AN ABSTRACT OF THE THESIS OF

Michael C. Ryan for the degree of Master of Science in Medical Physics presented on June 10, 2010.

Title: Characterization of the Onset of Charged Particle Equilibrium for Photon Dose to the Skin.

Abstract approved:

_____

Camille J. Lodwick

In the U.S., the Nuclear Regulatory Commission (NRC) is responsible for setting annual dose limits. For cases of hot particle contamination these limits are set at depths in skin of 7 mg/cm^2, 300 mg/cm^2, and 1000 mg/cm^2. However, at such shallow depths, the lack of charged particle equilibrium (CPE) precludes the use of traditional fluence-to-dose conversion methods.

In this work, an enhanced photon dosimetry model is constructed based on simulations of photon point sources using MCNP5 (Monte Carlo N Particle version 5) transport code. An empirical relationship between KERMA and absorbed dose was established, and used to develop a correction factor, f_{CPE}, accounting for the lack of charged particle equilibrium (CPE) at shallow depths. This correction factor, in conjunction with traditional point-kernel fluence-to-

dose conversion, provides a more accurate prediction of photon dose. The photon model is implemented such that empirical mathematical formulations, rather than look-up tables, drive the estimation of integrated dose over a disk up to 10 cm^2.

In addition to f_{CPE}, the creation of a secondary off-axis correction (s_C) was necessary in order to accurately calculate the integrated dose to a disc at shallow depths. When calculating the integrated dose to a disc of 10 cm^2 at a depth of 0.007 cm for photon energies of 0.662, 0.835, and 1.333 MeV the new model is within 2.0%, 3.7%, and 2.5%, respectively, of the dose calculated by MCNP5. This corresponds to improvements of 134.4%, 165.2%, and 275.5% over VARSKIN 3's results for the same shallow-depth calculations. The photon dosimetry model presented here also incorporates the parameters of energy, attenuation, and dose-averaging area, thereby addressing deficiencies in previous models.

Characterization of the Onset of Charged Particle of Equilibrium for Photon Dose to the Skin

by

Michael C. Ryan

A THESIS

submitted to

Oregon State University

in partial fulfillment of

the requirements for the

degree of

Master of Science

Presented June 10, 2010

Commencement June 2011

Master of Science thesis of Michael C. Ryan presented on June 10, 2010.

APPROVED:

_____

Major Professor, representing Medical Physics

_____

Head of the Department of Nuclear Engineering and Radiation Health Physics

_____

Dean of the Graduate School

I understand that my thesis will become part of the permanent collection of Oregon State University libraries. My signature below authorizes release of my thesis to any reader upon request.

_____

Michael C. Ryan, Author

ACKNOWLEDGEMENTS

I would like to thank Drs. Hamby, Higley, Reese, and Palmer, who have been more than gracious with their time, support, and expertise throughout my time at OSU. I would also like to thank all of my peers in the Department of Radiation Health Physics and Nuclear Engineering, particularly Kevin Makinson and Edward Cazalas, whose input and advice over the course of this project have proven invaluable. My sincere appreciation also goes to my family and friends, especially my wonderful fiancé Sam, for their love, encouragement, and ability to remind me what is truly important. Lastly, I want to express my deepest gratitude to my advisor Dr. Camille Lodwick. Her honesty, patience, and guidance not only made this project a success but have also made my time here an incredibly fun, invigorating, and unforgettable experience.

TABLE OF CONTENTS

Page

TABLE OF CONTENTS (CONTINUED)

Page

List Of Figures

Figure Page

LIST OF FIGURES (CONTINUED)

Figure Page

LIST OF TABLES

Table Page

LIST OF TABLES (CONTINUED)

Table Page

1 Background and Literature Review

1.1 Hot Particles

The term 'hot particle' was first coined roughly 50 years ago in reference to the types of particulate matter that soldiers on a battlefield contaminated by nuclear fallout may have encountered (Charles, 2002). Today the term is generally used to mean any small radioactive source of high activity. Such particles typically have a diameter of several μm to several mm and activities of 37 Bq to 37 MBq, although some samples with activities in the GBq range have been encountered (Reece, 1991). Due to their small physical size, hot particles can present a health risk either through direct deposition on the skin or through inhalation into the lungs. Clearly, the health physics mantra of 'time, distance, shielding' is difficult to enforce in these scenarios. The significance of hot particle dosimetry is best illustrated by a practical example: a single 5 kBq source of ^{60}Co is capable of delivering a dose large enough to violate the Nuclear Regulatory Commission's (NRC) mandated limit for members of the public with only a few hours of residence time (Darley, 2000).

The two most common sources of hot particles in the nuclear power industry are from the corrosion of irradiated fuel and from the neutron activation of corrosion product particles (Charles, 2007). These sources are of particular concern in the US where older pressurized water reactors (PWRs) and boiling water reactors (BWRs) pose a greater risk of exposure. In a 1988 survey of 61

U.S. operating nuclear power plants, forty-four plants reported incidents involving hot particles (Reece, 1991). In some cases extremity doses as large as 5120 mGy have been reported as a result of hot particle exposure (Reece, 1991). The most predominant radionuclide found in hot particles originating from water reactors is ^{60}Co, although ^{54}Mn, ^{58}Co, and ^{51}Cr may also be present.

How particle dosimetry is a challenge. Until relatively recently, no reliable data was available regarding either the stochastic or deterministic effects of hot particle exposure on humans to serve as a basis for setting informed regulatory limits. Secondly, traditional methods of dose evaluation are insufficient to describe the highly non-uniform spatial dose distribution surrounding hot particles. Fortunately, recent advances in dosimetric techniques and radiobiology have led to progress in addressing the issues presented by hot particle contamination.

Unfortunately, most of this progress has been limited to a better understanding of the beta component of hot particle dose, while the ability to accurately predict the gamma component has remained elusive. In fact, until recently there was debate as to whether or not the gamma component was even a significant contributor to the total dose (Lantz & Lambert, 1990). However, it is now generally accepted that there is a need for a method to accurately predict the gamma dose from hot particles, particularly in scenarios in which personal protective equipment (PPE) is worn. In situations such as this, the gamma

component of dose may constitute as much as 99.7% of the total dose to the basal cell layer of the skin (Lantz & Lambert, 1990).

1.2 Biological Considerations

Concern over the biological effect of hot particles was first raised in the 1960's and was mainly focused on the carcinogenicity of alpha-emitting radionuclides, particularly ^{239}Pu. As was previously mentioned, the dose distributions produced by hot particles tend to be highly non-uniform; alpha/beta particles experience rapid attenuation in tissue and the small dimensions of hot particles lead to a near inverse square fall-off for fluence. At the time it was thought that the very high local doses associated with inhalation and deposition of these contaminants in the lung might present a carcinogenic risk several orders of magnitude greater than what would be expected for an equivalent uniform exposure. This conjecture became known as the 'hot particle hypothesis' (Charles, 2007).

However, several decades of experimental and theoretical research have shown this not to be the case and the International Council on Radiological Protection (ICRP) has maintained that mean dose is an appropriate metric to use for evaluating risk (ICRP, 1980). This makes sense given that the origins of radiation-induced cancer lie in individual cells and that the dose-response relationship is linear. It follows from these suppositions that cancer risk is independent of the spatial dose distribution (Charles, 2002).

While the origins of the hot particle dosimetry arose from a concern over the inhalation of radioactive material, the overwhelming majority of current research is focused on the risks associated with hot particle contamination of the skin. This is due to the fact that most hot particles encountered in the nuclear power industry are "large" (dimensions > 10 μm) and are therefore incapable of depositing in the lung. As with lung exposures, the 'hot particle hypothesis' as it relates to skin exposure has been shown to be false (Charles, 2002). In fact, there is experimental evidence that suggests that the high local doses that result from hot particle contamination may actually lead to increased cell killing and a corresponding decrease in cancer risk (Charles, 2002). As a result, deterministic effects, primarily acute skin necrosis and moist desquamation, have been identified as the endpoints of concern (Hopewell, 1991).

1.3 Regulatory Limits

In the U.S., the Nuclear Regulatory Commission (NRC) is responsible for regulating and enforcing public and occupational dose limits. These regulations are codified in 10CFR20 and the limits for shallow-dose equivalent (SDE), lens dose equivalent (LDE), and deep-dose equivalent (DDE) are summarized in Tbl. 1-1. Shallow-dose equivalent is defined as the dose equivalent at a depth of 0.007 cm in tissue (the basal cell layer) that is the result of an external exposure to the skin. The lens dose equivalent is taken to be the equivalent dose at a depth of 0.3 cm in tissue from an external exposure to the lens of the eye and the deep-dose

equivalent is defined as the equivalent dose at a depth of 1 cm in tissue from an external whole-body exposure. It should be noted that while DDE is defined using a whole-body exposure criterion, the same limit applies in the case of hot particle contamination.

Table 1-1: Shallow-dose equivalent (SDE), lens dose equivalent (LDE), and deep-dose equivalent (DDE) limits as specified in 10CFR20.1201, *as averaged over the 10 cm^2 area receiving the highest exposure.

Location	Tissue Depth [cm]	Dose Limit* [Sv/y]
SDE	0.007	0.5
LDE	0.3	0.15
DDE	1.0	0.5

While the NRC is responsible for regulating doses, it bases its regulatory decisions on the recommendations of the ICRP and the National Council on Radiological Protection (NCRP, the U.S. counterpart of the ICRP). The dose limits and depths outlined in Tbl. 1-1 comply with ICRP recommendations first published in 1991 in Report 59 and then reiterated in 2007 in Report 106, except for one very notable difference: the ICRP recommends that an averaging area of 1 cm^2 be used rather than the 10 cm^2 mandated by 10CFR20. The dose limits set by the NRC once used the same averaging area recommended by the ICRP but were changed in 2002 to agree with the 10 cm^2 recommendation in NCRP's Report 130 to establish "a more risk-informed limit" (U.S. NRC, 2002). Nuclear power companies had successfully argued to the NRC that the 1 cm^2 constraint actually violated the long standing 'as low as reasonably achievable' (ALARA)

concept by requiring workers to frequently interrupt their work to check for contamination, thereby causing unproductive exposures (Xu, 2005). One unintended consequence of loosening this constraint is a push within the health physics community to determine whether or not the whole-body effective dose needs to be calculated when quantifying the risk from hot particles (Xu, 2006).

1.4 Basic Interactions

Charged particles, such as elections (e^-); protons (p); and alpha particles (α), are considered directly ionizing radiation because they are able to produce ionizations via direct collisions with the atoms of a given medium. Photons, being electrically neutral, are unable to produce direct ionizations and must first interact with matter to produce secondary electrons. There are three main mechanisms of interaction for photons with matter: the photoelectric effect, Compton scattering, and pair production.

1.4.1 Photoelectric Effect

The photoelectric effect is a threshold process by which a photon transfers its energy to an orbital electron, thereby causing the electron to be ejected. The threshold energy, or work function, required to remove an electron from its orbital is equal to the binding energy of the electron. Any photon energy in excess of the work function is imparted to the secondary electron as kinetic energy. As a consequence, not all of the incident photon energy is converted to kinetic energy; if the hole created by the ejection of the secondary electron is filed

by the de-excitation of another orbital electron, some energy may escape in the form of fluorescence (Johns and Cunningham, 1983). However, if an Auger electron is also ejected, the binding energy of the electron will appear as kinetic energy. Each orbital of an atom has a different work function associated with it, which is dependent upon the orbital's proximity to the nucleus. In a given material, the photoelectric cross section increases with increasing atomic number and decreases with increasing photon energy such that,

$$\sigma_{ph} \propto \frac{Z^4}{E^3}. \tag{1.1}$$

1.4.2 Compton (Incoherent) Scattering

In Compton or incoherent scattering, energy is transferred between a photon and a "free" electron via an inelastic collision. In this context the word "free" means that the binding energy of the electron is much less than the energy of the incident photon. The energy imparted to the Compton electron during the collision is given by,

$$E = h\nu \frac{\alpha(1-\cos\theta)}{1+\alpha(1-\cos\theta)} \tag{1.3}$$

where m_e is the rest mass of an electron, ν is the frequency of the incident photon, θ is the photon scattering angle measured with respect to the incident trajectory. The parameter α is simply the ratio of the incident photon energy to the rest energy of an electron,

$$\alpha = \frac{h\nu}{m_e c^2}. \tag{1.3}$$

It follows from Eqn. 1.3 that the energy of the Compton electron increases with increasing scattering angle. When the incident photon is completely backscattered (i.e., θ=180°) Eqn. 1.3 becomes,

$$E_{\max} = h\nu \frac{2\alpha}{1+2\alpha}. \tag{1.4}$$

As with the photoelectric effect, the probability of a Compton event is dependent upon the atomic number of the absorbing material such that,

$$\sigma_c = Z\sigma_{KN} \tag{1.5}$$

$$\sigma_{KN}(E,\theta) = \frac{r_e^2}{2}\frac{E'}{E}\left[1+\left(\frac{E'}{E}\right)^2 - (1-\cos^2\theta)\right] \tag{1.6}$$

where σ_{KN} is the Klein-Nishina cross section, r_e is the classical electron radius, and E'/E is the ratio of incident to scatted photon energy.

1.4.3 Pair Production

Similar to Compton scattering, pair production is a threshold process requiring a minimum photon energy of 1.022 MeV. When an incident photon passes in the vicinity of an atomic nucleus it strongly interacts with the associated electromagnetic field producing an electron/positron pair. It is the 0.511 MeV rest mass of each particle that leads to the 1.022 MeV threshold. Any

photon energy that is in excess of this threshold is imparted to the particles as kinetic energy, which is roughly shared equally. As the positron moves though matter, it deposits energy via the same mechanisms as electrons. As it nears the end of its track, however, the positron will combine with a nearby free electron thereby creating two annihilation photons, each having 0.511 MeV of energy. Pair production is an elegant example of the mass-energy interconversion that is predicted by Einstein's now-famous $E=mc^2$ equation. As a consequence of the relatively high threshold energy, pair production is the dominant mechanism of interaction for high-energy photons. Figure 1-1 shows the absorption coefficients for each of the previously described processes as well as the total absorption coefficient.

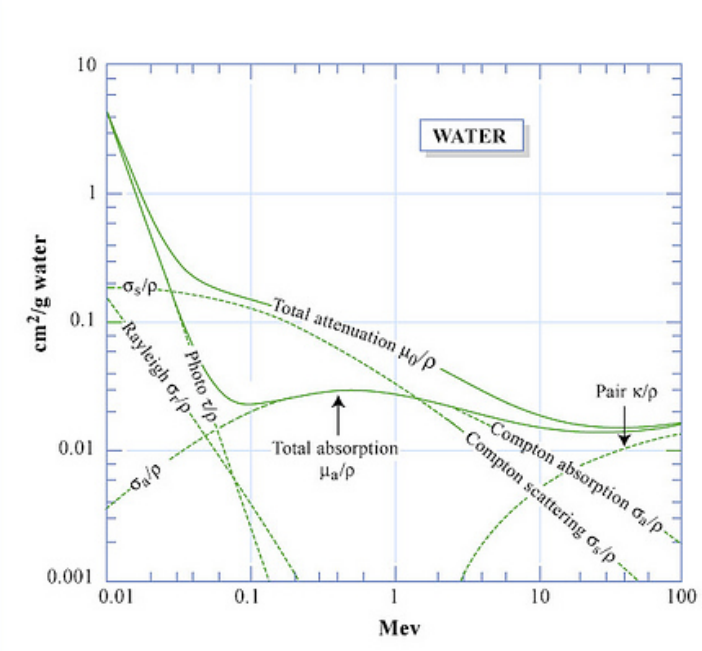

Figure 1-1: Individual process and total absorption coefficients as a function of photon energy. Modified from MIT Open Courseware (2006).

The interactions of the secondary electrons with other charged particles in the medium are governed by the Coulomb forces that exist between the various electric fields. These coulombic collisions give rise to the excitations and ionizations that break molecular bonds, thereby causing tissue damage. The range of electrons in matter can be calculated by using the Continuous Slowing Down Approximation (CSDA), which assumes that all collisions that occur result in very small and instantaneous energy exchange. Integrating over the path taken by the electron yields the range,

$$R_{CSDA} = \int_0^{E_0} \frac{dE}{S_{tot}(E)} \tag{1.7}$$

where E_0 is the initial electron energy and $S_{tot}(E)$ is the energy dependent total stopping power (Johns and Cunningham, 1983). In tissue, a further approximation can be made to determine the electron range (in mg/cm^2) for energies below 3.0 MeV:

$$R = 412E^{1.265-0.0954\ln(E)}. \tag{1.8}$$

1.5 Dose Theory

Indirectly ionizing radiations, such as photons, transfer their energy to material through a two-step mechanism. In the first step, a photon interacts in the medium and creates a secondary electron. In the second step, the secondary electron moves through the medium depositing its energy via excitations and ionizations. Figure 1-2 shows a schematic representation of these processes.

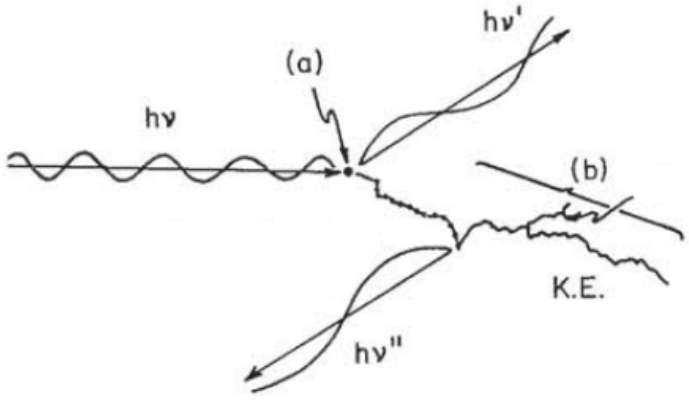

Figure 1-2: Schematic showing the complicated manner in which photons transfer their energy to matter. At (a) a photon interacts with a free electron thereby setting it in motion. In (b) the secondary electron transfers its energy to atomic electrons in the material. Modified from Johns and Cunningham (1983).

1.5.1 KERMA

The concept of KERMA (kinetic energy released in matter) has been developed as a way of describing step (a) in Fig. 1-2. KERMA (K) is defined as,

$$K = \frac{dE_{tr}}{dm} \tag{1.8}$$

where dE_{tr} is the energy transferred to the charged ionizing particles (e.g., electrons) that have been created by the uncharged particles (e.g., photons) in a volume element of mass dm. The units for KERMA are the same as those for dose, namely J/kg, although dose is commonly measured in its SI unit of gray (Gy). The KERMA for a volume of interest is easily calculated using,

$$K = \Psi\left(\frac{\mu_{tr}}{\rho}\right) \tag{1.9}$$

where Ψ is the energy fluence and μ_{tr}/ρ is the mass energy transfer coefficient. The energy fluence is the total average energy being carried by all radiations incident upon the volume of interest and for a monoenergetic photon source reduces to,

$$\Psi = \Phi E \tag{1.10}$$

where Φ is the photon fluence. Using Eqns. 1.9 and 1.10 to calculate KERMA at any point of interest is an easy task.

In low Z materials, such as tissue, most of the kinetic energy of the secondary electrons is expended through inelastic collisions (i.e. excitations and ionizations) with atomic electrons. However, a small fraction of the initial kinetic energy will be expended via radiative collisions with atomic nuclei (i.e., bremsstrahlung). Total KERMA can therefore be broken down into two parts,

$$K = k_{col} + k_{rad} \tag{1.11}$$

where k_{col} and k_{rad} are the collisional and radiative components of KERMA, respectively.

1.5.2 Absorbed Dose

Absorbed dose is defined as the energy deposited in the medium (dE_{en}) per unit mass (dm),

$$D = \frac{dE_{en}}{dm} \tag{1.12}$$

The mass dm, however, should be considered sufficiently small as to consider Eqn. 1.12 as describing the absorbed dose at a point. It is also important to note that energy transfer (KERMA) and absorption (dose) do not occur at the same location. As is shown in Fig. 1-2, energy deposition occurs downstream of electron creation due to the predominately forward motion of the secondary electrons.

If one assumes that equilibrium exists between dose and KERMA then dose can be related to fluence in a manner similar to Eqns. 1.9 and 1.10,

$$D = \Phi E\left(\frac{\mu_{en}}{\rho}\right) \tag{1.13}$$

where μ_{en}/ρ is the mass energy absorption coefficient. Equation 1.13 also assumes that the volume of interest is infinitely thin and that interactions occur only in the two dimensions that are normal to the beam of incident photons. Dose can also be related to KERMA,

$$D = K(1-g) = k_{col} \tag{1.14}$$

where g is the fraction of electron energy lost to radiative processes. These radiative losses are not considered in the calculation of dose since their energy is not deposited locally. It then follows from Eqns. 1.9, 1.13 and 1.14,

$$\left(\frac{\mu_{en}}{\rho}\right) = \left(\frac{\mu_{tr}}{\rho}\right)(1-g). \tag{1.15}$$

For photon energies less than 10 MeV in low Z material (e.g., tissue), radiative losses due to bremsstrahlung are negligible and so the mass energy absorption coefficient is equivalent to the mass energy transfer coefficient (Lantz and Lambert, 1990). This also means that dose, total KERMA, and collisional KERMA are all equivalent as well.

Equation 1.13 can be modified to calculate the dose rate at a point from a hot particle by noting that the uncollided flux (fluence rate) of the hot particle is proportional to its strength (S) in units of photons per second,

$$\phi_0 = \frac{d\Phi_0}{dt} = \frac{S}{4\pi r^2} \tag{1.16}$$

where r is the distance to the point of interest. The dose rate at point r is then given by,

$$\dot{D} = \frac{S}{4\pi r^2} E\left(\frac{\mu_{en}}{\rho}\right) e^{-\left(\frac{\mu}{\rho}\right)r} \tag{1.17}$$

where the exponential decay term is added to account for photon attenuation in the medium.

1.5.3 Charged Particle Equilibrium

Charged particle equilibrium (CPE) is said to exist when each particle that leaves a given volume is replaced by a particle of equivalent type and energy entering the volume. While KERMA is at a maximum at the skin surface and then

decreases exponentially with depth, dose must first build to a maximum after which it decreases at the same rate as KERMA. The region in which dose increases (see Fig. 1-3) is known as the 'build up region'. It is in this region that the number of charged particles being created increases until CPE is achieved. In the build up region, no analytical method for relating dose to fluence exists. The depth at which CPE is achieved is equal to the range of the most energetic secondary electrons that are created (Lantz & Lambert, 1990).

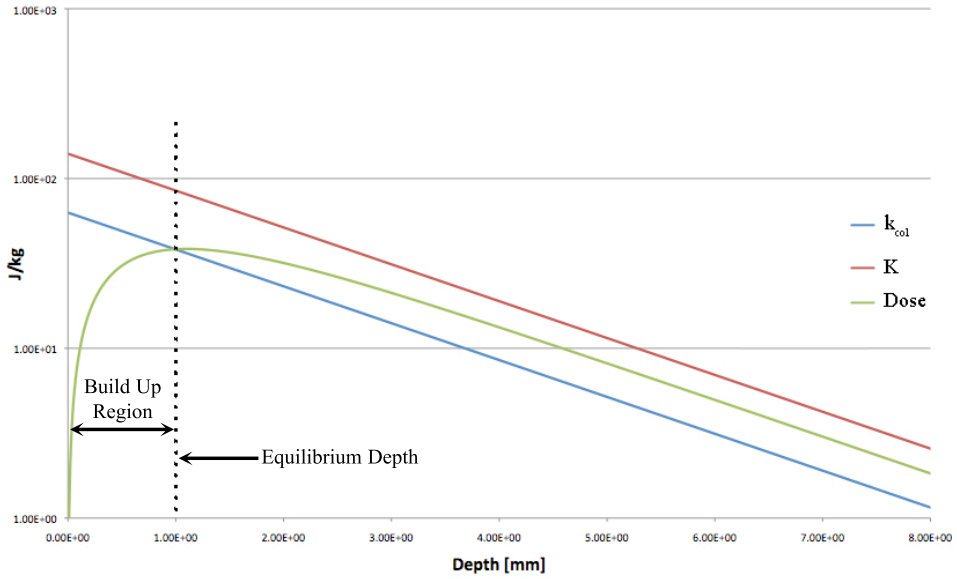

Figure 1-3: Comparison of absorbed dose, total KERMA and collisional KERMA.

As can be seen in Fig. 1-3, absorbed dose will generally be larger than collisional KERMA and less than total KERMA at a given depth. This is due to a portion of the total KERMA being carried away in the form of bremsstrahlung, which means it will not be deposited locally (i.e., converted to dose). Additionally, dose is larger than KERMA at a given depth as a result of the center

of electron production being located upstream relative to the point where dose is being deposited (see Fig. 1-2). At the energies relevant to hot particle dosimetry, radiative losses are minimal and so total KERMA and collisional KERMA are equal.

It is CPE, or lack thereof, that is partially exploited in radiation therapy treatments. By choosing beam energies that achieve CPE after a depth of a centimeter or more, the skin and normal tissues upstream of the tumor are spared the maximum dose as they lie in the build up region shown in Fig. 1-3.

1.5.4 Equivalent Dose

Section 1.5 has been primarily devoted to summarizing the basis for absorbed dose theory. The regulatory limits reported in Tbl. 1-1, however, are actually for the quantity of equivalent dose (H). The concept of equivalent dose was first formalized in ICRP 26 in 1977, although at the time it was referred to as "dose equivalent", as a means of accounting for the different biological effects of different radiation types. While the SI unit of Sievert (Sv) is used to differentiate equivalent dose from absorbed dose (SI unit Gy) their base units are the same, namely J/kg. Equivalent dose is defined in ICRP 60 as,

$$H_{T,R} = w_R D_{T,R}$$

where w_R is the dimensionless radiation weighting factor, $D_{T,R}$ is the absorbed dose to tissue T from radiation type R in Gy, and $H_{T,R}$ is the dose equivalent to

tissue T from radiation type R in Sv. For all x-ray, gamma, and beta energies, the radiation weighting factor is one and so the absorbed dose in Gy is also the dose equivalent in Sv.

1.6 Previous Work on Hot Particle Photon Dosimetry Models

1.6.1 Lantz, Lambert, and Chabot

The best known and most widely used hot particle photon dosimetry model was originally developed and reported by Michael W. Lantz and Michael W. Lambert in 1990. The rational behind their model begins with Cember's (1996) equation for calculating the dose from a point source to a disk, which itself is based on the Inverse Square Law,

$$\dot{D}_1 x_1^2 = \dot{D}_2 x_2^2 \tag{1.18}$$

where $\dot{D}$ and x are the dose rate at and distance to the point of interest respectively. Substituting the specific gamma ray constant (Γ) for the left side of equation 1.18 and solving for $\dot{D}_2$ yields,

$$\dot{D}_2 = \frac{\Gamma}{x_2^2}. \tag{1.19}$$

To find the dose to a disc, as illustrated in Fig. 1-4, equation 1.19 is simply integrated over the disc area,

$$\dot{D}_{Disc} = \int_0^R \frac{\Gamma}{(h+r)^2} 2\pi r \, dr = \pi \Gamma \, \ln\left(\frac{h^2 + R^2}{h^2}\right). \tag{1.20}$$

Lantz and Lambert repeatedly cite to Eqn. 1.20 as reporting the "average dose rate" to the disc per unit activity. However, Eqn. 1.20 actually reports the *total exposure* rate per unit activity to the disc in mR μCi^{-1} hr^{-1}. Implicit in the claim that Eqn. 1.20 calculates dose is the assumption that 1 Roentgen is equivalent to 1 rad in tissue, although the actual conversion is closer to 0.96 rad/R. Furthermore, in order to calculate the average dose rate to the disc the total dose must be divided by the averaging area,

$$\overline{\dot{D}}_{disc} = \frac{\int_0^R \frac{\Gamma}{(h+r)^2} 2\pi r\, dr}{\int_0^R 2\pi r\, dr} = \frac{\Gamma}{R^2} \ln\left(\frac{h^2+R^2}{h^2}\right). \qquad (1.21)$$

Finally, the equations for total dose and average dose both ignore the effect of photon attenuation in tissue, which was assumed to be negligible at the depths they were investigating (Lantz & Lambert, 1990).

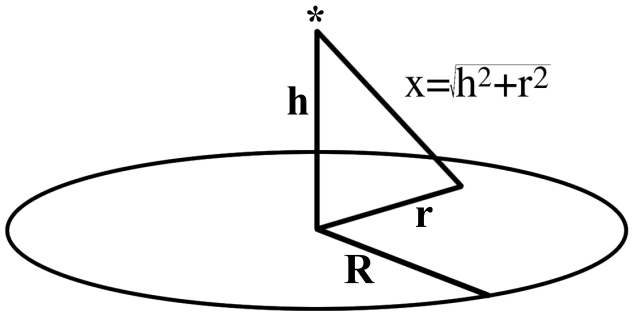

Figure 1-4: A point source irradiating a disc of fixed area.

Lantz and Lambert define a CPE correction factor that can be applied to Eqn. 1.19 such that the equilibrium corrected dose to a point on the disc can be calculated,

$$\dot{D}_{CPE} = (\text{CPE Fraction})\frac{\Gamma}{(h^2 + r^2)}. \quad (1.22)$$

Chabot provided Lantz and Lambert with three energy-dependent "CPE Path Length Coefficients" (μ), and the formula for determining the degree of CPE that has been achieved for a given path length (x) (1990),

$$\text{CPE Fraction} = 1 - e^{-\mu x}. \quad (1.23)$$

While the units (cm^{-1}) and the symbol used to represent the CPE Path Length Coefficient are the same as those for the linear attenuation coefficient, the two parameters are not equivalent.

Chabot obtained his values of μ by using unpublished radiotherapy depth dose curves and a modified form of Loevinger's equation for beta emitters. As such, the values of μ that were reported were based on a monodirectional photon source where every photon must travel the same distance to reach the area of interest. For a point source, photons are assumed to be emitted isotropically and as a result, some photons will travel through much more than 0.007 cm of tissue before reaching the basal cell layer (Lantz and Lambert, 1990). This leads to a much greater fraction of CPE being achieved as compared to the broad-beam

setup. Figure 1-5 illustrates this; note the path length of a photon traveling to a point in the basal cell layer directly below the hot particle is 0.007 cm. However, in order to reach a point on the edge of the averaging area (10 cm^2) a photon must travel 1.78 cm and a correspondingly larger degree of CPE is achieved. For a disc at 0.007 cm depth a monodirectional source is expected to achieve only 7% equilibrium whereas an isotropic source has achieved approximately 50% (Lantz and Lambert, 1990).

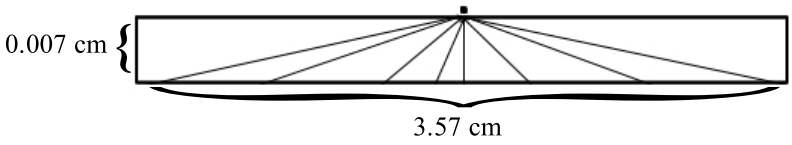

Figure 1-5: Representative path lengths of hot particle photons reaching the basal cell layer (not to scale).

Lantz and Lambert took the three values of the CPE Path Length Coefficient provided by Chabot (for energies 1.25, 0.8, and 0.3 MeV) and fit an equation that allowed them to determine the Path Length Coefficient at any energy of interest,

$$\mu = 139e^{-0.00209 \cdot E} \tag{1.24}$$

where E is the photon energy in keV. Equation 1.24 differs greatly from the expression that Chabot himself used to calculate μ,

$$\mu = 13(E - 0.036)^{-1.37}. \tag{1.25}$$

No explanation for this discrepancy was available in the literature. Table 1-2 shows a comparison of the CPE Path Length Coefficients as calculated by Eqns. 1.24 and 1.25.

Table 1-2: Comparison between the CPE Path Length Coefficients as calculated by Lantz and Lambert and Chabot.

Energy [MeV]	μ [cm^{-1}] (Chabot)	μ [cm^{-1}] (L&L)	% Difference
0.20	155	92	-40.9
0.40	52	60	16.1
0.60	28	40	39.2
0.80	19	26	38.9
1.00	14	17	25.8
1.25	10	10	2.3
1.50	8	6	-21.6
1.75	6	4	-42.3
2.00	5	2	-58.8

Equations 1.22, 1.23, and 1.24 were then combined to calculate the CPE-corrected dose rate to a disc for a variety of photon energies through a step-wise summation,

$$\dot{D}_{CPE,\,disc} = \sum_{i=1}^{N-1} \frac{\pi(r_1^2 - r_2^2)\Gamma}{h^2 + r^2} \left\{ 1 - Exp\left[-(139e^{-0.00209E})\sqrt{h^2 + r^2} \right] \right\} \qquad (1.26)$$

where R_1 and R_2 are the radii of concentric rings as measure from the center of the disc and r is the radius to the center of the annuli. Again, Eqn. 1.26 is reporting the *total* dose rate to the disc even though the literature indicates it is calculating the *average* dose.

Lantz and Lambert define and calculate a disc-averaged CPE fraction by taking the ratio of the CPE-corrected dose (Eqn. 1.26) to the uncorrected dose (Eqn. 1.20),

$$\text{CPE Fraction}_{\text{disc}} = \frac{\dot{D}_{\text{CPE, disc}}}{\dot{D}_{\text{disc}}}. \tag{1.27}$$

When determining the CPE fraction, the use of the total dose rate as opposed to the average dose rate is of no consequence since both the corrected and uncorrected doses are overestimated by the same factor, namely, the area of the averaging disc. Finally, Lantz and Lambert found a global fit for the disc-averaged CPE factor as a function of both depth in tissue (h) and photon energy (E),

$$\text{CPE Fraction} = 1 - ae^{-bh} \tag{1.28a}$$

where for h ≤ 0.02 cm,

$$\begin{aligned} a &= 0.129 + 0.000338E \\ b &= 171.8e^{-0.00162E} \end{aligned} \tag{1.28b}$$

and for h > 0.02 cm,

$$\begin{aligned} a &= 0.062 + 0.0003055E \\ b &= 156e^{-0.00193E} \end{aligned}. \tag{1.29c}$$

The formulation of this disc-averaged CPE factor allows the step-wise integration performed in Eqn. 1.26 to be bypassed when calculating the corrected dose rate,

$$\dot{D}_{CPE,\,disc} = \pi\Gamma \ln\left[\frac{h^2 + R^2}{h^2}\right](1 - ae^{-bh}) \tag{1.30}$$

where each of the variables are as previously defined. While Eqn. 1.30 appears to calculate the dose rate to a disc of arbitrary radius it is important to note that the CPE correction factor is only valid for discs of 1 cm^2 area (r=0.564 cm). Furthermore, Eqn. 1.30 assumes that photon attenuation is negligible at all depths, which is not a valid for low photon energies (U.S. NRC, 2006).

1.6.2 VARSKIN 3

While the dose limits outlined in Tbl. 1-1 are for planned exposures they are still enforced in circumstances of accidental exposure, which is often the case with hot particle contamination. Due to the unexpected nature of hot particle contamination, the affected personnel may not be wearing the monitoring equipment necessary for an accurate evaluation of dose. Even if monitoring equipment is being worn, the highly localized dose distributions that result are difficult to measure using traditional dosimeters (Cazalas, 2009). As such, there was a need for a fast and reasonably reliable method of dose reconstruction for skin contamination, hence the VARSKIN code was created. Originally developed for use by the NRC for regulatory purposes VARSKIN (currently in version 3) is now widely used in both industry and academia as a quick and efficient means of determining the severity of a skin contamination incident.

VARSKIN 3 contains beta and photon dosimetry models, with the photon component utilizing an expanded version of the previously described Lantz and Lambert model. The most significant difference between the two models is the disc averaging area that was used to determine the CPE correction factors; the Lantz and Lambert model uses 1 cm^2 while VARSKIN uses the 10 cm^2 area mandated by 10CFR20.1201. This discrepancy leads to a different set of equations for the coefficients of Eqn. 1.28a,

$$\begin{aligned} a &= 0.117 + 0.000272E \\ b &= 170.8e^{-0.001465E} \end{aligned} \tag{1.31a}$$

for h ≤ 0.02 cm and,

$$\begin{aligned} a &= 0.0458 + 0.000267E \\ b &= 147e^{-0.00166E} \end{aligned} \tag{1.31b}$$

for h > 0.02 cm, where h is the depth in tissue. As was the case with the Lantz and Lambert model, VARSKIN allows for the dose to be calculated to a disc of arbitrary radius despite the disc-averaged CPE corrections being calculated with a 10 cm^2 averaging area (r=1.784 cm).

Another limitation of VARSKIN 3 is that it fails to account for photon absorption. As a result, photon energies that would normally be attenuated are allowed to contribute to dose at deeper depths. As a workaround VARSKIN users must maintain an extensive library of depth-dependent radionuclides, each with the appropriate "photon energy cutoff". The VARSKIN user manual recommends

energy cutoffs of 2, 20, and 35 keV when calculating the SDE, LDE, and DDE respectively. Table 1-3 shows data from the VARSKIN user manual that demonstrates the strong energy dependence of the specific gamma ray constant.

Table 1-3: Modified specific gamma ray constant for Co-57 as a function of photon cutoff energy.

Energy Cutoff [keV]	Γ [rad $cm^2 mCi^{-1} hr^{-1}$]
2	14.38
10	0.96
20	0.53
100	0.53

Finally, while Lantz and Lambert's model and VARSKIN 3 compare well to other methods for calculating the degree of CPE correction needed, neither have been directly validated using experimental results. While both models are ostensibly based on Chabot's experimental results, these results and the corresponding analysis have never been published (Lantz & Lambert, 1990; Myrick, 1994).

2 MATERIALS AND METHODS

The model proposed in this work seeks to improve upon those described in Section 1.6 in several ways:

- A true point kernel approach is used to account for lack of CPE as opposed to a disc-averaged correction. Such an approach is more fundamentally sound and allows for the model to meet evolving user and regulatory needs that may require the use of averaging areas other than 10 cm^2.
- The use of the Specific Gamma Ray Constant is abandoned and with it the assumption that 1 R equals 1 rad.
- The average dose, not the total, to the disc of interest is calculated as mandated by the NRC.
- Photon attenuation in tissue is considered, thereby eliminating the need for an energy cutoff that excludes low-energy photons
- The model is based on independent measurements and the resultant dose profiles are independently verified.

2.1 Formulation of the Model

The proposed model starts with an assumption similar to that made by Lantz and Lambert (see Eqn. 1.22), but the use of the Specific Gamma Ray Constant is omitted:

$$\dot{D}_{CPE} = f_{CPE}\dot{D}_0 = f_{CPE}\dot{K} \tag{2.1}$$

where f_{CPE} is the degree of CPE that has been achieved, $\dot{D}_0$ is the uncollided dose rate and $\dot{K}$ is the KERMA rate. The substitution of KERMA for the uncollided dose in Eqn. 1.32 is allowed because losses from bremsstrahlung are negligible.

It then follows from Eqn. 2.1 that at a given depth in tissue, the fraction of CPE that has been established is,

$$f_{CPE} = \frac{\dot{D}_{CPE}}{\dot{K}} . \tag{2.2}$$

By using a Monte Carlo simulation package to estimate KERMA and dose as a function of depth (x), f_{CPE} curves can be constructed for various photon energies. This allows for the function $f_{CPE}(x)$ to be empirically determined using standard curve-fitting techniques, and an integration similar to the one performed in Eqn. 1.29 yields the CPE-corrected dose to the area of interest.

To construct the f_{CPE} curves the Monte Carlo N Particle code version 5 (MCNP5), developed and maintained by Los Alamos National Laboratories, was used to simulate hot particle contamination scenarios. The code was executed on Oregon State University's (OSU) High Performance Computing Cluster (HPC), which uses either 1.2, 2.2, or 2.8 GHz Dual-Core AMD Opteron processors, depending on what nodes are assigned to the job.

Because MCNP is unable to tally either the dose or KERMA to a point, each "kernel" was modeled as a cylinder with a radius of 0.01 cm and a height of 2 μm. The energy deposition tally (*F8 tally) determines the energy deposited in a given volume or 'cell' (in units of MeV) by summing the energy of all particles entering the cell and subtracting from that the energy of all particles that leave the cell. The result of the energy deposition tally must then be divided by the

cell's mass in order to obtain a direct measure of dose (MCNP5 Vol. II: Users Manual). The heating tally (F6 tally) is used to estimate the KERMA for a given cell in MeV/g. In the context of the MCNP output Eqn. 1.33 then becomes,

$$f_{CPE} = \frac{*F8}{F6 \cdot \pi r^2 h \rho} \tag{2.3}$$

where r and h are the radius and height of the cylindrical cell, and ρ is the density of liquid water. Figure 2-1 shows the geometry that was used in MCNP to construct the f_{CPE} factors, where a cylinder of water (fuchsia) was used to model tissue. The f_{CPE} factors were measured in 2 μm increments between 2 μm to 70 μm depth, and in 100 μm increments from 70 μm to 1 cm depth. The use of the 2 μm increment at shallow depths was necessary to resolve the large dose gradient in this region. The photon energy range was from 0.1 MeV to 1 MeV in 0.1 MeV increments and from 1 MeV to 2 MeV in 0.2 MeV increments. Simulations of photons with energies of 5, 20, 50, and 90 keV were also performed.

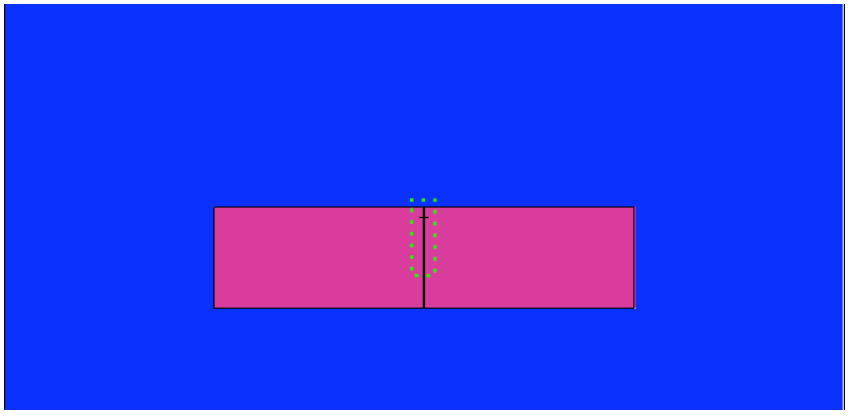

Figure 2-1: Picture of the geometry used in MCNP5 to calculate the f_{CPE} correction factors. Each color in the figure represents a different material; blue is air and fuchsia is tissue.

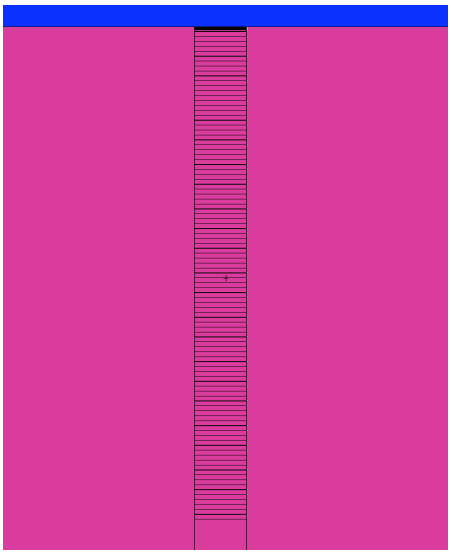

Figure 2-2: A magnified view (green square in Fig. 2-1) of the MCNP geometry.

While the small kernel size (~6E-8 mL) was required to accurately model the dose to a point, it also necessitated the simulation of a large number of photons to reduce statistical uncertainty given that individual photons have a very low probability of interacting in each target volume. This required segmenting the input file for a given energy into 24 smaller input files, each simulating 50 million photons. By apportioning the inputs in this manner, the multiple nodes offered by the HPC could be utilized to decrease computing time despite the fact that a parallel installation of MCNP5 was not available. MCNP5's "RAND SEED" parameter was changed for each input to ensure that different sequences of random numbers were used for each run. In total, over 20 billion photons were simulated, which required over 400 days of CPU-time. The results

from each of the inputs were later combined during post-processing, which took an estimated 230 hours. The hours listed here do not include time spent on data analysis.

Once the MCNP5 results were processed to yield the desired f_{CPE} curves TableCurve 3D® was used to find the function $f_{CPE}(x)$. TableCurve 3D® is a linear and non-linear surface fitting package that fits and ranks 36,000 equations, out of a library of over 450 million, for user supplied 3D data. This eliminates the need for the tedious and time-consuming trial and error approach typically associated with curve fitting. However, the 36,000 equations returned by TableCurve 3D® were scrutinized and an expression common to each energy was found, which was itself a tedious and time-consuming task. Finding an expression common to each energy allowed for the coefficients of the expression to be fit as functions of photon energy, thereby creating a global fit for f_{CPE}.

TableCurve 3D® was also used to find fits for the energy-dependent mass attenuation coefficient $(\mu/\rho)_{tissue}$ and the mass energy-absorption coefficient $(\mu_{en}/\rho)_{tissue}$ using data obtained from the National Institute of Standards and Technology (NIST) and the International Commission on Radiation Units and Measurement (ICRU) Report 44. While tables of the coefficient data are readily available, a fit is necessary if the model is to allow users to arbitrarily pick photon energies.

By definition, once CPE is achieved f_{CPE} is equal to one. As such, $f_{CPE}(x)$ will be a piecewise function,

$$f_{CPE}(x) = \begin{cases} 0; & x = 0 \\ f_{CPE}; & x < x_{CPE} \\ 1; & x > x_{CPE} \end{cases} \tag{2.4}$$

where x_{CPE} is the equilibrium depth. As was discussed in Section 1.5.3, CPE depth is approximately equal to the range of the most energetic secondary electrons that are created. Using Eqn. 1.8, x_{CPE} (in mg/cm^2) is given by,

$$x_{CPE} = 412 E_{\max}^{1.265 - 0.0954 \ln(E_{\max})} \tag{2.5}$$

where E_{max} is the maximum secondary electron energy. For this model it is assumed that the mechanism of interaction for photons of 100 keV or less is the photoelectric effect, while photons of greater energy are Compton scattered through 180°. The energy of the secondary electrons is therefore also a piecewise function,

$$E_{\max}(E_{photon}) = \begin{cases} E_{photon}; & E_{photon} \le 0.1 \text{ MeV} \\ E_{photon} \dfrac{2\alpha}{1+2\alpha}; & E_{photon} > 0.1 \text{ MeV} \end{cases} \tag{2.5}$$

where the parameter α has previously been defined in Eqn. 1.3.

By combining Eqns. 1.14, 1.17, 2.1, and 2.4, the average dose rate the disc of interest is given by,

$$\dot{D}_{disc}(h,E,A) = \frac{\int f_{CPE}(x)\cdot\dot{K}(x,E)\cdot dA}{\int dA} = \frac{S}{2A}\left(\int_0^R f_{CPE}(\sqrt{h^2+r^2})\cdot E\cdot\left(\frac{\mu_{en}}{\rho}\right)_{tissue}(h^2+r^2)^{-1/2}e^{-(\mu/\rho)\sqrt{h^2+r^2}}dr\right) \quad (2.6)$$

where R is the radius of the disc and all variables are as previously defined. Equation 2.6 yields an analytic solution with complex components and so a stepwise integration is necessary. One way to accomplish this is by segmenting the disc area into concentric rings (annuli) of equal area (A'). If the averaging area is split into N annuli it follows that the area of each annuli will be A'=A/N. It also follows that the distance from the averaging area to the outer radius (R_j) of each annuli is,

$$R_j = \sqrt{\frac{A'}{\pi} + R_{j-1}^2} \quad (2.7)$$

where j runs from 1 to N. Note that R_N=R, the radius of the disc. Once the values of R_j have been calculated the dose rate to the disc is,

$$\dot{D}_{disc}(h,E,A) = \frac{S}{2N}\sum_{i=1}^{N} f_{CPE}(\sqrt{h^2+r_i^2})\cdot E\cdot\left(\frac{\mu_{en}}{\rho}\right)_{tissue}(h^2+r_i^2)^{-1/2}e^{-(\mu/\rho)\sqrt{h^2+r_i^2}} \quad (2.8)$$

where r_i is measured to the center of each annuli.

3 RESULTS

3.1 Fitting f_{CPE}

Figures 3-1, 3-2, and 3-3 show the f_{CPE} curves that were constructed for 0.5 MeV, 1.0 MeV, and 1.6 MeV photon sources respectively (see Appendix A for all f_{CPE} data). While the results look as expected (i.e., the dose build up region is clearly visible), they are not of the form predicted by Chabot, Lantz, and Lambert as evidenced by the lack of agreement between the VARSKIN 3 curve (see Eqn. 1.28a) and the MCNP5 results. Instead, using the TableCurve® package, $f_{CPE}(x)$ was found to have the general form,

$$f_{CPE}(x) = \frac{1}{\left(a + b \cdot \ln(x) + {}^{c}\!/\!_{\sqrt{x}}\right)} \tag{3.1}$$

where the coefficients a, b, and c are themselves functions of energy (in units of MeV) such that,

$$\begin{aligned} a(E) = {} & 19.77986 + 149 + 1.85868 \cdot E \cdot \ln(E) - 0.00838988 \cdot E^{1.5} \\ & + 3.62352 \cdot 10^{-5} \cdot E^{2} + 3.34309091\sqrt{E} \cdot \ln(E) - 10.7243496 \frac{E}{\ln(E)} \end{aligned} \tag{3.2a}$$

$$\begin{aligned} b(E) = {} & 1.2166 \cdot 10^{-12} \cdot E^{4} - 5.673 \cdot 10^{-9} \cdot E^{3} + 7.9415 \cdot 10^{-6} \cdot E^{2} \\ & - 2.0276 \cdot 10^{-3} \cdot E + 0.32959 \end{aligned} \tag{3.2b}$$

$$\begin{aligned} c(E) = {} & 9.694 \cdot 10^{-13} \cdot E^{4} - 4.861 \cdot 10^{-9} \cdot E^{3} \\ & + 7.765 \cdot 10^{-6} \cdot E^{2} - 1.856 \cdot E + 0.1467 \end{aligned} . \tag{3.2c}$$

This new expression for $f_{CPE}(x)$ is shown in Figs. 3-1, 3-2, and 3-3 and there is excellent agreement with the MCNP5 results.

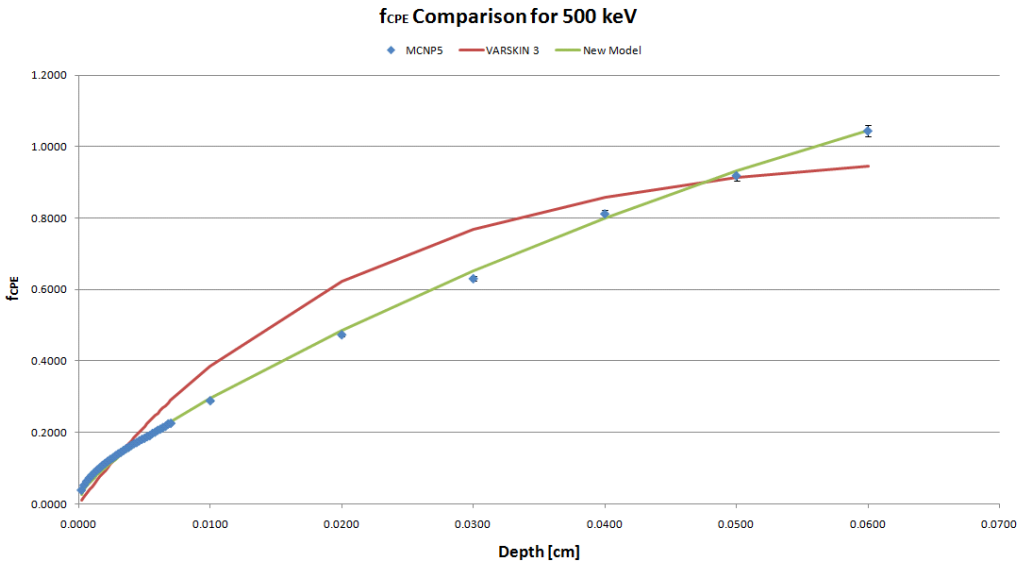

Figure 3-1: f_{CPE} curve for a 0.5 MeV photon source.

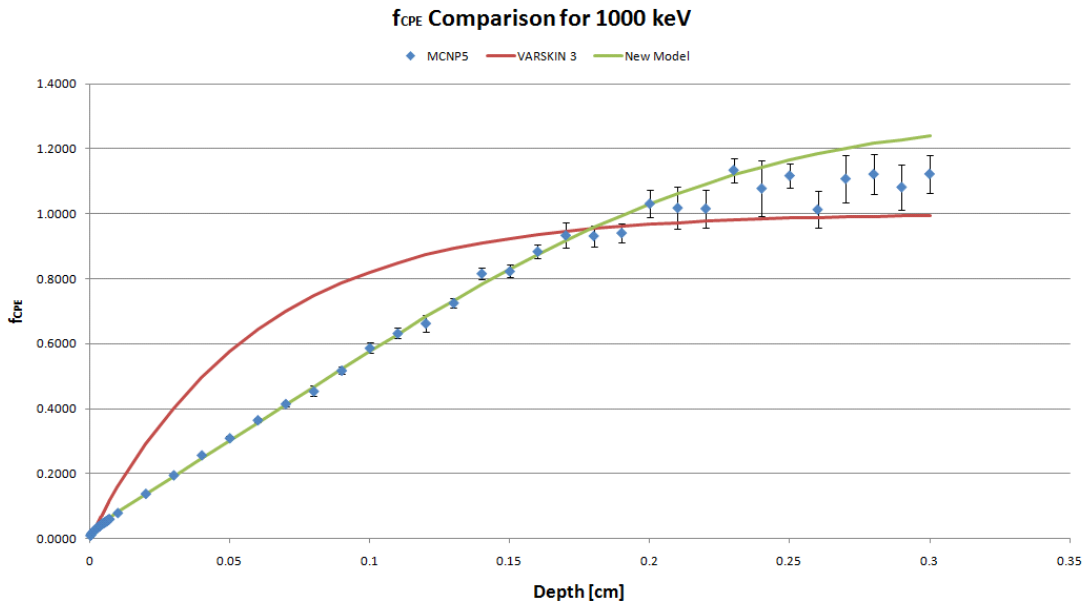

Figure 3-2: f_{CPE} curve for a 1.0 MeV photon source.

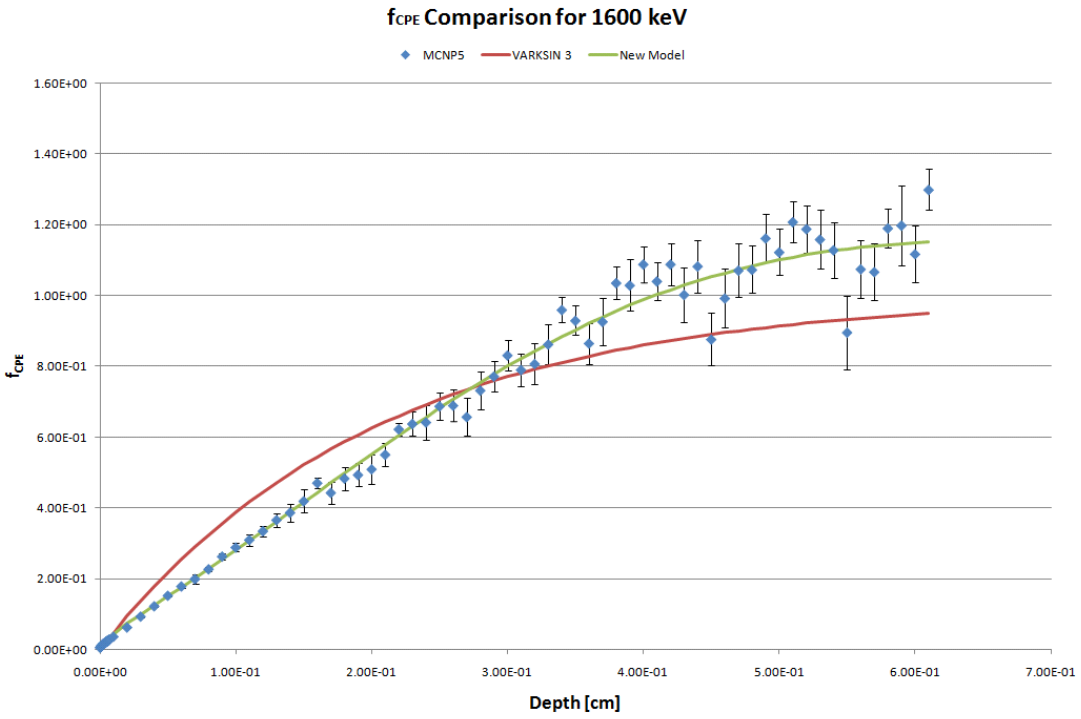

Figure 3-3: f_{CPE} curve for a 1.6 MeV photon source.

3.2 Fitting the Attenuation and Absorption Coefficients

The TableCurve 3D® package was also used to construct fits for the mass attenuation and mass-energy absorption coefficients in soft tissue, which were found to be piecewise functions:

$$\left(\frac{\mu}{\rho}\right)_{tissue}(E) = \begin{cases} \dfrac{1}{1.45\cdot 10^{-5} + 3810\cdot E^{2.5} + 134400\cdot E^{3}}; & \text{E} \le 0.02 \text{ MeV} \\ e^{-3.22-0.11\cdot \ln(E)^2 + 0.5566\sqrt{E} - 0.7713\cdot \ln(E) + 7.21\cdot 10^{-4}/E^2}; & \text{E} > 0.02 \text{ MeV} \end{cases} \tag{3.3}$$

$$\left(\frac{\mu}{\rho}\right)_{tissue}(E) = \frac{a + b\cdot \ln(E) + c\cdot \ln(E)^2 + d\cdot \ln(E)^3 + e\cdot \ln(E)^4}{1 + f\cdot \ln(E) + g\cdot \ln(E)^2 + h\cdot \ln(E)^3 + i\cdot \ln(E)^4 + j\cdot \ln(E)^5} \tag{3.4}$$

where E is the incident photon energy in MeV. The coefficients in Eqn 3.4 are different depending on whether the incident photon energy is greater or less than 0.03 MeV (see Tbl. 3-1).

Table 3-1: Coefficients for the empirical fit for the mass-energy absorption coefficient.

Coefficient	E≤0.03 MeV	E>0.03 MeV
a	2.97E-02	3.07E-02
b	7.45E-01	4.97E-01
c	1.52E-02	9.88E-03
d	2.24E-01	1.82E-01
e	9.56E-04	-2.39E-04
f	3.37E-02	7.30E-02
g	-1.51E-04	6.93E-04
h	2.55E-03	1.52E-02
i	6.02E-05	3.24E-04
j	7.74E-05	1.08E-03

Figures 3-4 and 3-5 demonstrate the degree to which Eqns. 3.3 and 3.4 adhere to the accepted values for each coefficient.

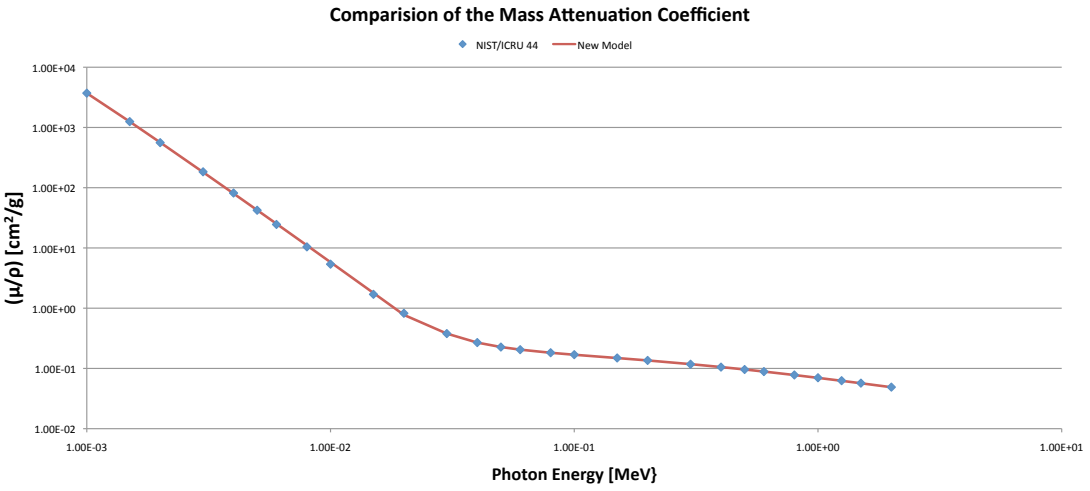

Figure 3-4: Comparison of the fit found for the mass attenuation coefficient and the NIST/ICRU data.

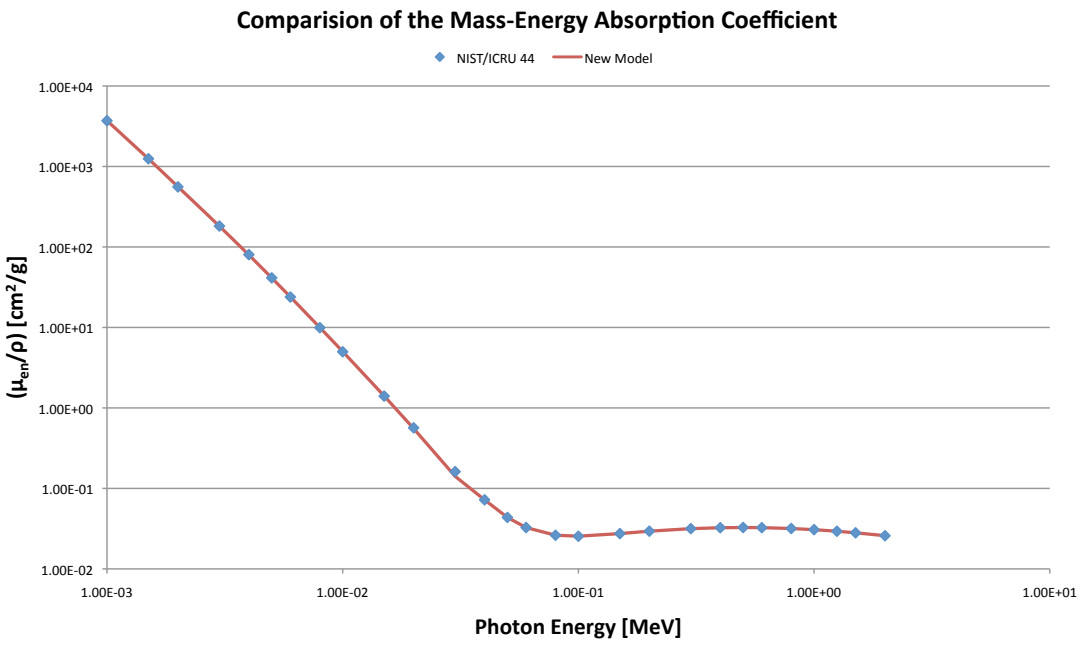

Figure 3-5: Comparison of the fit found for the mass-energy absorption coefficient and the NIST/ICRU data.

3.3 Calculating Dose

To calculate the average dose to a disc the new expression for $f_{CPE}(x)$ (Eqns. 3.1 and 3.2) is substituted into Eqn. 2.8 and the summation is executed. Figures 3-6, 3-7, and 3-8 show a comparison of the disc-averaged dose as calculated by the new model with that calculated by MCNP5 and VARSKIN 3.

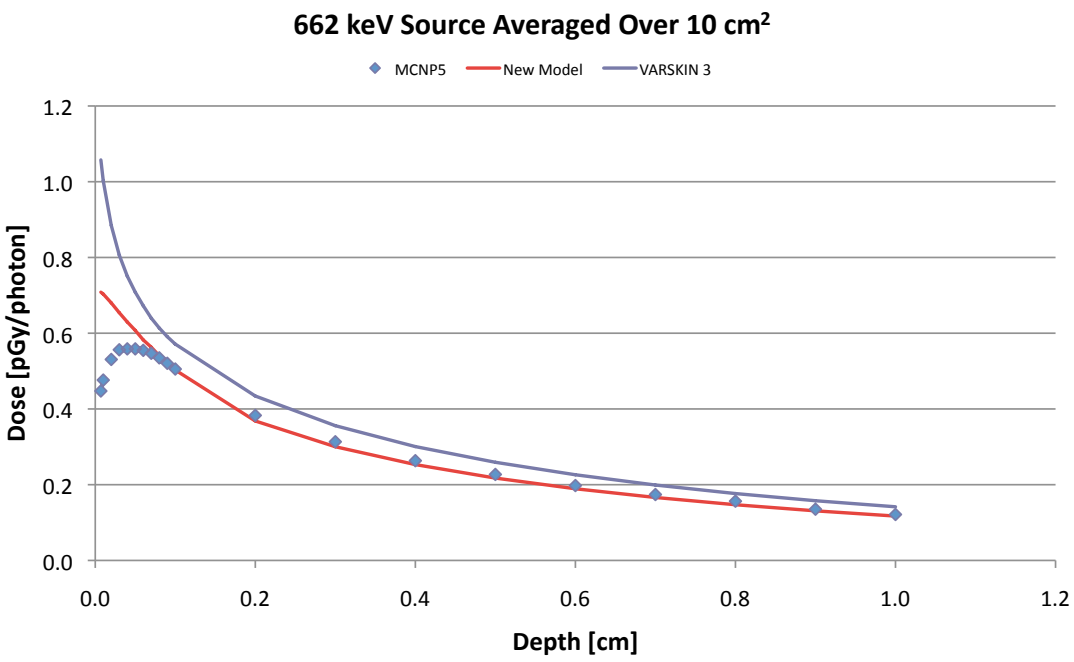

Figure 3-6: Comparison of calculated dose rates from MCNP5, VARSKIN 3, and the new model for a 0.662 MeV photon source averaged over 10 cm².

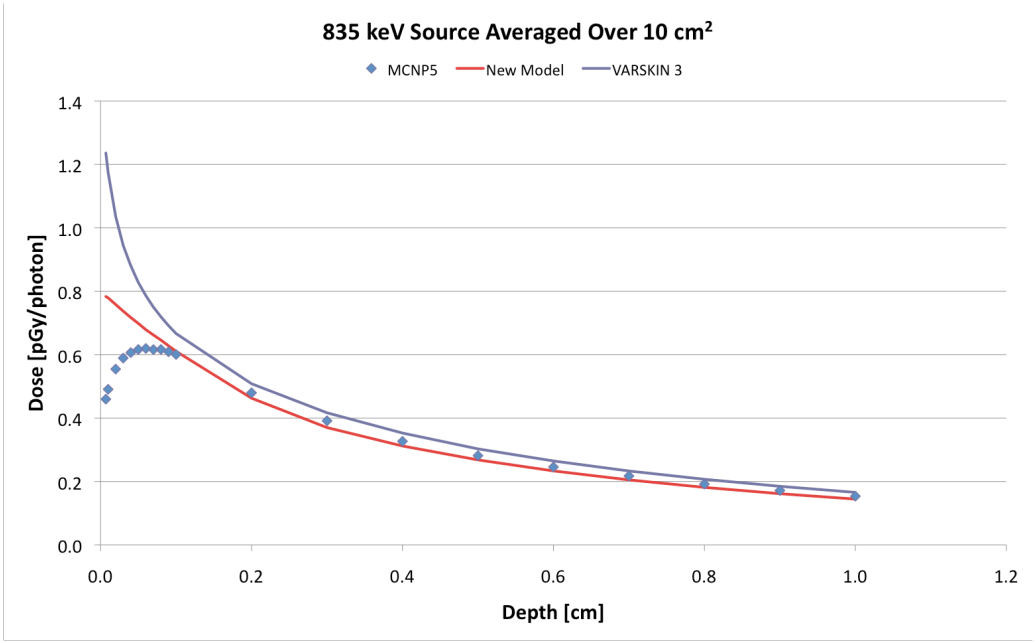

Figure 3-7: Comparison of calculated dose rates from MCNP5, VARSKIN 3, and the new model for a 0.835 MeV photon source averaged over 10 cm².

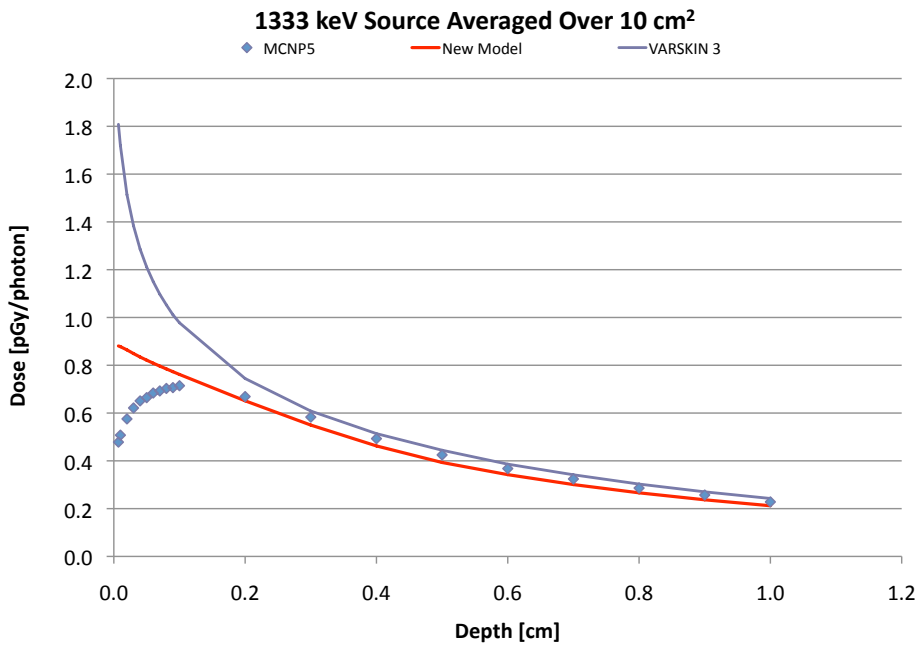

Figure 3-8; Comparison of calculated dose rates from MCNP5, VARSKIN 3, and the new model for a 1.333 MeV photon source averaged over 10 cm².

These figures show that the new model offers a significant improvement over VARSKIN 3, but significantly overestimates dose at shallow depths. Table 3-2 shows a summary of the performance of the new model for the energies of 0.662 and 1.333 MeV. The percent differences reported in Tbl. 3-2 are relative to the MCNP5 dose estimates and percent improvement is defined as the difference between the new model and VARSKIN 3 over the corresponding MCNP5 result.

Initially, the inability of the model to accurately calculate dose at shallow depths is puzzling, especially given the close agreement between $f_{CPE}(x)$ and MCNP5 in Section 3.1. If the dose to a point can be accurately predicted, it seems that the weighted average of all the points on the disc of interest should provide

an equally accurate measure of the average dose. The origin of this inaccuracy stems from an assumption that is implicit in the definition of $f_{CPE}(x)$ itself.

Table 3-2: Summary of the comparisons made in Figs. 3-6, 3-7, and 3-8.

Photon Energy	0.662 MeV		1.333 MeV	
Depth [cm]	% Difference	% Improvement	% Difference	% Improvement
0.007	58.34	78.06	84.12	193.88
0.010	47.68	62.73	72.98	165.82
0.020	28.14	38.54	50.19	112.87
0.030	17.60	27.35	36.64	86.01
0.040	12.72	21.67	28.24	69.37
0.050	8.72	18.07	23.62	58.67
0.060	4.97	16.25	18.28	49.90
0.070	2.93	14.03	15.00	43.42
0.080	1.04	13.68	11.64	38.12
0.090	0.55	12.96	9.43	33.69
0.100	-0.52	13.55	6.61	30.27

3.4 The Need for a Scatter Correction

When using MCNP5 to estimate f_{CPE} at various depths and energies, the geometry of the simulations were constructed so that only those particle tracks that coincided with the axis of the source were examined (see Figs. 2-1 and 2-2). Inherent in this setup is the assumption that there is no photon or electron loss at the air-tissue interface. However, as Fig. 3-9 shows, with increasing angle (θ) the kernel of interest is brought closer to the skin surface and is therefore more likely to experience a decreased dose due to particles leaving the volume. In other words, the CPE correction as previously constructed assumed that $D_I=D_{II}=D_{III}$, when in actuality $D_I>D_{II}>D_{III}$.

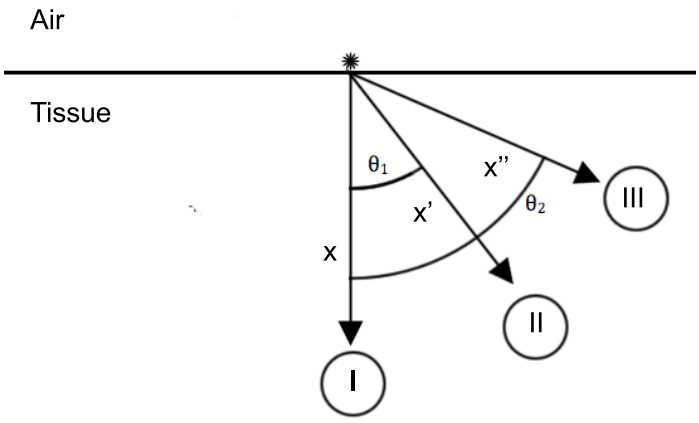

Figure 3-9: Schematic showing the orientation of θ and its effect on the target kernel.

To correct for this error a scatter correction factor (s_c) is defined such that,

$$s_c(x,\theta,E) = \frac{D(x,\theta,E)}{D(x,0,E)} \tag{3.5}$$

where x is the path length to the kernel, θ is as defined in Fig. 3-9, and E is the photon energy. The scatter correction is then incorporated into Eqn. 2.8,

$$\dot{D}_{disc}(h,E,A) = \frac{S}{2N}\sum_{i=1}^{N}\left[f_{CPE}(\sqrt{r_i^2+h^2})\cdot E\cdot\left(\frac{\mu_{en}}{\rho}\right)_{tissue} s_c(\sqrt{r_i^2+h^2},\tan^{-1}(r_i/h),E)\cdot(h^2+r_i^2)^{-1/2}e^{-(\mu/\rho)\sqrt{h^2+r_i^2}}\right], \tag{3.6}$$

where,

$$\theta = \tan^{-1}(r/h). \tag{3.7}$$

MCNP5 was used to estimate s_c at energies ranging from 0.2 to 2 MeV in 0.2 MeV increments; angles from 0˚ to 80˚ in 10˚ increments as well as an additional angle of 87˚; and the path lengths 0.23, 0.4, 0.7, 1.5, and 2 cm. The geometry of the simulations was identical to that used for the determination of f_{CPE} with the exception of the kernel shape and size, which was modeled as a sphere of radius 0.01 cm. Figure 3-10 shows a magnification of the geometry.

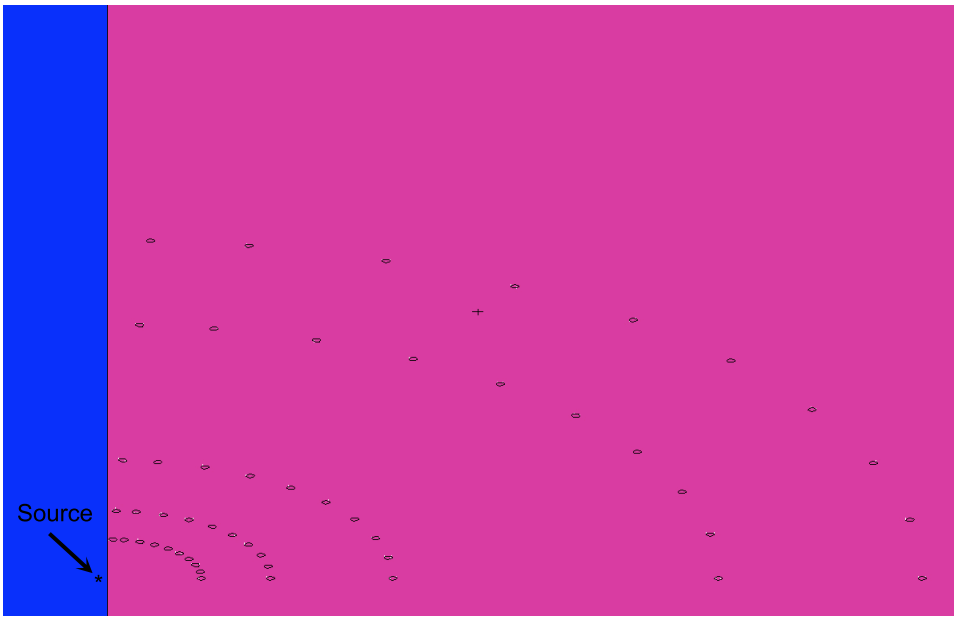

Figure 3-10.: Schematic of the geometry used in MCNP5 to determine the scatter correction factor (s_c). Blue is used to represent air and fuchsia is tissue. Note: the source point has been highlighted to orient the simulation.

Figures 3-11 and 3-12 show the estimated values of the scatter factor, which exhibits a strong dependence on the angle to the axis (θ). Of particular interest is the relative independence of s_c with respect to photon path length (x) and energy (E). The relative stability of s_c in relation to these variables allows for the formulation proposed in Eqn. 3.5 to be simplified so that s_c is a function of

angle only. Also of note is that s_c is very nearly one at all angles for energies less than 0.6 MeV, which allows for further simplification.

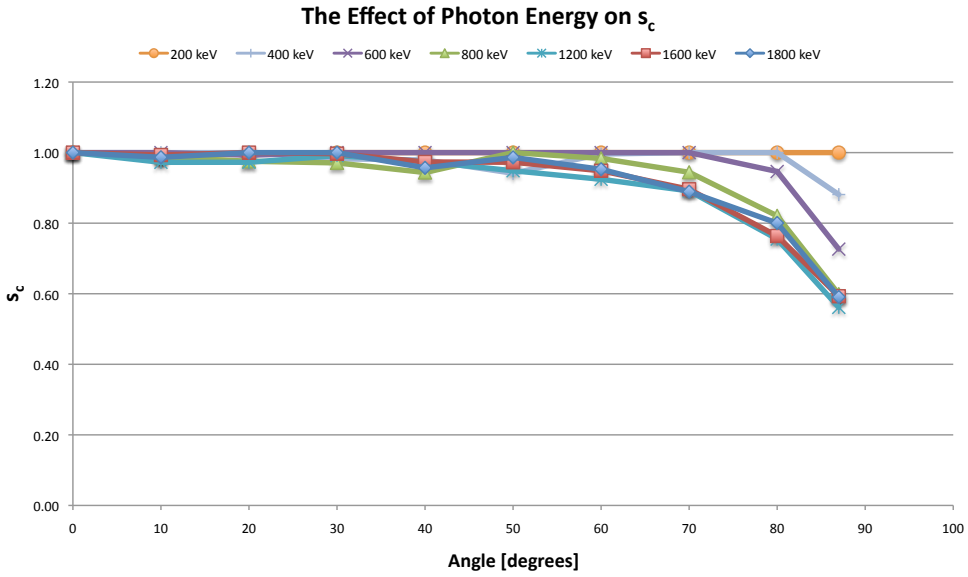

Figure 3-11: Summary of the MCNP5 results for the effect of energy on the scatter factor (s_c).

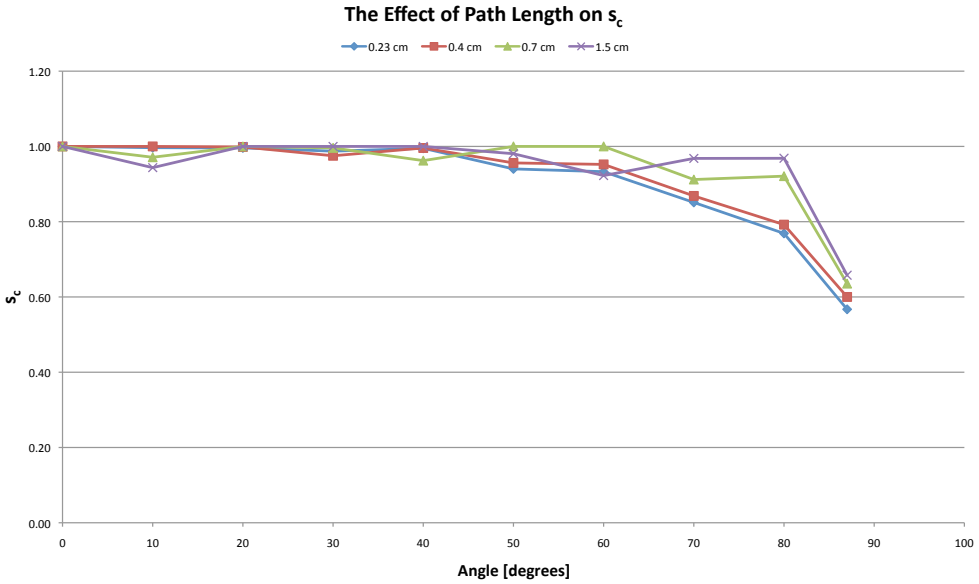

Figure 3-12: Summary of the MCNP5 results for the effect of path length on the scatter factor (s_c) for a 1.6 MeV source.

Using TableCurve®, the fit for the scatter factor was found to be,

$$s_c(\theta) = \frac{1}{-1.57 + 3.34 \cdot 10^{-4}\theta^{2.5} - 3.25 \cdot 10^{-5}\theta^{3}}. \quad (3.8)$$

Figure 3-13 provides a comparison of the scatter factor fit to the MCNP 5 results. Given the approximations that have been made in an effort to simply the model, the expression for $s_c(\theta)$ matches the experimental results well. However, as can also be seen in Fig. 3-13, the values of s_c calculated by Eqn. 3.8 experience their greatest deviation from the MCNP5 estimates at large angles (>70˚) and lower energies (<0.6 MeV).

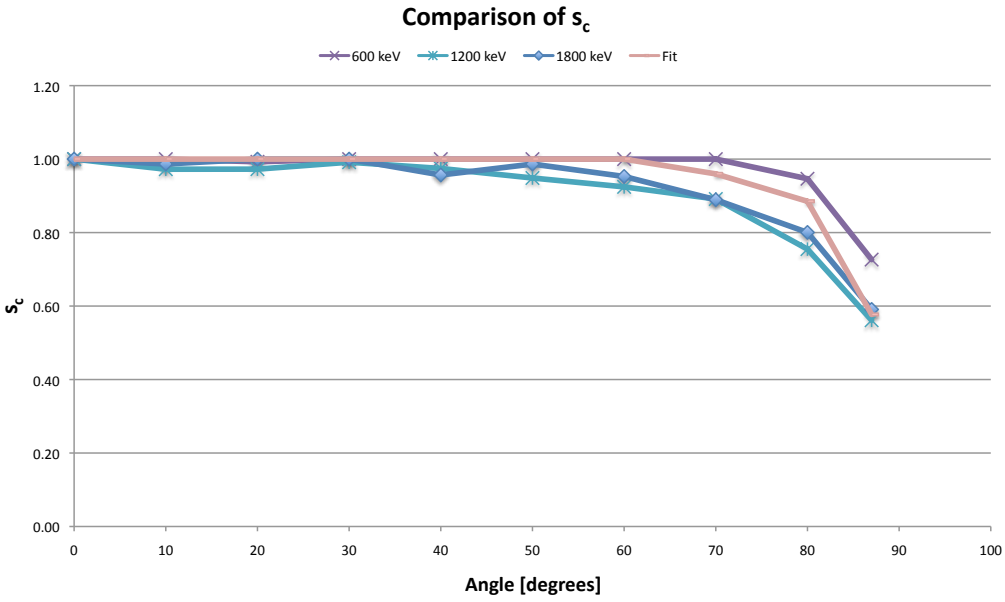

Figure 3-13: Comparison of $s_c(\theta)$ to the MCNP5 results.

Using Eqn. 3.6 to calculate the CPE- and scatter-corrected dose yields the results presented in Figs. 3-14, 3-15, and 3-16. Table 3-3 summarizes the same data for the energies of 0.662 and 1.333 MeV. Again, the percent differences reported in Tbl. 3-3 are relative to the MCNP5 dose estimates and percent improvement is defined as the difference between the new model and VARSKIN 3 over the corresponding MCNP5 result. These results show that there is excellent agreement between the new model and the dose estimated by MCNP5. The underestimation of dose at larger depths for the 0.662 MeV simulation is a result of the simplifications made when determining the expression for s_c. At lower energies Eqn. 3.8 underestimates the value of s_c (see Fig. 3-13), and this effect persists when the dose is integrated over the disc surface.

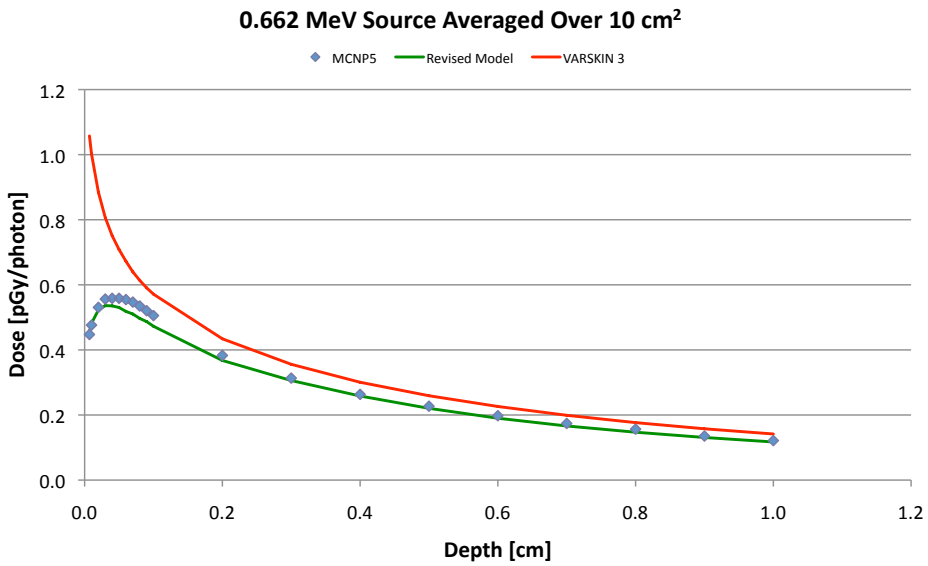

Figure 3-14: Comparison of dose rates calculated by MCNP5, VARSKIN 3, and this work for a 0.662 MeV photon source averaged over 10 cm².

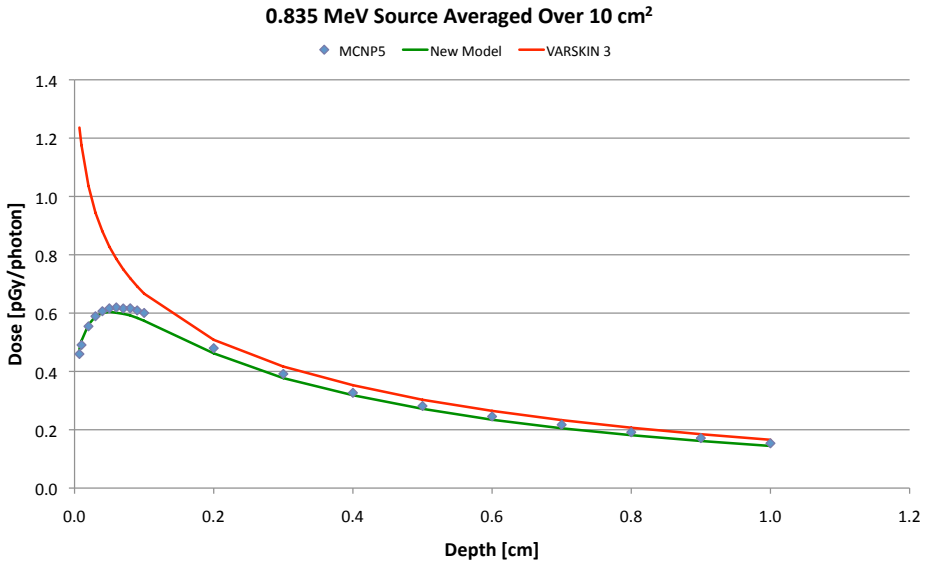

Figure 3-15: Comparison of dose rates calculated by MCNP5, VARSKIN 3, and this work for a 0.835 MeV photon source averaged over 10 cm².

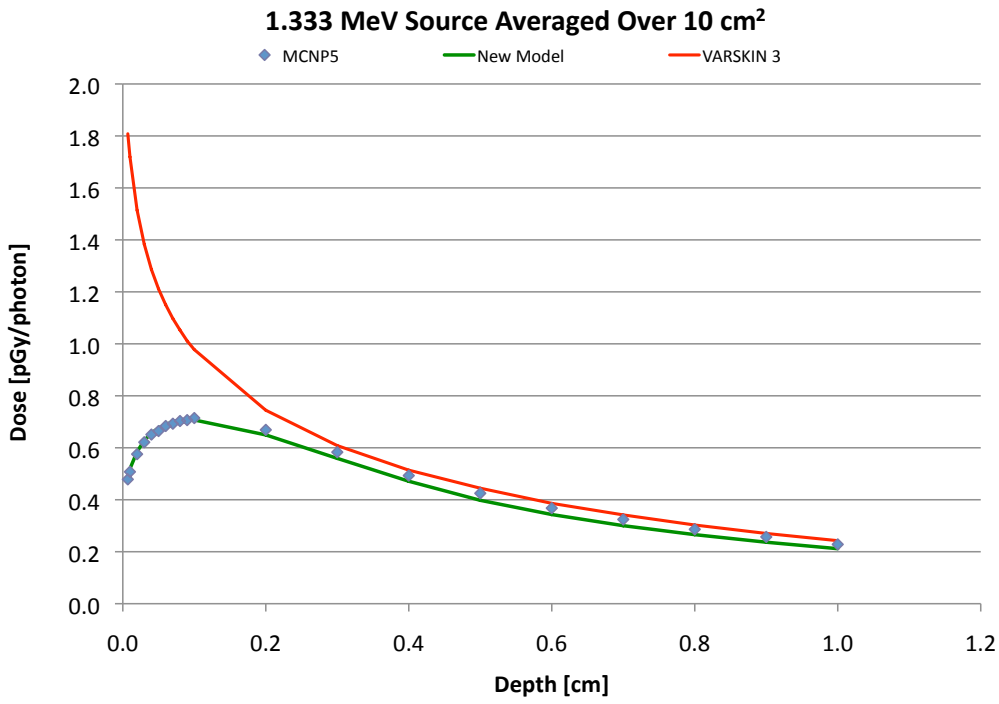

Figure 3-16: Comparison of dose rates calculated by MCNP5, VARSKIN 3, and this work for a 1.333 MeV photon source averaged over 10 cm².

Table 3-3: Summary of the comparisons made in Figs. 3-14, 3-15, and 3-16.

Photon Energy	0.662 MeV		1.333 MeV	
Depth [cm]	% Difference	% Improvement	% Difference	% Improvement
0.007	2.02	134.37	2.53	275.46
0.010	1.14	109.27	2.29	236.50
0.020	-1.48	68.16	1.67	161.39
0.030	-3.63	48.58	1.06	121.58
0.040	-4.17	38.56	0.84	96.77
0.050	-5.08	31.88	1.79	80.49
0.060	-6.55	27.77	0.89	67.29
0.070	-6.73	23.69	0.93	57.49
0.080	-7.13	21.85	0.23	49.54
0.090	-6.42	19.93	0.10	43.03
0.100	-6.49	19.51	-1.03	37.90

3.5 Cover Materials and Air Gaps

Much of the work presented in this thesis has served as the basis for a recent update to the VARSKIN code (distributed as version 4). Throughout this work the assumed scenario has been one in which a hot particle is deposited directly on the skin surface. However, another commonly occurring scenario is one in which the contamination occurs on a layer of clothing covering the skin (Charles, 1991; Gimadiva & Keirim-Markus, 1991; Taylor, Hussein, & Yuen, 1997). In these situations, the thickness of the clothing and the presence of an air gap can significantly alter the skin dose distribution and needs to be incorporated into any dosimetric model (Reece, 1991; Taylor, Hussein, & Yuen, 1997). Figure 3-17 illustrates the typical geometry involved in clothing contamination.

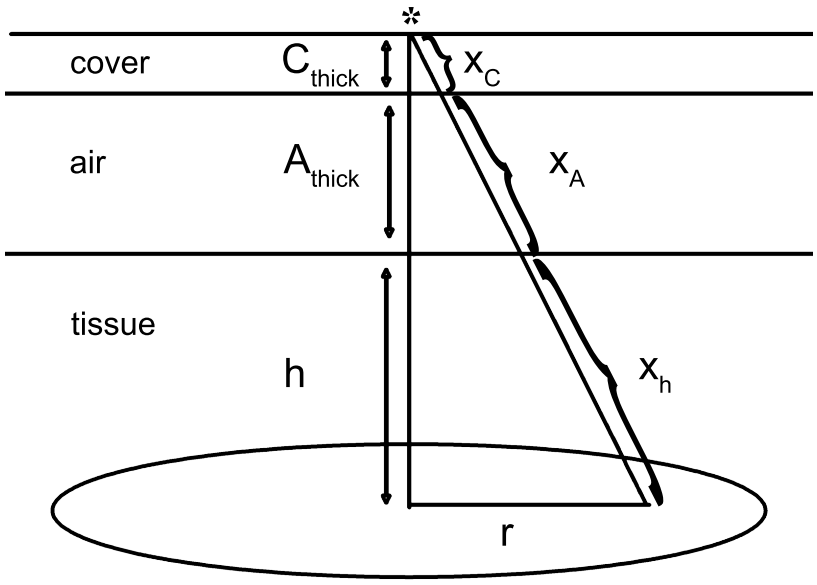

Figure 3-17: Typical geometry for a hot particle contamination of the clothing.

VARSKIN 3's cover model assumes any material between the source particle and the skin to be tissue equivalent, which is typically not a valid approximation given the densities and chemical composition of commonly encountered materials (Taylor, Hussein, & Yuen, 1997). VARSKIN 4 improves upon this assumption by appropriately accounting for attenuation through cotton and latex. One issue with the cover model that needs to be addressed is the path length used when calculating $f_{CPE}(x)$.

Figure 3-17 shows that the total photon path length consists of three parts: the portion that passes though the cover material (x_C), the portion that passes though air (x_A), and the portion that passes through tissue (x_h). The law of similar triangles allows the length of each of these tracks to de expressed in

terms of the cover material thickness (C_{thick}), the air gap thickness (A_{thick}), and the depth of the averaging area (h),

$$x_C = C_{thick}\left(\frac{\sqrt{(C_{thick} + A_{thick} + h)^2 + r^2}}{C_{thick} + A_{thick} + h}\right) \quad (3.9a)$$

$$x_A = A_{thick}\left(\frac{\sqrt{(C_{thick} + A_{thick} + h)^2 + r^2}}{C_{thick} + A_{thick} + h}\right) \quad (3.9b)$$

$$x_h = h\left(\frac{\sqrt{(C_{thick} + A_{thick} + h)^2 + r^2}}{C_{thick} + A_{thick} + h}\right). \quad (3.9c)$$

VARSKIN 4 currently assumes that the total path length (x) contributes to the CPE correction factor to be applied. However, it is unlikely that CPE persists across an interface of two media since the rate of charged particle creation is different in each respective medium. As an alternative, only the path length through tissue could be used to calculate CPE. Figures 3-18 and 3-19 demonstrate that neither of these assumptions are correct. These figures show the results of simulations where 0.37 mm of cotton was used as the cover material, there was no air gap, and the disc averaging area was 10 cm^2. The "VARSKIN 4 (current)" curve shows the results of using the total path length in determining f_{CPE}, while the "VARSKIN 4 (modified)" curve uses only the path length through tissue. The larger dose predicted by the current implementation of VARSKIN 4 can be attributed to an overestimation of the degree of CPE that has been achieved as a result of using a too long of a path length. Conversely, the

lower dose predicted by the modified version of VARSKIN 4 is a consequence of a shorter-than-necessary path length.

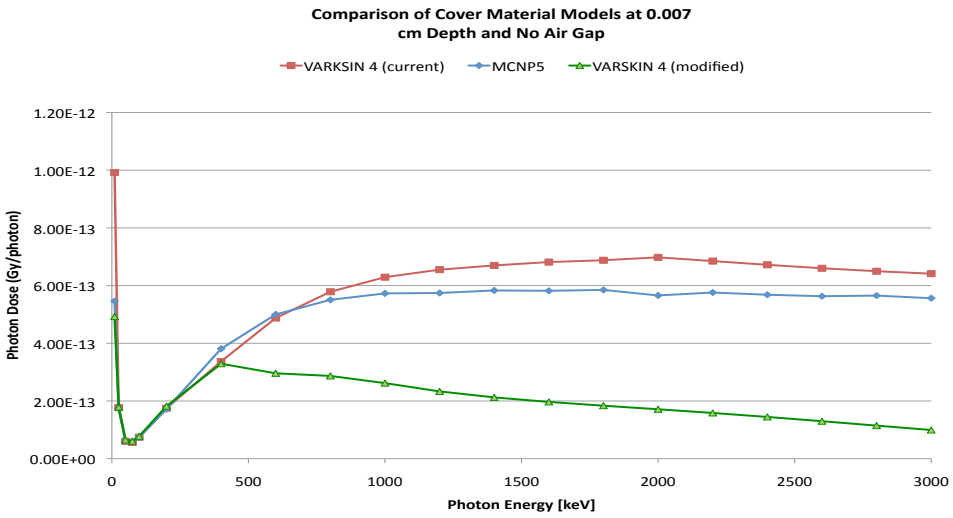

Figure 3-18: Comparison of different cover model assumptions to MCNP5. All results are for a 10 cm² averaging area, a depth of 0.007 cm in tissue, 0.37 mm of cotton as the cover material, and no air gap.

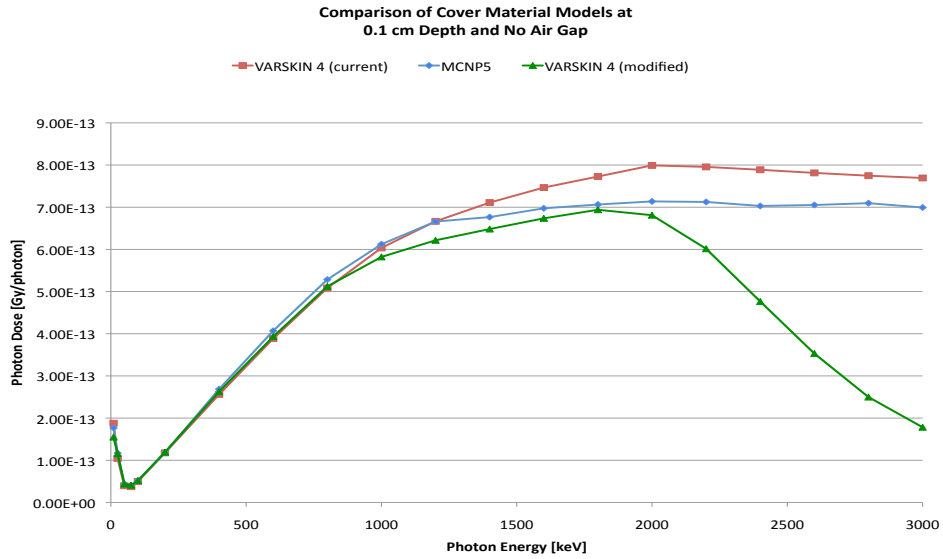

Figure 3-19: Comparison of different cover model assumptions to MCNP5. All results are for a 10 cm² averaging area, a depth of 0.1 cm in tissue, 0.37 mm of cotton as the cover material, and no air gap.

The results summarized in Figs. 3-18 and 3-19 suggest that while CPE is not maintained across the cover/tissue interface, the charged particles created in the cover material do contribute towards CPE in tissue. This also explains why the deviation of both methods from the MCNP results is more pronounced at higher photon energies, since the CPE correction factor is more heavily applied.

The issue becomes even more complicated when an air gap is added, as in Figs. 3-20 and 3-21. These figures show that the addition of an air gap results in a decreased contribution to CPE from the charged particles created in the cover material. This is evidenced by the larger degree of overestimation by the current implementation of VARSKIN 4. This is expected, as charged particles created in the cover material must now traverse the air gap, experiencing a greater degree of attenuation before being able to contribute to CPE. In fact, the earlier assumption that only the path length in tissue will affect CPE seems to hold true at the 0.007 cm depth shown in Fig. 3-20, as the modified version of VARSKIN 4 accurately predicts dose at higher photon energies. Surprisingly, Fig. 3-21 illustrates that this assumption appears invalid as the depth is increased to 0.1 cm.

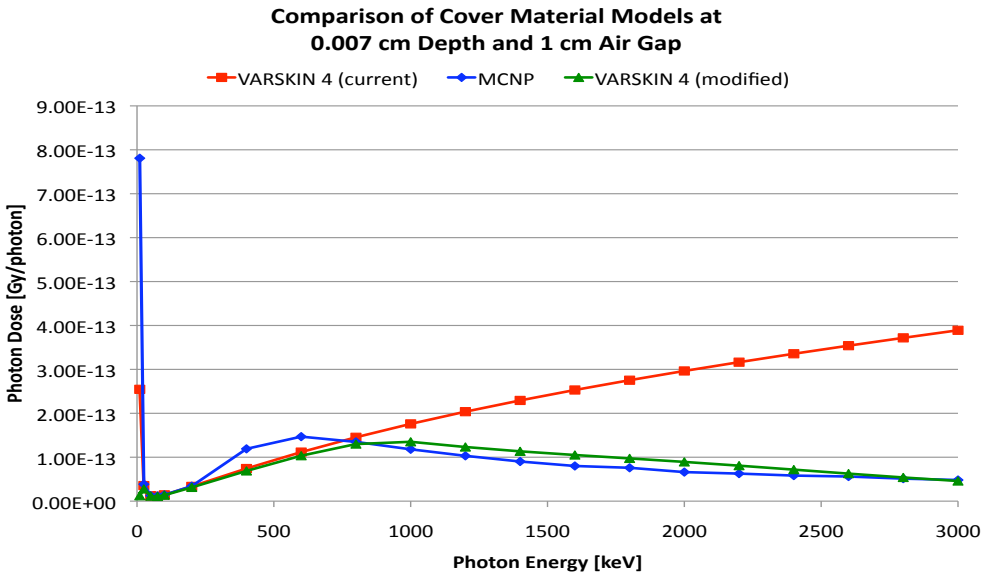

Figure 3-20: Comparison of different cover model assumptions to MCNP5. All results are for a 10 cm² averaging area, a depth of 0.007 cm in tissue, 0.37 mm of cotton as the cover material, and a 1 cm air gap.

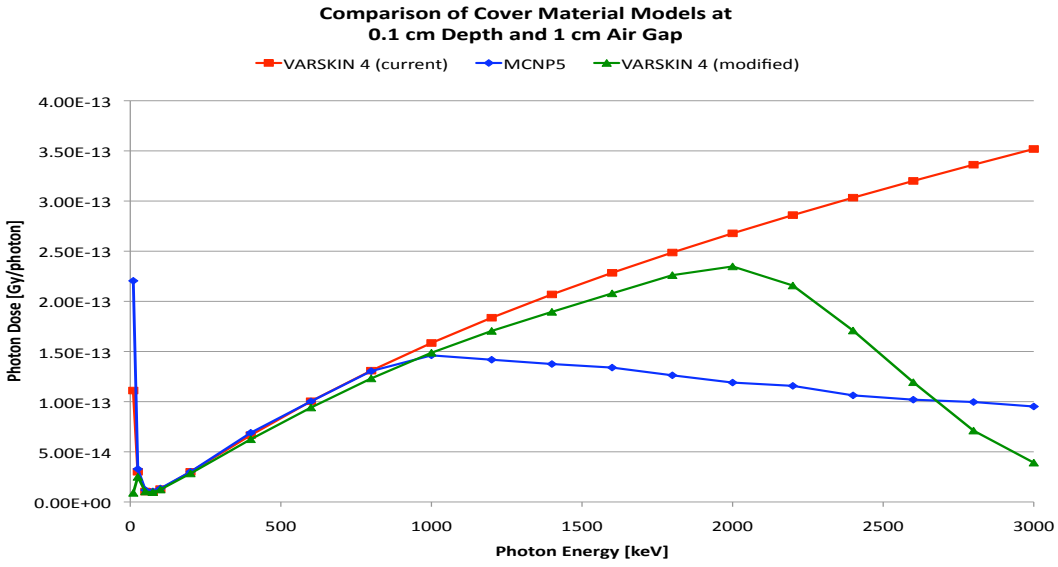

Figure 3-21: Comparison of different cover model assumptions to MCNP5. All results are for a 10 cm² averaging area, a depth of 0.1 cm in tissue, 0.37 mm of cotton as the cover material, and a 1 cm air gap.

While these preliminary results give insight into the effect of cover materials on hot particle dose distributions, the inability to fully explain the observed CPE behavior highlights the need for further investigation. Perhaps another correction factor that accounts for the contribution of the cover material to CPE needs to be added to Eqn. 3.6.

4 CONCLUSION

4.1 Conclusion

Overall, the new photon dosimetry model can be considered a success as it delivers improved accuracy over a wide range of energies and depths. When calculating the integrated dose to a disc of 10 cm^2 at a depth of 0.007 cm for photon energies of 0.662, 0.835, and 1.333 MeV the new model is within 2.0%, 3.7%, and 2.5% of the dose calculated by MCNP5, respectively. This corresponds to improvements of 134.4%, 165.2%, and 275.5% over VARSKIN 3's results for the same scenario. Figure 4-1 presents an expanded comparison of the new model to MCNP5.

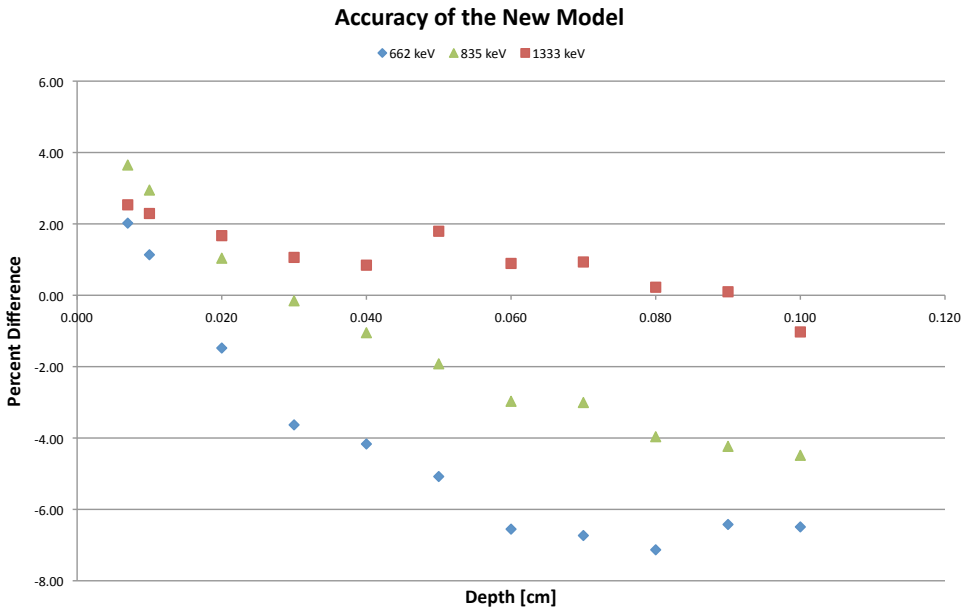

Figure 4-1: Summary of the accuracy of the new model for the photon energies of 0.662, 0.835, and 1.333 MeV.

While the 'hot particle problem' may be conceptually easy to understand, a 'solution' has proved elusive. Despite the many advances that have been made in addressing the risk presented by hot particles in the past 50 years there remains much room for improvement. The work presented in the previous chapters represents a large step forward, as it is the most successful attempt to date at a point kernel approach for accounting for CPE. Such an approach allows for the model to meet the challenges presented by an evolving regulatory environment and an increasing variety of contamination scenarios.

5 BIBLIOGRAPHY

Attix, Frank H. *Introduction to Radiological Physics and Radiation Dosimetry*. New York: Wiley, 1986.

Bakali, M., et al. "Hot Particle Dosimetry at Nuclear Power Plants." *Radiation Measurements* 34 (2001): 487-90.

Baum, J. W. , and D. G. Kaurin. "Reassessment of Data Used in Setting Exposure Limits for Hot Particles." *Radiation Protection Management* 39 1/3 (1991): 49-54.

Cazalas, Edward J. "Design, Construction, and Analysis of a Skin Contamination Dosimeter." Oregon State University, 2009.

Cember, Herman. "Introduction to Health Physics". New York, 1996. 3rd: xviii, 733 p. McGraw-Hill, Health Professions Division.

Charles, M. W. "The Hot Particle Problem." *Radiation Protection Dosimetry* 39 1/3 (1991): 39-47.

Charles, M. W., and J. D. Harrison. "Hot Particle Dosimetry and Radiobiology--Past and Present." *J Radiol Prot* 27 3A (2007): A97-109.

Charles, M. W., A. J. Mill, and P. J. Darley. "Carcinogenic Risk of Hot-Particle Exposures." *J Radiol Prot* 23 1 (2003): 5-28.

Durham, J. S. "Considerations for Applying Varskin Mod 2 to Skin Dose Calculations Averaged over 10 Cm2." *Health Phys* 86 2 Suppl (2004): S11-4.

Durham, J. S. "Hot Particle Dose Calculations Using the Computer Code Varskin Mod 2." *Radiation Protection Dosimetry* 39 1/3 (1991): 75-78.

Hamby, David M. "An Improved Method for Charged Particle Equilibrium Corrections for Photon Dosimetry of the Skin." Corvallis: Oregon State University, 2008.

Hopewell, J. W. "Biological Effects of Irradiation on Skin and Recommended Dose Limits." *Radiation Protection Dosimetry* 39 1/3 (1991): 11-24.

International Commission on Radiological Protection. *Recommendations of the International Commission on Radiological Protection*. Annals of the ICRP Publication 26, 1977.

International Commission on Radiological Protection. *Biological effects of inhaled radionuclides*. Annals of the ICRP Publication 31, 1980

International Commission of Radiological Protection. *Recommendations of the International Commission on Radiological Protection*. Annals of the ICRP Publication 60, 1991.

Johns, Harold Elford, and John Robert Cunningham. "The Physics of Radiology". Springfield, Ill., U.S.A., 1983. 4th: xix, 796 p. Charles C. Thomas.

Khan, Faiz M. *The Physics of Radiation Therapy*. 3rd ed. Philadelphia: Lippincott Williams & Wilkins, 2003.

Lantz, Michael W., and Michael W. Lambert. "Charged Particle Equilibrium Corrections for the Gamma Component of Hot Particle Skin Doses." *Radiation Protection Management* 7 5 (1990): 38-48.

Makinson, Kevin A. "Tissue Weighting Factors for Radiation Protection: Derivation and Parametric Analysis ". Oregon State University, 2009.

Myrick, J. A. "Electronic Equilibrium as a Function of Depth in Tissue from Cobalt-60 Point Source Exposures." Texas A&M, 1994.

National Council on Radiation Protection and Measurements. *Extension of the Skin Dose Limit for Hot Particles to Other External Sources of Skin Irradiation*. Washington D.C.: NCRP, 2001.

National Council on Radiation Protection and Measurments. *Report No. 106: Limit for Exposure To "Hot Particles" On the Skin*. Washington: NCRP, 1989.

Osanov, D. "The Problem of Adequacy in Skin Dosimetry for the Case of a Nuclear Reactor Emergency and for Occupational Exposure." *Radiation Protection Dosimetry* 39 1/3 (1991): 85-90.

Reece, W. D. "Experiences and Problems of Skin Irradiation Due to Hot Particle Exposures at Workplaces in the United States." *Radiation Protection Dosimetry* 39 1/3 (1991): 165-71.

Sherbini, S., et al. "Verification of the Varskin Beta Skin Dose Calculation Computer Code." *Health Phys* 94 6 (2008): 527-38.

Taylor, D. C., E. M. Hussein, and P. S. Yuen. "Skin Dose from Radionuclide Contamination on Clothing." *Health Phys* 72 6 (1997): 835-41.

U.S. Nuclear Regulatory Commission. *Standards for Protection Against Radiation*. Washington, DC. U.S. Governemtn Printing Office; Title 10, Chapter I, Code of Federal Regulations, Part 20 (10 CFR 20)

U.S. Nuclear Regulatory Commission. *Varskin 3: A Computer Code for Assessing Skin Dose from Skin Dose Contamination*. Ed. Durham, J. S. NUREG/CR-6918 ed. Washington, DC, 2006.

Walters, M. D., et al. "Effective Dose Equivalent Due to Gamma-Ray Emissions from Hot Particles." *Health Phys* 76 5 (1999): 564-6.

Xu, X. G. "The Effective Dose Equivalent and Effective Dose for Hot Particles on the Skin." *Health Phys* 89 1 (2005): 53-70.

Xu, X. G., H. Su, and S. Bushart. "The Epri Ede Calculator--a Software Package for Assessing Effective Dose Equivalent from Hot Particles on the Skin." *Health Phys* 91 4 (2006): 373-8.

Yip, S. "Mit Open Courseware". Boston, 2006. May 2010. http://ocw.mit.edu/courses/nuclear-engineering/22-101-applied-nuclear-physics-fall-2006/

APPENDICES

6 APPENDIX A - MCNP5 f_{CPE} DATA AND COMPARISONS

The MCNP5 results used to construct the f_{CPE} curves described in the previous chapters are presented. For comparison, the values of f_{CPE} as calculated by VARSKIN 3 and the new model are also provided. Not all of the data that were produced for this project is presented, as doing so would be unnecessarily cumbersome. Instead only the data collected for the photon energies from 0.5 to 2 MeV is given, and only to the equilibrium depth.

Table 6-1: The MCNP5 data that was used to construct the 500 keV f_{CPE} curve and the corresponding values as calculated by VARSKIN 3 and the new model.

Depth [cm]	KERMA [J/kg Y]	σ_{KERMA} [%]	Dose [J/kg•Y]	σ_{dose} [%]	f_{CPE}	σ_{fCPE} [%]	VARSKIN 3 f_{CPE}	New Model f_{CPE}
2.00E-04	1.03E+02	5.77E-05	3.97E+00	5.83E-03	3.87E-02	5.83E-03	9.73E-03	2.63E-02
4.00E-04	8.42E+01	5.77E-05	4.43E+00	5.52E-03	5.26E-02	5.52E-03	1.94E-02	3.88E-02
6.00E-04	7.37E+01	2.89E-05	4.68E+00	5.23E-03	6.35E-02	5.23E-03	2.89E-02	4.90E-02
8.00E-04	6.62E+01	2.89E-05	4.82E+00	5.09E-03	7.28E-02	5.09E-03	3.84E-02	5.80E-02
1.00E-03	6.04E+01	2.89E-05	4.88E+00	5.06E-03	8.07E-02	5.06E-03	4.77E-02	6.62E-02
1.20E-03	5.57E+01	2.89E-05	4.91E+00	4.98E-03	8.81E-02	4.98E-03	5.70E-02	7.39E-02
1.40E-03	5.18E+01	2.89E-05	4.94E+00	4.91E-03	9.54E-02	4.91E-03	6.61E-02	8.11E-02
1.60E-03	4.84E+01	2.89E-05	4.88E+00	4.94E-03	1.01E-01	4.94E-03	7.52E-02	8.81E-02
1.80E-03	4.54E+01	2.89E-05	4.90E+00	4.80E-03	1.08E-01	4.80E-03	8.42E-02	9.47E-02
2.00E-03	4.27E+01	2.89E-05	4.85E+00	4.87E-03	1.14E-01	4.87E-03	9.31E-02	1.01E-01
2.20E-03	4.03E+01	2.89E-05	4.82E+00	4.91E-03	1.20E-01	4.91E-03	1.02E-01	1.07E-01
2.40E-03	3.82E+01	2.89E-05	4.76E+00	4.87E-03	1.25E-01	4.87E-03	1.11E-01	1.13E-01
2.60E-03	3.62E+01	2.89E-05	4.68E+00	4.88E-03	1.29E-01	4.88E-03	1.19E-01	1.19E-01
2.80E-03	3.44E+01	2.89E-05	4.64E+00	4.88E-03	1.35E-01	4.88E-03	1.28E-01	1.25E-01
3.00E-03	3.27E+01	2.89E-05	4.59E+00	4.84E-03	1.40E-01	4.84E-03	1.36E-01	1.31E-01
3.20E-03	3.12E+01	2.89E-05	4.50E+00	4.90E-03	1.44E-01	4.90E-03	1.45E-01	1.36E-01
3.40E-03	2.97E+01	2.89E-05	4.45E+00	4.92E-03	1.50E-01	4.92E-03	1.53E-01	1.42E-01

Depth [cm]	KERMA [J/kg Y]	σ_{KERMA} [%]	Dose [J/kg•Y]	σ_{dose} [%]	f_{CPE}	σ_{fCPE} [%]	VARSKIN 3 f_{CPE}	New Model f_{CPE}
3.60E-03	2.84E+01	2.89E-05	4.39E+00	4.84E-03	1.55E-01	4.84E-03	1.61E-01	1.47E-01
3.80E-03	2.71E+01	2.89E-05	4.31E+00	5.01E-03	1.59E-01	5.01E-03	1.70E-01	1.53E-01
4.00E-03	2.60E+01	2.89E-05	4.26E+00	4.94E-03	1.64E-01	4.94E-03	1.78E-01	1.58E-01
4.20E-03	2.49E+01	2.89E-05	4.20E+00	5.00E-03	1.69E-01	5.00E-03	1.86E-01	1.63E-01
4.40E-03	2.39E+01	2.89E-05	4.11E+00	5.04E-03	1.72E-01	5.04E-03	1.94E-01	1.68E-01
4.60E-03	2.29E+01	2.89E-05	4.05E+00	4.99E-03	1.77E-01	4.99E-03	2.01E-01	1.73E-01
4.80E-03	2.20E+01	2.89E-05	3.98E+00	5.12E-03	1.81E-01	5.12E-03	2.09E-01	1.78E-01
5.00E-03	2.11E+01	2.89E-05	3.88E+00	5.03E-03	1.84E-01	5.03E-03	2.17E-01	1.83E-01
5.20E-03	2.03E+01	2.89E-05	3.83E+00	5.07E-03	1.89E-01	5.07E-03	2.24E-01	1.88E-01
5.40E-03	1.95E+01	2.89E-05	3.74E+00	5.29E-03	1.91E-01	5.29E-03	2.32E-01	1.93E-01
5.60E-03	1.88E+01	2.89E-05	3.71E+00	5.22E-03	1.98E-01	5.22E-03	2.39E-01	1.98E-01
5.80E-03	1.81E+01	2.89E-05	3.64E+00	5.34E-03	2.01E-01	5.34E-03	2.47E-01	2.02E-01
6.00E-03	1.74E+01	2.89E-05	3.60E+00	5.26E-03	2.06E-01	5.26E-03	2.54E-01	2.07E-01
6.20E-03	1.68E+01	5.77E-05	3.52E+00	5.33E-03	2.09E-01	5.33E-03	2.61E-01	2.12E-01
6.40E-03	1.62E+01	5.77E-05	3.47E+00	5.44E-03	2.14E-01	5.44E-03	2.69E-01	2.16E-01
6.60E-03	1.56E+01	5.77E-05	3.40E+00	5.46E-03	2.18E-01	5.46E-03	2.76E-01	2.21E-01
6.80E-03	1.51E+01	5.77E-05	3.38E+00	5.41E-03	2.24E-01	5.41E-03	2.83E-01	2.26E-01
7.00E-03	1.46E+01	5.77E-05	3.29E+00	5.54E-03	2.26E-01	5.54E-03	2.90E-01	2.30E-01
1.00E-02	9.10E+00	5.77E-05	2.63E+00	6.10E-03	2.89E-01	6.10E-03	3.87E-01	2.95E-01
2.00E-02	2.93E+00	1.15E-04	1.39E+00	8.02E-03	4.74E-01	8.03E-03	6.24E-01	4.87E-01
3.00E-02	1.38E+00	1.73E-04	8.72E-01	1.10E-02	6.31E-01	1.10E-02	7.69E-01	6.53E-01
4.00E-02	7.96E-01	2.31E-04	6.46E-01	1.23E-02	8.12E-01	1.23E-02	8.58E-01	8.01E-01
5.00E-02	5.15E-01	2.89E-04	4.73E-01	1.48E-02	9.19E-01	1.48E-02	9.13E-01	9.31E-01
6.00E-02	3.60E-01	3.46E-04	3.75E-01	1.60E-02	1.04E+00	1.60E-02	9.47E-01	1.04E+00
7.00E-02	2.65E-01	4.04E-04	2.78E-01	1.88E-02	1.05E+00	1.88E-02	9.67E-01	1.14E+00
8.00E-02	2.03E-01	4.62E-04	2.23E-01	2.27E-02	1.10E+00	2.27E-02	9.80E-01	1.23E+00
9.00E-02	1.61E-01	5.20E-04	1.78E-01	2.28E-02	1.11E+00	2.28E-02	9.88E-01	1.30E+00
1.00E-01	1.30E-01	5.77E-04	1.35E-01	3.08E-02	1.03E+00	3.08E-02	9.92E-01	1.00E+00
1.10E-01	1.08E-01	6.35E-04	1.17E-01	3.01E-02	1.08E+00	3.01E-02	9.95E-01	1.00E+00

Table 6-2: The MCNP5 data that was used to construct the 600 keV f_{CPE} curve and the corresponding values as calculated by VARSKIN 3 and the new model.

Depth [cm]	KERMA [J/kg ϒ]	σ_{KERMA} [%]	Dose [J/kg•ϒ]	σ_{dose} [%]	f_{CPE}	σ_{fCPE} [%]	VARSKIN 3 f_{CPE}	New Model f_{CPE}
2.00E-04	1.23E+02	5.77E-05	3.35E+00	6.49E-03	2.73E-02	6.50E-03	7.90E-03	1.78E-02
4.00E-04	1.01E+02	5.77E-05	3.69E+00	6.17E-03	3.66E-02	6.18E-03	1.57E-02	2.62E-02
6.00E-04	8.80E+01	2.89E-05	3.89E+00	5.79E-03	4.42E-02	5.79E-03	2.35E-02	3.30E-02
8.00E-04	7.91E+01	2.89E-05	4.01E+00	5.75E-03	5.07E-02	5.75E-03	3.12E-02	3.91E-02
1.00E-03	7.22E+01	2.89E-05	4.03E+00	5.70E-03	5.58E-02	5.70E-03	3.89E-02	4.46E-02
1.20E-03	6.66E+01	2.89E-05	4.04E+00	5.64E-03	6.07E-02	5.64E-03	4.65E-02	4.98E-02
1.40E-03	6.19E+01	2.89E-05	4.07E+00	5.67E-03	6.58E-02	5.67E-03	5.40E-02	5.47E-02
1.60E-03	5.78E+01	2.89E-05	4.05E+00	5.53E-03	7.00E-02	5.53E-03	6.15E-02	5.94E-02
1.80E-03	5.42E+01	2.89E-05	4.07E+00	5.45E-03	7.50E-02	5.45E-03	6.89E-02	6.39E-02
2.00E-03	5.10E+01	2.89E-05	3.99E+00	5.47E-03	7.81E-02	5.47E-03	7.63E-02	6.82E-02
2.20E-03	4.82E+01	2.89E-05	3.99E+00	5.43E-03	8.28E-02	5.43E-03	8.36E-02	7.24E-02
2.40E-03	4.56E+01	2.89E-05	3.91E+00	5.68E-03	8.58E-02	5.69E-03	9.08E-02	7.65E-02
2.60E-03	4.32E+01	2.89E-05	3.89E+00	5.61E-03	9.00E-02	5.61E-03	9.80E-02	8.06E-02
2.80E-03	4.11E+01	2.89E-05	3.88E+00	5.46E-03	9.44E-02	5.46E-03	1.05E-01	8.45E-02
3.00E-03	3.91E+01	2.89E-05	3.82E+00	5.44E-03	9.77E-02	5.44E-03	1.12E-01	8.84E-02
3.20E-03	3.72E+01	2.89E-05	3.77E+00	5.37E-03	1.01E-01	5.37E-03	1.19E-01	9.21E-02
3.40E-03	3.55E+01	2.89E-05	3.74E+00	5.37E-03	1.05E-01	5.37E-03	1.26E-01	9.59E-02
3.60E-03	3.39E+01	2.89E-05	3.65E+00	5.43E-03	1.07E-01	5.43E-03	1.33E-01	9.96E-02
3.80E-03	3.24E+01	2.89E-05	3.59E+00	5.59E-03	1.11E-01	5.59E-03	1.40E-01	1.03E-01
4.00E-03	3.11E+01	2.89E-05	3.56E+00	5.39E-03	1.14E-01	5.39E-03	1.47E-01	1.07E-01
4.20E-03	2.97E+01	2.89E-05	3.47E+00	5.62E-03	1.17E-01	5.62E-03	1.53E-01	1.10E-01
4.40E-03	2.85E+01	2.89E-05	3.44E+00	5.54E-03	1.21E-01	5.54E-03	1.60E-01	1.14E-01
4.60E-03	2.74E+01	2.89E-05	3.38E+00	5.65E-03	1.24E-01	5.65E-03	1.67E-01	1.17E-01
4.80E-03	2.63E+01	2.89E-05	3.33E+00	5.73E-03	1.27E-01	5.73E-03	1.73E-01	1.21E-01
5.00E-03	2.52E+01	2.89E-05	3.28E+00	5.56E-03	1.30E-01	5.56E-03	1.80E-01	1.24E-01
5.20E-03	2.43E+01	2.89E-05	3.22E+00	5.70E-03	1.33E-01	5.70E-03	1.86E-01	1.27E-01
5.40E-03	2.33E+01	2.89E-05	3.15E+00	5.84E-03	1.35E-01	5.84E-03	1.93E-01	1.31E-01
5.60E-03	2.25E+01	2.89E-05	3.11E+00	5.97E-03	1.38E-01	5.97E-03	1.99E-01	1.34E-01
5.80E-03	2.16E+01	2.89E-05	3.09E+00	5.84E-03	1.43E-01	5.84E-03	2.06E-01	1.37E-01
6.00E-03	2.08E+01	2.89E-05	3.03E+00	5.85E-03	1.45E-01	5.85E-03	2.12E-01	1.41E-01
6.20E-03	2.01E+01	5.77E-05	2.99E+00	6.02E-03	1.49E-01	6.02E-03	2.18E-01	1.44E-01

Depth [cm]	KERMA [J/kg ϒ]	σ_{KERMA} [%]	Dose [J/kg•ϒ]	σ_{dose} [%]	f_{CPE}	σ_{fCPE} [%]	VARSKIN 3 f_{CPE}	New Model f_{CPE}
6.40E-03	1.94E+01	5.77E-05	2.92E+00	5.96E-03	1.51E-01	5.96E-03	2.24E-01	1.47E-01
6.60E-03	1.87E+01	5.77E-05	2.89E+00	5.93E-03	1.54E-01	5.93E-03	2.30E-01	1.50E-01
6.80E-03	1.81E+01	5.77E-05	2.86E+00	5.92E-03	1.58E-01	5.92E-03	2.36E-01	1.53E-01
7.00E-03	1.74E+01	5.77E-05	2.81E+00	6.08E-03	1.61E-01	6.08E-03	2.42E-01	1.57E-01
1.00E-02	1.09E+01	5.77E-05	2.24E+00	6.65E-03	2.06E-01	6.65E-03	3.27E-01	2.02E-01
2.00E-02	3.50E+00	1.15E-04	1.21E+00	9.08E-03	3.46E-01	9.08E-03	5.48E-01	3.43E-01
3.00E-02	1.65E+00	1.73E-04	7.89E-01	1.09E-02	4.77E-01	1.09E-02	6.96E-01	4.73E-01
4.00E-02	9.51E-01	2.31E-04	5.68E-01	1.36E-02	5.97E-01	1.36E-02	7.95E-01	5.97E-01
5.00E-02	6.15E-01	2.89E-04	4.44E-01	1.33E-02	7.22E-01	1.33E-02	8.62E-01	7.15E-01
6.00E-02	4.30E-01	3.46E-04	3.42E-01	1.84E-02	7.96E-01	1.84E-02	9.07E-01	8.26E-01
7.00E-02	3.17E-01	4.04E-04	2.81E-01	1.93E-02	8.88E-01	1.93E-02	9.38E-01	9.29E-01
8.00E-02	2.43E-01	4.62E-04	2.41E-01	2.34E-02	9.91E-01	2.34E-02	9.58E-01	1.02E+00
9.00E-02	1.92E-01	5.20E-04	2.00E-01	2.09E-02	1.04E+00	2.09E-02	9.72E-01	1.11E+00
1.00E-01	1.56E-01	5.77E-04	1.69E-01	2.55E-02	1.09E+00	2.55E-02	9.81E-01	1.19E+00
1.10E-01	1.29E-01	6.35E-04	1.36E-01	3.61E-02	1.06E+00	3.61E-02	9.87E-01	1.26E+00
1.20E-01	1.08E-01	6.93E-04	1.15E-01	2.92E-02	1.06E+00	2.92E-02	9.91E-01	1.32E+00

Table 6-3: The MCNP5 data that was used to construct the 700 keV f_{CPE} curve and the corresponding values as calculated by VARSKIN 3 and the new model.

Depth [cm]	KERMA [J/kg ϒ]	σ_{KERMA} [%]	Dose [J/kg•ϒ]	σ_{dose} [%]	f_{CPE}	σ_{fCPE} [%]	VARSKIN 3 f_{CPE}	New Model f_{CPE}
2.00E-04	1.42E+02	5.77E-05	2.88E+00	7.63E-03	2.03E-02	7.63E-03	6.42E-03	1.31E-02
4.00E-04	1.16E+02	5.77E-05	3.19E+00	6.84E-03	2.74E-02	6.84E-03	1.28E-02	1.93E-02
6.00E-04	1.02E+02	2.89E-05	3.30E+00	6.76E-03	3.25E-02	6.76E-03	1.91E-02	2.44E-02
8.00E-04	9.15E+01	2.89E-05	3.42E+00	6.44E-03	3.74E-02	6.44E-03	2.54E-02	2.88E-02
1.00E-03	8.35E+01	2.89E-05	3.44E+00	6.28E-03	4.12E-02	6.28E-03	3.17E-02	3.29E-02
1.20E-03	7.70E+01	2.89E-05	3.41E+00	6.45E-03	4.43E-02	6.45E-03	3.79E-02	3.67E-02
1.40E-03	7.15E+01	2.89E-05	3.46E+00	6.30E-03	4.83E-02	6.30E-03	4.41E-02	4.03E-02
1.60E-03	6.68E+01	2.89E-05	3.46E+00	6.12E-03	5.18E-02	6.12E-03	5.02E-02	4.38E-02
1.80E-03	6.27E+01	2.89E-05	3.45E+00	6.01E-03	5.51E-02	6.01E-03	5.63E-02	4.71E-02
2.00E-03	5.90E+01	2.89E-05	3.46E+00	5.82E-03	5.86E-02	5.82E-03	6.23E-02	5.03E-02
2.20E-03	5.57E+01	2.89E-05	3.43E+00	6.17E-03	6.15E-02	6.17E-03	6.84E-02	5.34E-02

Depth [cm]	KERMA [J/kg Y]	σ_{KERMA} [%]	Dose [J/kg•Y]	σ_{dose} [%]	f_{CPE}	σ_{fCPE} [%]	VARSKIN 3 f_{CPE}	New Model f_{CPE}
2.40E-03	5.27E+01	2.89E-05	3.36E+00	6.30E-03	6.38E-02	6.30E-03	7.43E-02	5.64E-02
2.60E-03	5.00E+01	2.89E-05	3.33E+00	5.98E-03	6.66E-02	5.98E-03	8.03E-02	5.93E-02
2.80E-03	4.75E+01	2.89E-05	3.27E+00	6.35E-03	6.90E-02	6.35E-03	8.62E-02	6.22E-02
3.00E-03	4.52E+01	2.89E-05	3.26E+00	6.15E-03	7.23E-02	6.15E-03	9.20E-02	6.51E-02
3.20E-03	4.30E+01	2.89E-05	3.20E+00	6.02E-03	7.43E-02	6.02E-03	9.79E-02	6.79E-02
3.40E-03	4.11E+01	2.89E-05	3.15E+00	6.05E-03	7.67E-02	6.05E-03	1.04E-01	7.06E-02
3.60E-03	3.92E+01	2.89E-05	3.15E+00	6.00E-03	8.03E-02	6.00E-03	1.09E-01	7.33E-02
3.80E-03	3.75E+01	2.89E-05	3.07E+00	6.10E-03	8.18E-02	6.10E-03	1.15E-01	7.60E-02
4.00E-03	3.59E+01	2.89E-05	3.06E+00	6.18E-03	8.53E-02	6.19E-03	1.21E-01	7.86E-02
4.20E-03	3.44E+01	2.89E-05	2.99E+00	6.10E-03	8.71E-02	6.10E-03	1.26E-01	8.12E-02
4.40E-03	3.30E+01	2.89E-05	2.95E+00	6.22E-03	8.94E-02	6.22E-03	1.32E-01	8.38E-02
4.60E-03	3.16E+01	2.89E-05	2.90E+00	6.60E-03	9.16E-02	6.60E-03	1.38E-01	8.64E-02
4.80E-03	3.04E+01	2.89E-05	2.87E+00	6.35E-03	9.45E-02	6.35E-03	1.43E-01	8.89E-02
5.00E-03	2.92E+01	2.89E-05	2.84E+00	6.30E-03	9.75E-02	6.30E-03	1.49E-01	9.14E-02
5.20E-03	2.80E+01	2.89E-05	2.74E+00	6.53E-03	9.78E-02	6.53E-03	1.54E-01	9.39E-02
5.40E-03	2.70E+01	2.89E-05	2.72E+00	6.61E-03	1.01E-01	6.61E-03	1.60E-01	9.64E-02
5.60E-03	2.60E+01	2.89E-05	2.68E+00	6.48E-03	1.03E-01	6.48E-03	1.65E-01	9.88E-02
5.80E-03	2.50E+01	2.89E-05	2.64E+00	6.41E-03	1.06E-01	6.41E-03	1.70E-01	1.01E-01
6.00E-03	2.41E+01	2.89E-05	2.61E+00	6.35E-03	1.08E-01	6.35E-03	1.76E-01	1.04E-01
6.20E-03	2.32E+01	5.77E-05	2.54E+00	6.80E-03	1.09E-01	6.80E-03	1.81E-01	1.06E-01
6.40E-03	2.24E+01	5.77E-05	2.50E+00	6.95E-03	1.12E-01	6.95E-03	1.86E-01	1.08E-01
6.60E-03	2.16E+01	5.77E-05	2.44E+00	7.08E-03	1.13E-01	7.08E-03	1.91E-01	1.11E-01
6.80E-03	2.09E+01	5.77E-05	2.42E+00	6.95E-03	1.16E-01	6.95E-03	1.97E-01	1.13E-01
7.00E-03	2.02E+01	5.77E-05	2.41E+00	6.35E-03	1.20E-01	6.35E-03	2.02E-01	1.15E-01
1.00E-02	1.26E+01	5.77E-05	1.95E+00	7.40E-03	1.55E-01	7.40E-03	2.75E-01	1.49E-01
2.00E-02	4.05E+00	1.15E-04	1.07E+00	1.00E-02	2.65E-01	1.00E-02	4.75E-01	2.55E-01
3.00E-02	1.91E+00	1.73E-04	7.09E-01	1.10E-02	3.71E-01	1.10E-02	6.19E-01	3.56E-01
4.00E-02	1.10E+00	2.31E-04	4.95E-01	1.71E-02	4.51E-01	1.71E-02	7.24E-01	4.56E-01
5.00E-02	7.11E-01	2.89E-04	3.99E-01	1.54E-02	5.61E-01	1.54E-02	8.00E-01	5.53E-01
6.00E-02	4.97E-01	3.46E-04	3.23E-01	1.97E-02	6.50E-01	1.97E-02	8.55E-01	6.48E-01
7.00E-02	3.66E-01	4.04E-04	2.68E-01	1.64E-02	7.33E-01	1.64E-02	8.95E-01	7.41E-01
8.00E-02	2.81E-01	4.62E-04	2.32E-01	2.30E-02	8.25E-01	2.30E-02	9.24E-01	8.29E-01
9.00E-02	2.22E-01	5.20E-04	1.97E-01	2.57E-02	8.85E-01	2.57E-02	9.45E-01	9.13E-01

Depth [cm]	KERMA [J/kg ϒ]	σ_{KERMA} [%]	Dose [J/kg•ϒ]	σ_{dose} [%]	f_{CPE}	σ_{fCPE} [%]	VARSKIN 3 f_{CPE}	New Model f_{CPE}
1.00E-01	1.80E-01	5.77E-04	1.79E-01	2.05E-02	9.93E-01	2.05E-02	9.60E-01	9.92E-01
1.10E-01	1.49E-01	6.35E-04	1.52E-01	2.78E-02	1.02E+00	2.78E-02	9.71E-01	1.07E+00
1.20E-01	1.25E-01	6.93E-04	1.27E-01	3.19E-02	1.02E+00	3.19E-02	9.79E-01	1.13E+00
1.30E-01	1.07E-01	7.51E-04	1.17E-01	3.06E-02	1.10E+00	3.06E-02	9.85E-01	1.20E+00
1.40E-01	9.20E-02	8.08E-04	1.00E-01	4.35E-02	1.09E+00	4.36E-02	9.89E-01	1.25E+00

Table 6-4: The MCNP5 data that was used to construct the 800 keV f_{CPE} curve and the corresponding values as calculated by VARSKIN 3 and the new model.

Depth [cm]	KERMA [J/kg ϒ]	σ_{KERMA} [%]	Dose [J/kg•ϒ]	σ_{dose} [%]	f_{CPE}	σ_{fCPE} [%]	VARSKIN 3 f_{CPE}	New Model f_{CPE}
2.00E-04	1.60E+02	5.77E-05	2.53E+00	8.33E-03	1.58E-02	8.33E-03	5.21E-03	1.03E-02
4.00E-04	1.31E+02	5.77E-05	2.79E+00	7.35E-03	2.12E-02	7.35E-03	1.04E-02	1.52E-02
6.00E-04	1.15E+02	2.89E-05	2.89E+00	7.40E-03	2.52E-02	7.40E-03	1.55E-02	1.92E-02
8.00E-04	1.03E+02	2.89E-05	2.98E+00	6.77E-03	2.89E-02	6.77E-03	2.07E-02	2.27E-02
1.00E-03	9.42E+01	2.89E-05	3.00E+00	7.15E-03	3.18E-02	7.15E-03	2.58E-02	2.59E-02
1.20E-03	8.68E+01	2.89E-05	2.99E+00	7.08E-03	3.45E-02	7.08E-03	3.09E-02	2.88E-02
1.40E-03	8.07E+01	2.89E-05	3.03E+00	6.68E-03	3.76E-02	6.68E-03	3.59E-02	3.17E-02
1.60E-03	7.53E+01	2.89E-05	2.99E+00	6.84E-03	3.97E-02	6.84E-03	4.09E-02	3.43E-02
1.80E-03	7.07E+01	2.89E-05	3.02E+00	6.88E-03	4.28E-02	6.88E-03	4.59E-02	3.69E-02
2.00E-03	6.65E+01	2.89E-05	3.01E+00	6.73E-03	4.53E-02	6.73E-03	5.09E-02	3.94E-02
2.20E-03	6.28E+01	2.89E-05	2.96E+00	7.02E-03	4.71E-02	7.02E-03	5.58E-02	4.18E-02
2.40E-03	5.94E+01	2.89E-05	2.96E+00	6.77E-03	4.98E-02	6.77E-03	6.08E-02	4.42E-02
2.60E-03	5.64E+01	2.89E-05	2.92E+00	6.82E-03	5.18E-02	6.82E-03	6.56E-02	4.65E-02
2.80E-03	5.36E+01	2.89E-05	2.91E+00	6.74E-03	5.44E-02	6.74E-03	7.05E-02	4.88E-02
3.00E-03	5.10E+01	2.89E-05	2.88E+00	6.48E-03	5.65E-02	6.48E-03	7.54E-02	5.10E-02
3.20E-03	4.86E+01	2.89E-05	2.82E+00	6.79E-03	5.81E-02	6.79E-03	8.02E-02	5.32E-02
3.40E-03	4.63E+01	2.89E-05	2.77E+00	7.16E-03	5.97E-02	7.16E-03	8.50E-02	5.53E-02
3.60E-03	4.42E+01	2.89E-05	2.76E+00	6.66E-03	6.23E-02	6.66E-03	8.97E-02	5.74E-02
3.80E-03	4.23E+01	2.89E-05	2.74E+00	6.39E-03	6.49E-02	6.39E-03	9.45E-02	5.95E-02
4.00E-03	4.05E+01	2.89E-05	2.69E+00	6.77E-03	6.64E-02	6.77E-03	9.92E-02	6.16E-02
4.20E-03	3.88E+01	2.89E-05	2.64E+00	6.75E-03	6.82E-02	6.75E-03	1.04E-01	6.36E-02
4.40E-03	3.72E+01	2.89E-05	2.59E+00	6.78E-03	6.96E-02	6.78E-03	1.09E-01	6.56E-02

Depth [cm]	KERMA [J/kg Y]	σ_{KERMA} [%]	Dose [J/kg•Y]	σ_{dose} [%]	f_{CPE}	σ_{fCPE} [%]	VARSKIN 3 f_{CPE}	New Model f_{CPE}
4.60E-03	3.57E+01	2.89E-05	2.53E+00	7.29E-03	7.10E-02	7.29E-03	1.13E-01	6.76E-02
4.80E-03	3.42E+01	2.89E-05	2.49E+00	7.36E-03	7.28E-02	7.36E-03	1.18E-01	6.96E-02
5.00E-03	3.29E+01	2.89E-05	2.47E+00	6.92E-03	7.52E-02	6.92E-03	1.22E-01	7.15E-02
5.20E-03	3.16E+01	2.89E-05	2.43E+00	7.24E-03	7.67E-02	7.24E-03	1.27E-01	7.35E-02
5.40E-03	3.04E+01	2.89E-05	2.39E+00	7.60E-03	7.85E-02	7.60E-03	1.32E-01	7.54E-02
5.60E-03	2.93E+01	2.89E-05	2.36E+00	6.99E-03	8.07E-02	6.99E-03	1.36E-01	7.73E-02
5.80E-03	2.82E+01	2.89E-05	2.31E+00	7.63E-03	8.20E-02	7.63E-03	1.41E-01	7.92E-02
6.00E-03	2.72E+01	2.89E-05	2.27E+00	7.19E-03	8.34E-02	7.19E-03	1.45E-01	8.11E-02
6.20E-03	2.62E+01	5.77E-05	2.25E+00	7.14E-03	8.60E-02	7.14E-03	1.49E-01	8.29E-02
6.40E-03	2.53E+01	5.77E-05	2.19E+00	7.84E-03	8.65E-02	7.84E-03	1.54E-01	8.48E-02
6.60E-03	2.44E+01	5.77E-05	2.14E+00	8.33E-03	8.78E-02	8.33E-03	1.58E-01	8.66E-02
6.80E-03	2.35E+01	5.77E-05	2.13E+00	7.90E-03	9.04E-02	7.90E-03	1.63E-01	8.85E-02
7.00E-03	2.27E+01	5.77E-05	2.11E+00	7.62E-03	9.27E-02	7.62E-03	1.67E-01	9.03E-02
1.00E-02	1.42E+01	5.77E-05	1.72E+00	8.28E-03	1.21E-01	8.28E-03	2.30E-01	1.17E-01
2.00E-02	4.56E+00	1.15E-04	9.43E-01	1.17E-02	2.07E-01	1.17E-02	4.07E-01	2.00E-01
3.00E-02	2.15E+00	1.73E-04	6.08E-01	1.51E-02	2.82E-01	1.51E-02	5.43E-01	2.80E-01
4.00E-02	1.24E+00	2.31E-04	4.52E-01	1.62E-02	3.65E-01	1.62E-02	6.48E-01	3.59E-01
5.00E-02	8.02E-01	2.89E-04	3.60E-01	1.95E-02	4.49E-01	1.95E-02	7.29E-01	4.39E-01
6.00E-02	5.60E-01	3.46E-04	2.96E-01	1.82E-02	5.29E-01	1.82E-02	7.91E-01	5.18E-01
7.00E-02	4.13E-01	4.04E-04	2.49E-01	2.15E-02	6.03E-01	2.15E-02	8.39E-01	5.96E-01
8.00E-02	3.17E-01	4.62E-04	2.04E-01	2.92E-02	6.45E-01	2.92E-02	8.76E-01	6.73E-01
9.00E-02	2.51E-01	5.20E-04	1.79E-01	2.93E-02	7.16E-01	2.93E-02	9.05E-01	7.47E-01
1.00E-01	2.03E-01	5.77E-04	1.62E-01	2.67E-02	7.99E-01	2.67E-02	9.27E-01	8.19E-01
1.10E-01	1.68E-01	6.35E-04	1.49E-01	2.84E-02	8.85E-01	2.84E-02	9.43E-01	8.88E-01
1.20E-01	1.41E-01	6.93E-04	1.28E-01	3.10E-02	9.07E-01	3.10E-02	9.56E-01	9.54E-01
1.30E-01	1.20E-01	7.51E-04	1.18E-01	3.38E-02	9.80E-01	3.38E-02	9.66E-01	1.02E+00
1.40E-01	1.04E-01	8.08E-04	1.06E-01	2.77E-02	1.02E+00	2.78E-02	9.74E-01	1.07E+00
1.50E-01	9.05E-02	8.66E-04	8.95E-02	3.50E-02	9.89E-01	3.50E-02	9.80E-01	1.13E+00
1.60E-01	7.95E-02	9.24E-04	8.65E-02	3.26E-02	1.09E+00	3.26E-02	9.85E-01	1.17E+00
1.70E-01	7.05E-02	9.81E-04	8.23E-02	4.21E-02	1.17E+00	4.21E-02	9.88E-01	1.22E+00
1.80E-01	6.28E-02	1.04E-03	6.93E-02	4.65E-02	1.10E+00	4.65E-02	9.91E-01	1.26E+00
1.90E-01	5.64E-02	1.10E-03	6.30E-02	4.43E-02	1.12E+00	4.43E-02	9.93E-01	1.30E+00
2.00E-01	5.09E-02	1.15E-03	5.44E-02	4.69E-02	1.07E+00	4.70E-02	9.95E-01	1.33E+00

Table 6-5: The MCNP5 data that was used to construct the 900 keV f_{CPE} curve and the corresponding values as calculated by VARSKIN 3 and the new model.

Depth [cm]	KERMA [J/kg ϒ]	σ_{KERMA} [%]	Dose [J/kg•ϒ]	σ_{dose} [%]	f_{CPE}	σ_{fCPE} [%]	VARSKIN 3 f_{CPE}	New Model f_{CPE}
2.00E-04	1.77E+02	5.77E-05	2.21E+00	9.85E-03	1.25E-02	9.85E-03	4.23E-03	8.54E-03
4.00E-04	1.45E+02	5.77E-05	2.47E+00	8.00E-03	1.70E-02	8.00E-03	8.44E-03	1.26E-02
6.00E-04	1.27E+02	2.89E-05	2.58E+00	7.98E-03	2.03E-02	7.98E-03	1.26E-02	1.58E-02
8.00E-04	1.14E+02	2.89E-05	2.67E+00	7.41E-03	2.34E-02	7.41E-03	1.68E-02	1.87E-02
1.00E-03	1.04E+02	2.89E-05	2.67E+00	7.89E-03	2.56E-02	7.89E-03	2.10E-02	2.13E-02
1.20E-03	9.61E+01	2.89E-05	2.68E+00	8.12E-03	2.79E-02	8.12E-03	2.51E-02	2.37E-02
1.40E-03	8.93E+01	2.89E-05	2.67E+00	7.99E-03	2.99E-02	7.99E-03	2.92E-02	2.60E-02
1.60E-03	8.34E+01	2.89E-05	2.70E+00	7.02E-03	3.23E-02	7.02E-03	3.33E-02	2.82E-02
1.80E-03	7.82E+01	2.89E-05	2.68E+00	7.76E-03	3.43E-02	7.76E-03	3.74E-02	3.03E-02
2.00E-03	7.36E+01	2.89E-05	2.69E+00	7.40E-03	3.65E-02	7.40E-03	4.15E-02	3.24E-02
2.20E-03	6.95E+01	2.89E-05	2.65E+00	7.37E-03	3.81E-02	7.37E-03	4.55E-02	3.44E-02
2.40E-03	6.58E+01	2.89E-05	2.62E+00	7.79E-03	3.98E-02	7.79E-03	4.96E-02	3.63E-02
2.60E-03	6.24E+01	2.89E-05	2.57E+00	7.67E-03	4.11E-02	7.67E-03	5.36E-02	3.82E-02
2.80E-03	5.93E+01	2.89E-05	2.55E+00	7.82E-03	4.30E-02	7.82E-03	5.76E-02	4.00E-02
3.00E-03	5.64E+01	2.89E-05	2.54E+00	7.18E-03	4.51E-02	7.18E-03	6.16E-02	4.18E-02
3.20E-03	5.37E+01	2.89E-05	2.50E+00	7.29E-03	4.66E-02	7.29E-03	6.56E-02	4.36E-02
3.40E-03	5.13E+01	2.89E-05	2.46E+00	7.81E-03	4.80E-02	7.81E-03	6.95E-02	4.54E-02
3.60E-03	4.90E+01	2.89E-05	2.44E+00	7.17E-03	4.99E-02	7.17E-03	7.34E-02	4.71E-02
3.80E-03	4.68E+01	2.89E-05	2.43E+00	7.21E-03	5.19E-02	7.21E-03	7.74E-02	4.88E-02
4.00E-03	4.48E+01	2.89E-05	2.39E+00	7.26E-03	5.34E-02	7.26E-03	8.13E-02	5.04E-02
4.20E-03	4.29E+01	2.89E-05	2.35E+00	7.42E-03	5.47E-02	7.42E-03	8.51E-02	5.21E-02
4.40E-03	4.11E+01	2.89E-05	2.32E+00	7.01E-03	5.65E-02	7.01E-03	8.90E-02	5.37E-02
4.60E-03	3.95E+01	2.89E-05	2.27E+00	8.52E-03	5.75E-02	8.52E-03	9.29E-02	5.54E-02
4.80E-03	3.79E+01	2.89E-05	2.23E+00	8.54E-03	5.88E-02	8.54E-03	9.67E-02	5.70E-02
5.00E-03	3.64E+01	2.89E-05	2.23E+00	7.20E-03	6.12E-02	7.20E-03	1.01E-01	5.86E-02
5.20E-03	3.50E+01	2.89E-05	2.17E+00	7.82E-03	6.21E-02	7.82E-03	1.04E-01	6.01E-02
5.40E-03	3.37E+01	2.89E-05	2.12E+00	8.22E-03	6.30E-02	8.22E-03	1.08E-01	6.17E-02
5.60E-03	3.24E+01	2.89E-05	2.09E+00	7.56E-03	6.46E-02	7.56E-03	1.12E-01	6.32E-02
5.80E-03	3.12E+01	2.89E-05	2.07E+00	8.06E-03	6.62E-02	8.06E-03	1.16E-01	6.48E-02

Depth [cm]	KERMA [J/kg Y]	σ_{KERMA} [%]	Dose [J/kg•Y]	σ_{dose} [%]	f_{CPE}	σ_{fCPE} [%]	VARSKIN 3 f_{CPE}	New Model f_{CPE}
6.00E-03	3.01E+01	2.89E-05	2.02E+00	7.83E-03	6.73E-02	7.83E-03	1.19E-01	6.63E-02
6.20E-03	2.90E+01	5.77E-05	2.00E+00	8.24E-03	6.89E-02	8.24E-03	1.23E-01	6.78E-02
6.40E-03	2.80E+01	5.77E-05	1.98E+00	8.13E-03	7.08E-02	8.13E-03	1.27E-01	6.93E-02
6.60E-03	2.70E+01	5.77E-05	1.93E+00	8.77E-03	7.17E-02	8.77E-03	1.31E-01	7.08E-02
6.80E-03	2.60E+01	5.77E-05	1.90E+00	9.17E-03	7.30E-02	9.17E-03	1.34E-01	7.23E-02
7.00E-03	2.52E+01	5.77E-05	1.88E+00	8.18E-03	7.46E-02	8.19E-03	1.38E-01	7.38E-02
1.00E-02	1.57E+01	5.77E-05	1.54E+00	8.88E-03	9.82E-02	8.89E-03	1.91E-01	9.53E-02
2.00E-02	5.05E+00	1.15E-04	8.56E-01	1.21E-02	1.69E-01	1.21E-02	3.45E-01	1.62E-01
3.00E-02	2.38E+00	1.73E-04	5.71E-01	1.52E-02	2.39E-01	1.52E-02	4.70E-01	2.28E-01
4.00E-02	1.37E+00	2.31E-04	4.23E-01	1.98E-02	3.09E-01	1.98E-02	5.72E-01	2.93E-01
5.00E-02	8.87E-01	2.89E-04	3.42E-01	1.82E-02	3.86E-01	1.82E-02	6.53E-01	3.58E-01
6.00E-02	6.20E-01	3.46E-04	2.66E-01	2.27E-02	4.29E-01	2.27E-02	7.20E-01	4.24E-01
7.00E-02	4.57E-01	4.04E-04	2.25E-01	2.42E-02	4.93E-01	2.42E-02	7.73E-01	4.90E-01
8.00E-02	3.51E-01	4.62E-04	1.93E-01	3.55E-02	5.50E-01	3.55E-02	8.16E-01	5.55E-01
9.00E-02	2.77E-01	5.20E-04	1.70E-01	3.10E-02	6.13E-01	3.10E-02	8.51E-01	6.19E-01
1.00E-01	2.25E-01	5.77E-04	1.47E-01	3.49E-02	6.52E-01	3.49E-02	8.80E-01	6.82E-01
1.10E-01	1.86E-01	6.35E-04	1.36E-01	3.47E-02	7.33E-01	3.47E-02	9.03E-01	7.43E-01
1.20E-01	1.56E-01	6.93E-04	1.27E-01	2.19E-02	8.11E-01	2.20E-02	9.21E-01	8.03E-01
1.30E-01	1.33E-01	7.51E-04	1.10E-01	3.56E-02	8.25E-01	3.56E-02	9.36E-01	8.59E-01
1.40E-01	1.15E-01	8.08E-04	1.05E-01	3.74E-02	9.16E-01	3.74E-02	9.49E-01	9.13E-01
1.50E-01	1.00E-01	8.66E-04	9.33E-02	5.81E-02	9.32E-01	5.82E-02	9.58E-01	9.65E-01
1.60E-01	8.80E-02	9.24E-04	8.37E-02	4.00E-02	9.50E-01	4.01E-02	9.66E-01	1.01E+00
1.70E-01	7.80E-02	9.81E-04	7.76E-02	3.97E-02	9.95E-01	3.97E-02	9.73E-01	1.06E+00
1.80E-01	6.95E-02	1.04E-03	7.35E-02	4.30E-02	1.06E+00	4.31E-02	9.78E-01	1.10E+00
1.90E-01	6.24E-02	1.10E-03	7.15E-02	3.36E-02	1.15E+00	3.37E-02	9.82E-01	1.14E+00
2.00E-01	5.63E-02	1.15E-03	6.30E-02	3.32E-02	1.12E+00	3.32E-02	9.86E-01	1.17E+00
2.10E-01	5.11E-02	1.21E-03	5.93E-02	5.29E-02	1.16E+00	5.29E-02	9.88E-01	1.20E+00
2.20E-01	4.65E-02	1.27E-03	5.27E-02	4.08E-02	1.13E+00	4.08E-02	9.91E-01	1.23E+00

Table 6-6: The MCNP5 data that was used to construct the 1.0 MeV f_{CPE} curve and the corresponding values as calculated by VARSKIN 3 and the new model.

Depth [cm]	KERMA [J/kg ϒ]	σ_{KERMA} [%]	Dose [J/kg•ϒ]	σ_{dose} [%]	f_{CPE}	σ_{fCPE} [%]	VARSKIN 3 f_{CPE}	New Model f_{CPE}
2.00E-04	1.93E+02	4.17E-05	2.00E+00	7.31E-03	1.04E-02	7.31E-03	3.43E-03	7.31E-03
4.00E-04	1.59E+02	4.17E-05	2.21E+00	6.40E-03	1.39E-02	6.40E-03	6.85E-03	1.07E-02
6.00E-04	1.39E+02	2.09E-05	2.31E+00	6.57E-03	1.67E-02	6.57E-03	1.03E-02	1.35E-02
8.00E-04	1.25E+02	2.09E-05	2.35E+00	6.35E-03	1.88E-02	6.35E-03	1.37E-02	1.59E-02
1.00E-03	1.14E+02	2.09E-05	2.35E+00	7.10E-03	2.07E-02	7.10E-03	1.70E-02	1.81E-02
1.20E-03	1.05E+02	2.09E-05	2.40E+00	6.37E-03	2.28E-02	6.37E-03	2.04E-02	2.02E-02
1.40E-03	9.76E+01	2.09E-05	2.42E+00	6.54E-03	2.48E-02	6.54E-03	2.38E-02	2.22E-02
1.60E-03	9.11E+01	2.09E-05	2.44E+00	5.81E-03	2.68E-02	5.81E-03	2.71E-02	2.40E-02
1.80E-03	8.55E+01	2.09E-05	2.39E+00	6.33E-03	2.79E-02	6.33E-03	3.05E-02	2.58E-02
2.00E-03	8.05E+01	2.09E-05	2.40E+00	5.98E-03	2.99E-02	5.98E-03	3.38E-02	2.76E-02
2.20E-03	7.60E+01	2.09E-05	2.38E+00	6.30E-03	3.13E-02	6.30E-03	3.71E-02	2.92E-02
2.40E-03	7.19E+01	2.09E-05	2.36E+00	5.85E-03	3.28E-02	5.85E-03	4.04E-02	3.09E-02
2.60E-03	6.82E+01	2.09E-05	2.33E+00	6.14E-03	3.41E-02	6.14E-03	4.37E-02	3.25E-02
2.80E-03	6.48E+01	2.09E-05	2.30E+00	6.07E-03	3.55E-02	6.07E-03	4.70E-02	3.40E-02
3.00E-03	6.16E+01	2.09E-05	2.28E+00	6.02E-03	3.70E-02	6.02E-03	5.03E-02	3.55E-02
3.20E-03	5.87E+01	2.09E-05	2.27E+00	5.81E-03	3.87E-02	5.81E-03	5.35E-02	3.70E-02
3.40E-03	5.60E+01	2.09E-05	2.22E+00	5.63E-03	3.97E-02	5.63E-03	5.68E-02	3.85E-02
3.60E-03	5.35E+01	2.09E-05	2.19E+00	6.04E-03	4.09E-02	6.04E-03	6.00E-02	4.00E-02
3.80E-03	5.12E+01	2.09E-05	2.16E+00	5.76E-03	4.23E-02	5.76E-03	6.32E-02	4.14E-02
4.00E-03	4.90E+01	2.09E-05	2.16E+00	5.92E-03	4.41E-02	5.92E-03	6.65E-02	4.28E-02
4.20E-03	4.69E+01	2.09E-05	2.11E+00	5.96E-03	4.51E-02	5.96E-03	6.97E-02	4.42E-02
4.40E-03	4.50E+01	2.09E-05	2.09E+00	5.91E-03	4.65E-02	5.91E-03	7.29E-02	4.56E-02
4.60E-03	4.31E+01	2.09E-05	2.05E+00	6.09E-03	4.76E-02	6.09E-03	7.60E-02	4.70E-02
4.80E-03	4.14E+01	2.09E-05	2.02E+00	6.31E-03	4.89E-02	6.31E-03	7.92E-02	4.83E-02
5.00E-03	3.98E+01	2.09E-05	1.98E+00	6.32E-03	4.98E-02	6.32E-03	8.24E-02	4.96E-02
5.20E-03	3.82E+01	2.09E-05	1.94E+00	6.52E-03	5.07E-02	6.52E-03	8.55E-02	5.10E-02
5.40E-03	3.68E+01	2.09E-05	1.92E+00	6.24E-03	5.23E-02	6.24E-03	8.87E-02	5.23E-02
5.60E-03	3.54E+01	2.09E-05	1.88E+00	6.38E-03	5.32E-02	6.38E-03	9.18E-02	5.36E-02
5.80E-03	3.41E+01	2.09E-05	1.85E+00	6.48E-03	5.43E-02	6.48E-03	9.49E-02	5.49E-02
6.00E-03	3.29E+01	2.09E-05	1.84E+00	6.14E-03	5.60E-02	6.14E-03	9.80E-02	5.62E-02
6.20E-03	3.17E+01	4.17E-05	1.78E+00	6.71E-03	5.62E-02	6.71E-03	1.01E-01	5.74E-02

Depth [cm]	KERMA [J/kg Y]	σ_{KERMA} [%]	Dose [J/kg•Y]	σ_{dose} [%]	f_{CPE}	σ_{fCPE} [%]	VARSKIN 3 f_{CPE}	New Model f_{CPE}
6.40E-03	3.06E+01	4.17E-05	1.78E+00	6.30E-03	5.83E-02	6.30E-03	1.04E-01	5.87E-02
6.60E-03	2.95E+01	4.17E-05	1.75E+00	6.53E-03	5.93E-02	6.53E-03	1.07E-01	6.00E-02
6.80E-03	2.85E+01	4.17E-05	1.72E+00	6.59E-03	6.03E-02	6.59E-03	1.10E-01	6.12E-02
7.00E-03	2.75E+01	4.17E-05	1.68E+00	7.10E-03	6.12E-02	7.10E-03	1.13E-01	6.25E-02
1.00E-02	1.71E+01	4.17E-05	1.37E+00	7.35E-03	8.01E-02	7.35E-03	1.58E-01	8.05E-02
2.00E-02	5.52E+00	8.34E-05	7.67E-01	8.96E-03	1.39E-01	8.96E-03	2.91E-01	1.37E-01
3.00E-02	2.61E+00	1.25E-04	5.11E-01	1.41E-02	1.96E-01	1.41E-02	4.03E-01	1.91E-01
4.00E-02	1.50E+00	1.67E-04	3.86E-01	1.32E-02	2.58E-01	1.32E-02	4.97E-01	2.45E-01
5.00E-02	9.70E-01	2.09E-04	3.01E-01	1.58E-02	3.10E-01	1.58E-02	5.77E-01	3.00E-01
6.00E-02	6.78E-01	2.50E-04	2.48E-01	1.67E-02	3.65E-01	1.67E-02	6.44E-01	3.55E-01
7.00E-02	5.00E-01	2.92E-04	2.07E-01	2.08E-02	4.15E-01	2.08E-02	7.00E-01	4.11E-01
8.00E-02	3.83E-01	3.34E-04	1.74E-01	3.50E-02	4.54E-01	3.50E-02	7.47E-01	4.66E-01
9.00E-02	3.03E-01	3.75E-04	1.57E-01	2.26E-02	5.18E-01	2.26E-02	7.87E-01	5.21E-01
1.00E-01	2.46E-01	4.17E-04	1.44E-01	2.76E-02	5.87E-01	2.76E-02	8.21E-01	5.76E-01
1.10E-01	2.03E-01	4.59E-04	1.28E-01	2.58E-02	6.32E-01	2.58E-02	8.49E-01	6.30E-01
1.20E-01	1.71E-01	5.00E-04	1.13E-01	3.75E-02	6.63E-01	3.75E-02	8.73E-01	6.82E-01
1.30E-01	1.46E-01	5.42E-04	1.06E-01	2.00E-02	7.25E-01	2.00E-02	8.93E-01	7.33E-01
1.40E-01	1.26E-01	5.84E-04	1.03E-01	2.33E-02	8.16E-01	2.34E-02	9.10E-01	7.83E-01
1.50E-01	1.10E-01	6.26E-04	9.01E-02	2.34E-02	8.23E-01	2.34E-02	9.24E-01	8.30E-01
1.60E-01	9.63E-02	6.67E-04	8.51E-02	2.37E-02	8.84E-01	2.37E-02	9.36E-01	8.75E-01
1.70E-01	8.53E-02	7.09E-04	7.97E-02	4.16E-02	9.34E-01	4.16E-02	9.46E-01	9.18E-01
1.80E-01	7.61E-02	7.51E-04	7.09E-02	3.43E-02	9.32E-01	3.43E-02	9.55E-01	9.58E-01
1.90E-01	6.83E-02	7.92E-04	6.42E-02	3.12E-02	9.41E-01	3.12E-02	9.62E-01	9.96E-01
2.00E-01	6.16E-02	8.34E-04	6.35E-02	4.17E-02	1.03E+00	4.18E-02	9.68E-01	1.03E+00
2.10E-01	5.59E-02	8.76E-04	5.69E-02	6.40E-02	1.02E+00	6.40E-02	9.73E-01	1.06E+00
2.20E-01	5.09E-02	9.17E-04	5.17E-02	5.77E-02	1.02E+00	5.77E-02	9.77E-01	1.09E+00
2.30E-01	4.66E-02	9.59E-04	5.28E-02	3.21E-02	1.13E+00	3.21E-02	9.81E-01	1.12E+00
2.40E-01	4.28E-02	1.00E-03	4.61E-02	8.01E-02	1.08E+00	8.01E-02	9.84E-01	1.14E+00

Table 6-7: The MCNP5 data that was used to construct the 1.2 MeV f_{CPE} curve and the corresponding values as calculated by VARSKIN 3 and the new model.

Depth [cm]	KERMA [J/kg ϒ]	σ_{KERMA} [%]	Dose [J/kg•ϒ]	σ_{dose} [%]	f_{CPE}	σ_{fCPE} [%]	VARSKIN 3 f_{CPE}	New Model f_{CPE}
2.00E-04	2.24E+02	4.08E-05	1.69E+00	8.20E-03	7.56E-03	8.20E-03	2.26E-03	5.79E-03
4.00E-04	1.84E+02	4.08E-05	1.85E+00	7.71E-03	1.00E-02	7.71E-03	4.52E-03	8.48E-03
6.00E-04	1.61E+02	2.04E-05	1.94E+00	7.56E-03	1.21E-02	7.56E-03	6.77E-03	1.06E-02
8.00E-04	1.44E+02	2.04E-05	1.95E+00	7.76E-03	1.35E-02	7.76E-03	9.01E-03	1.25E-02
1.00E-03	1.32E+02	2.04E-05	2.00E+00	7.81E-03	1.52E-02	7.81E-03	1.13E-02	1.43E-02
1.20E-03	1.22E+02	2.04E-05	2.00E+00	7.83E-03	1.65E-02	7.83E-03	1.35E-02	1.59E-02
1.40E-03	1.13E+02	2.04E-05	2.02E+00	7.28E-03	1.79E-02	7.28E-03	1.57E-02	1.74E-02
1.60E-03	1.05E+02	2.04E-05	2.02E+00	6.72E-03	1.92E-02	6.72E-03	1.79E-02	1.89E-02
1.80E-03	9.89E+01	2.04E-05	1.99E+00	7.07E-03	2.02E-02	7.07E-03	2.02E-02	2.02E-02
2.00E-03	9.31E+01	2.04E-05	2.01E+00	6.70E-03	2.16E-02	6.70E-03	2.24E-02	2.16E-02
2.20E-03	8.79E+01	2.04E-05	1.97E+00	7.65E-03	2.24E-02	7.65E-03	2.46E-02	2.29E-02
2.40E-03	8.32E+01	2.04E-05	1.98E+00	6.83E-03	2.38E-02	6.83E-03	2.68E-02	2.41E-02
2.60E-03	7.89E+01	2.04E-05	1.96E+00	6.96E-03	2.49E-02	6.96E-03	2.90E-02	2.54E-02
2.80E-03	7.49E+01	2.04E-05	1.91E+00	7.38E-03	2.55E-02	7.38E-03	3.12E-02	2.66E-02
3.00E-03	7.13E+01	2.04E-05	1.89E+00	7.49E-03	2.65E-02	7.49E-03	3.34E-02	2.77E-02
3.20E-03	6.79E+01	2.04E-05	1.91E+00	6.71E-03	2.81E-02	6.71E-03	3.56E-02	2.89E-02
3.40E-03	6.48E+01	2.04E-05	1.88E+00	6.85E-03	2.90E-02	6.85E-03	3.78E-02	3.00E-02
3.60E-03	6.19E+01	2.04E-05	1.84E+00	7.76E-03	2.97E-02	7.76E-03	3.99E-02	3.11E-02
3.80E-03	5.92E+01	2.04E-05	1.82E+00	6.90E-03	3.07E-02	6.90E-03	4.21E-02	3.22E-02
4.00E-03	5.66E+01	2.04E-05	1.82E+00	6.58E-03	3.21E-02	6.58E-03	4.43E-02	3.33E-02
4.20E-03	5.43E+01	2.04E-05	1.76E+00	7.32E-03	3.24E-02	7.32E-03	4.64E-02	3.44E-02
4.40E-03	5.20E+01	2.04E-05	1.75E+00	6.94E-03	3.37E-02	6.94E-03	4.86E-02	3.54E-02
4.60E-03	4.99E+01	2.04E-05	1.72E+00	7.31E-03	3.45E-02	7.31E-03	5.07E-02	3.65E-02
4.80E-03	4.79E+01	2.04E-05	1.69E+00	7.59E-03	3.52E-02	7.59E-03	5.29E-02	3.75E-02
5.00E-03	4.60E+01	2.04E-05	1.64E+00	8.27E-03	3.57E-02	8.27E-03	5.50E-02	3.85E-02
5.20E-03	4.42E+01	2.04E-05	1.62E+00	8.06E-03	3.65E-02	8.06E-03	5.72E-02	3.96E-02
5.40E-03	4.26E+01	2.04E-05	1.60E+00	7.53E-03	3.76E-02	7.53E-03	5.93E-02	4.06E-02
5.60E-03	4.10E+01	2.04E-05	1.57E+00	8.49E-03	3.83E-02	8.49E-03	6.14E-02	4.16E-02
5.80E-03	3.95E+01	2.04E-05	1.57E+00	6.93E-03	3.98E-02	6.93E-03	6.35E-02	4.25E-02
6.00E-03	3.80E+01	2.04E-05	1.56E+00	7.04E-03	4.09E-02	7.04E-03	6.57E-02	4.35E-02
6.20E-03	3.67E+01	4.08E-05	1.49E+00	8.55E-03	4.06E-02	8.55E-03	6.78E-02	4.45E-02

Depth [cm]	KERMA [J/kg Y]	σ_{KERMA} [%]	Dose [J/kg•Y]	σ_{dose} [%]	f_{CPE}	σ_{fCPE} [%]	VARSKIN 3 f_{CPE}	New Model f_{CPE}
6.40E-03	3.54E+01	4.08E-05	1.49E+00	7.18E-03	4.22E-02	7.18E-03	6.99E-02	4.55E-02
6.60E-03	3.41E+01	4.08E-05	1.45E+00	7.96E-03	4.25E-02	7.96E-03	7.20E-02	4.64E-02
6.80E-03	3.29E+01	4.08E-05	1.42E+00	8.04E-03	4.32E-02	8.04E-03	7.41E-02	4.74E-02
7.00E-03	3.18E+01	4.08E-05	1.42E+00	8.36E-03	4.46E-02	8.36E-03	7.62E-02	4.83E-02
1.00E-02	1.98E+01	4.08E-05	1.14E+00	9.60E-03	5.76E-02	9.60E-03	1.07E-01	6.20E-02
2.00E-02	6.39E+00	8.16E-05	6.65E-01	1.11E-02	1.04E-01	1.11E-02	2.03E-01	1.04E-01
3.00E-02	3.02E+00	1.22E-04	4.37E-01	1.55E-02	1.45E-01	1.55E-02	2.88E-01	1.44E-01
4.00E-02	1.74E+00	1.63E-04	3.28E-01	1.93E-02	1.89E-01	1.93E-02	3.64E-01	1.84E-01
5.00E-02	1.12E+00	2.04E-04	2.67E-01	1.73E-02	2.38E-01	1.73E-02	4.32E-01	2.25E-01
6.00E-02	7.84E-01	2.45E-04	2.20E-01	1.91E-02	2.81E-01	1.91E-02	4.93E-01	2.66E-01
7.00E-02	5.78E-01	2.86E-04	1.87E-01	1.87E-02	3.23E-01	1.87E-02	5.47E-01	3.07E-01
8.00E-02	4.43E-01	3.27E-04	1.59E-01	3.95E-02	3.59E-01	3.95E-02	5.96E-01	3.48E-01
9.00E-02	3.51E-01	3.67E-04	1.44E-01	2.23E-02	4.10E-01	2.23E-02	6.39E-01	3.90E-01
1.00E-01	2.85E-01	4.08E-04	1.19E-01	4.95E-02	4.19E-01	4.95E-02	6.78E-01	4.31E-01
1.10E-01	2.35E-01	4.49E-04	1.15E-01	1.97E-02	4.89E-01	1.97E-02	7.12E-01	4.73E-01
1.20E-01	1.98E-01	4.90E-04	1.01E-01	5.20E-02	5.08E-01	5.20E-02	7.43E-01	5.14E-01
1.30E-01	1.69E-01	5.31E-04	9.58E-02	3.15E-02	5.69E-01	3.15E-02	7.70E-01	5.54E-01
1.40E-01	1.45E-01	5.72E-04	8.78E-02	4.39E-02	6.04E-01	4.39E-02	7.95E-01	5.94E-01
1.50E-01	1.27E-01	6.12E-04	8.14E-02	2.47E-02	6.42E-01	2.47E-02	8.17E-01	6.34E-01
1.60E-01	1.11E-01	6.53E-04	7.50E-02	5.53E-02	6.73E-01	5.53E-02	8.37E-01	6.72E-01
1.70E-01	9.87E-02	6.94E-04	6.62E-02	6.47E-02	6.71E-01	6.47E-02	8.54E-01	7.09E-01
1.80E-01	8.80E-02	7.35E-04	6.90E-02	2.85E-02	7.83E-01	2.85E-02	8.70E-01	7.45E-01
1.90E-01	7.90E-02	7.76E-04	6.37E-02	5.03E-02	8.07E-01	5.03E-02	8.84E-01	7.80E-01
2.00E-01	7.13E-02	8.16E-04	6.13E-02	5.81E-02	8.61E-01	5.81E-02	8.96E-01	8.13E-01
2.10E-01	6.46E-02	8.57E-04	5.81E-02	4.69E-02	8.99E-01	4.69E-02	9.07E-01	8.44E-01
2.20E-01	5.89E-02	8.98E-04	5.14E-02	5.27E-02	8.73E-01	5.27E-02	9.17E-01	8.74E-01
2.30E-01	5.39E-02	9.39E-04	4.91E-02	4.13E-02	9.12E-01	4.13E-02	9.26E-01	9.03E-01
2.40E-01	4.95E-02	9.80E-04	4.97E-02	2.78E-02	1.00E+00	2.79E-02	9.34E-01	9.29E-01
2.50E-01	4.56E-02	1.02E-03	4.51E-02	5.59E-02	9.89E-01	5.59E-02	9.41E-01	9.54E-01
2.60E-01	4.22E-02	1.06E-03	4.25E-02	3.28E-02	1.01E+00	3.28E-02	9.47E-01	9.77E-01
2.70E-01	3.91E-02	1.10E-03	4.10E-02	6.94E-02	1.05E+00	6.94E-02	9.53E-01	9.99E-01
2.80E-01	3.63E-02	1.14E-03	3.70E-02	6.88E-02	1.02E+00	6.88E-02	9.58E-01	1.02E+00
2.90E-01	3.39E-02	1.18E-03	3.78E-02	5.19E-02	1.12E+00	5.19E-02	9.62E-01	1.04E+00

Depth [cm]	KERMA [J/kg ϒ]	σ_{KERMA} [%]	Dose [J/kg•ϒ]	σ_{dose} [%]	f_{CPE}	σ_{fCPE} [%]	VARSKIN 3 f_{CPE}	New Model f_{CPE}
3.00E-01	3.17E-02	1.22E-03	3.31E-02	7.78E-02	1.05E+00	7.78E-02	9.66E-01	1.05E+00

Table 6-8: The MCNP5 data that was used to construct the 1.4 MeV f_{CPE} curve and the corresponding values as calculated by VARSKIN 3 and the new model.

Depth [cm]	KERMA [J/kg ϒ]	σ_{KERMA} [%]	Dose [J/kg•ϒ]	σ_{dose} [%]	f_{CPE}	σ_{fCPE} [%]	VARSKIN 3 f_{CPE}	New Model f_{CPE}
2.00E-04	2.52E+02	4.08E-05	1.46E+00	9.80E-03	5.80E-03	9.80E-03	1.49E-03	4.94E-03
4.00E-04	2.07E+02	4.08E-05	1.59E+00	9.04E-03	7.71E-03	9.04E-03	2.98E-03	7.21E-03
6.00E-04	1.81E+02	2.04E-05	1.68E+00	8.38E-03	9.29E-03	8.38E-03	4.46E-03	9.04E-03
8.00E-04	1.62E+02	2.04E-05	1.69E+00	8.88E-03	1.04E-02	8.88E-03	5.94E-03	1.06E-02
1.00E-03	1.48E+02	2.04E-05	1.73E+00	8.95E-03	1.17E-02	8.95E-03	7.42E-03	1.21E-02
1.20E-03	1.37E+02	2.04E-05	1.76E+00	8.54E-03	1.29E-02	8.54E-03	8.90E-03	1.34E-02
1.40E-03	1.27E+02	2.04E-05	1.75E+00	8.33E-03	1.38E-02	8.33E-03	1.04E-02	1.47E-02
1.60E-03	1.19E+02	2.04E-05	1.75E+00	8.35E-03	1.47E-02	8.35E-03	1.19E-02	1.59E-02
1.80E-03	1.11E+02	2.04E-05	1.74E+00	8.05E-03	1.56E-02	8.05E-03	1.33E-02	1.71E-02
2.00E-03	1.05E+02	2.04E-05	1.75E+00	7.32E-03	1.67E-02	7.32E-03	1.48E-02	1.82E-02
2.20E-03	9.89E+01	2.04E-05	1.71E+00	8.80E-03	1.73E-02	8.80E-03	1.63E-02	1.93E-02
2.40E-03	9.36E+01	2.04E-05	1.71E+00	8.10E-03	1.83E-02	8.10E-03	1.77E-02	2.03E-02
2.60E-03	8.87E+01	2.04E-05	1.70E+00	7.71E-03	1.91E-02	7.71E-03	1.92E-02	2.13E-02
2.80E-03	8.43E+01	2.04E-05	1.66E+00	9.42E-03	1.96E-02	9.42E-03	2.06E-02	2.23E-02
3.00E-03	8.02E+01	2.04E-05	1.65E+00	8.65E-03	2.05E-02	8.65E-03	2.21E-02	2.33E-02
3.20E-03	7.64E+01	2.04E-05	1.64E+00	8.13E-03	2.14E-02	8.13E-03	2.36E-02	2.42E-02
3.40E-03	7.29E+01	2.04E-05	1.60E+00	7.99E-03	2.20E-02	7.99E-03	2.50E-02	2.52E-02
3.60E-03	6.96E+01	2.04E-05	1.58E+00	8.51E-03	2.27E-02	8.51E-03	2.65E-02	2.61E-02
3.80E-03	6.66E+01	2.04E-05	1.57E+00	8.73E-03	2.35E-02	8.73E-03	2.79E-02	2.70E-02
4.00E-03	6.37E+01	2.04E-05	1.56E+00	8.28E-03	2.45E-02	8.28E-03	2.94E-02	2.79E-02
4.20E-03	6.10E+01	2.04E-05	1.54E+00	7.99E-03	2.52E-02	7.99E-03	3.08E-02	2.88E-02
4.40E-03	5.85E+01	2.04E-05	1.52E+00	8.26E-03	2.60E-02	8.26E-03	3.23E-02	2.96E-02
4.60E-03	5.61E+01	2.04E-05	1.48E+00	8.43E-03	2.64E-02	8.43E-03	3.37E-02	3.05E-02
4.80E-03	5.39E+01	2.04E-05	1.45E+00	9.34E-03	2.70E-02	9.34E-03	3.51E-02	3.13E-02
5.00E-03	5.18E+01	2.04E-05	1.41E+00	1.01E-02	2.72E-02	1.01E-02	3.66E-02	3.22E-02
5.20E-03	4.98E+01	2.04E-05	1.40E+00	9.82E-03	2.81E-02	9.82E-03	3.80E-02	3.30E-02

Depth [cm]	KERMA [J/kg Y]	σ_{KERMA} [%]	Dose [J/kg•Y]	σ_{dose} [%]	f_{CPE}	σ_{fCPE} [%]	VARSKIN 3 f_{CPE}	New Model f_{CPE}
5.40E-03	4.79E+01	2.04E-05	1.41E+00	8.02E-03	2.94E-02	8.02E-03	3.94E-02	3.38E-02
5.60E-03	4.61E+01	2.04E-05	1.36E+00	1.07E-02	2.95E-02	1.07E-02	4.09E-02	3.46E-02
5.80E-03	4.44E+01	2.04E-05	1.37E+00	7.57E-03	3.08E-02	7.57E-03	4.23E-02	3.55E-02
6.00E-03	4.28E+01	2.04E-05	1.32E+00	9.47E-03	3.09E-02	9.47E-03	4.37E-02	3.63E-02
6.20E-03	4.12E+01	4.08E-05	1.31E+00	9.37E-03	3.18E-02	9.37E-03	4.52E-02	3.70E-02
6.40E-03	3.98E+01	4.08E-05	1.30E+00	8.48E-03	3.27E-02	8.48E-03	4.66E-02	3.78E-02
6.60E-03	3.84E+01	4.08E-05	1.27E+00	8.55E-03	3.30E-02	8.55E-03	4.80E-02	3.86E-02
6.80E-03	3.70E+01	4.08E-05	1.24E+00	9.67E-03	3.34E-02	9.67E-03	4.94E-02	3.94E-02
7.00E-03	3.58E+01	4.08E-05	1.22E+00	9.87E-03	3.41E-02	9.87E-03	5.08E-02	4.02E-02
1.00E-02	2.23E+01	4.08E-05	9.90E-01	1.06E-02	4.44E-02	1.06E-02	7.18E-02	5.13E-02
2.00E-02	7.18E+00	8.16E-05	5.81E-01	1.25E-02	8.08E-02	1.25E-02	1.38E-01	8.49E-02
3.00E-02	3.39E+00	1.22E-04	3.94E-01	1.50E-02	1.16E-01	1.50E-02	2.00E-01	1.17E-01
4.00E-02	1.95E+00	1.63E-04	2.94E-01	1.64E-02	1.51E-01	1.64E-02	2.58E-01	1.48E-01
5.00E-02	1.26E+00	2.04E-04	2.33E-01	4.07E-02	1.85E-01	4.07E-02	3.11E-01	1.80E-01
6.00E-02	8.82E-01	2.45E-04	1.95E-01	2.45E-02	2.21E-01	2.45E-02	3.61E-01	2.11E-01
7.00E-02	6.50E-01	2.86E-04	1.67E-01	1.94E-02	2.56E-01	1.94E-02	4.06E-01	2.43E-01
8.00E-02	4.99E-01	3.27E-04	1.44E-01	2.58E-02	2.89E-01	2.58E-02	4.49E-01	2.76E-01
9.00E-02	3.95E-01	3.67E-04	1.23E-01	5.33E-02	3.11E-01	5.33E-02	4.89E-01	3.08E-01
1.00E-01	3.20E-01	4.08E-04	1.14E-01	2.89E-02	3.55E-01	2.89E-02	5.25E-01	3.41E-01
1.10E-01	2.65E-01	4.49E-04	1.01E-01	5.64E-02	3.82E-01	5.64E-02	5.59E-01	3.74E-01
1.20E-01	2.22E-01	4.90E-04	8.96E-02	5.36E-02	4.03E-01	5.36E-02	5.91E-01	4.07E-01
1.30E-01	1.90E-01	5.31E-04	8.53E-02	4.37E-02	4.50E-01	4.37E-02	6.20E-01	4.40E-01
1.40E-01	1.64E-01	5.72E-04	7.87E-02	3.78E-02	4.82E-01	3.78E-02	6.48E-01	4.72E-01
1.50E-01	1.42E-01	6.12E-04	7.52E-02	3.10E-02	5.28E-01	3.11E-02	6.73E-01	5.05E-01
1.60E-01	1.25E-01	6.53E-04	6.19E-02	7.22E-02	4.94E-01	7.23E-02	6.96E-01	5.37E-01
1.70E-01	1.11E-01	6.94E-04	6.04E-02	5.03E-02	5.44E-01	5.04E-02	7.18E-01	5.69E-01
1.80E-01	9.90E-02	7.35E-04	6.40E-02	3.13E-02	6.46E-01	3.14E-02	7.39E-01	6.01E-01
1.90E-01	8.88E-02	7.76E-04	5.76E-02	6.32E-02	6.48E-01	6.32E-02	7.57E-01	6.31E-01
2.00E-01	8.02E-02	8.16E-04	5.48E-02	3.48E-02	6.84E-01	3.48E-02	7.75E-01	6.62E-01
2.10E-01	7.27E-02	8.57E-04	5.63E-02	2.22E-02	7.75E-01	2.22E-02	7.91E-01	6.91E-01
2.20E-01	6.62E-02	8.98E-04	4.88E-02	4.80E-02	7.37E-01	4.81E-02	8.06E-01	7.20E-01
2.30E-01	6.06E-02	9.39E-04	4.66E-02	4.86E-02	7.68E-01	4.86E-02	8.20E-01	7.47E-01
2.40E-01	5.57E-02	9.80E-04	4.42E-02	5.17E-02	7.94E-01	5.17E-02	8.33E-01	7.74E-01

Depth [cm]	KERMA [J/kg ϒ]	σ_{KERMA} [%]	Dose [J/kg•ϒ]	σ_{dose} [%]	f_{CPE}	σ_{fCPE} [%]	VARSKIN 3 f_{CPE}	New Model f_{CPE}
2.50E-01	5.13E-02	1.02E-03	4.02E-02	5.47E-02	7.84E-01	5.47E-02	8.45E-01	8.00E-01
2.60E-01	4.74E-02	1.06E-03	4.36E-02	2.81E-02	9.19E-01	2.81E-02	8.56E-01	8.25E-01
2.70E-01	4.40E-02	1.10E-03	3.84E-02	4.96E-02	8.73E-01	4.96E-02	8.66E-01	8.49E-01
2.80E-01	4.09E-02	1.14E-03	3.33E-02	8.97E-02	8.14E-01	8.97E-02	8.76E-01	8.71E-01
2.90E-01	3.81E-02	1.18E-03	3.38E-02	6.82E-02	8.88E-01	6.82E-02	8.85E-01	8.93E-01
3.00E-01	3.56E-02	1.22E-03	3.50E-02	6.94E-02	9.82E-01	6.94E-02	8.93E-01	9.13E-01
3.10E-01	3.33E-02	1.27E-03	3.33E-02	3.22E-02	9.98E-01	3.22E-02	9.01E-01	9.33E-01
3.20E-01	3.13E-02	1.31E-03	2.96E-02	5.77E-02	9.46E-01	5.77E-02	9.08E-01	9.51E-01
3.30E-01	2.94E-02	1.35E-03	2.87E-02	7.15E-02	9.75E-01	7.15E-02	9.14E-01	9.68E-01
3.40E-01	2.76E-02	1.39E-03	2.31E-02	8.94E-02	8.37E-01	8.94E-02	9.21E-01	9.84E-01
3.50E-01	2.61E-02	1.43E-03	2.90E-02	5.38E-02	1.11E+00	5.38E-02	9.26E-01	9.99E-01
3.60E-01	2.47E-02	1.47E-03	2.69E-02	4.11E-02	1.09E+00	4.11E-02	9.32E-01	1.01E+00
3.70E-01	2.33E-02	1.51E-03	2.45E-02	7.50E-02	1.05E+00	7.50E-02	9.37E-01	1.03E+00
3.80E-01	2.21E-02	1.56E-03	2.48E-02	4.14E-02	1.12E+00	4.14E-02	9.41E-01	1.04E+00
3.90E-01	2.10E-02	1.60E-03	2.16E-02	6.37E-02	1.03E+00	6.37E-02	9.45E-01	1.05E+00
4.00E-01	1.99E-02	1.64E-03	2.15E-02	4.36E-02	1.08E+00	4.37E-02	9.49E-01	1.06E+00
4.10E-01	1.90E-02	1.68E-03	2.13E-02	5.45E-02	1.12E+00	5.45E-02	9.53E-01	1.07E+00
4.20E-01	1.81E-02	1.72E-03	1.95E-02	6.88E-02	1.08E+00	6.89E-02	9.56E-01	1.07E+00
4.30E-01	1.72E-02	1.76E-03	1.95E-02	7.04E-02	1.13E+00	7.04E-02	9.59E-01	1.08E+00

Table 6-9: The MCNP5 data that was used to construct the 1.6 MeV f_{CPE} curve and the corresponding values as calculated by VARSKIN 3 and the new model.

Depth [cm]	KERMA [J/kg ϒ]	σ_{KERMA} [%]	Dose [J/kg•ϒ]	σ_{dose} [%]	f_{CPE}	σ_{fCPE} [%]	VARSKIN 3 f_{CPE}	New Model f_{CPE}
2.00E-04	2.78E+02	4.08E-05	1.29E+00	1.26E-02	4.65E-03	1.26E-02	9.81E-04	4.42E-03
4.00E-04	2.28E+02	4.08E-05	1.42E+00	1.18E-02	6.22E-03	1.18E-02	1.96E-03	6.43E-03
6.00E-04	2.00E+02	2.04E-05	1.49E+00	1.02E-02	7.48E-03	1.02E-02	2.94E-03	8.05E-03
8.00E-04	1.79E+02	2.04E-05	1.53E+00	9.95E-03	8.52E-03	9.95E-03	3.92E-03	9.45E-03
1.00E-03	1.64E+02	2.04E-05	1.55E+00	1.06E-02	9.46E-03	1.06E-02	4.89E-03	1.07E-02
1.20E-03	1.51E+02	2.04E-05	1.57E+00	9.11E-03	1.04E-02	9.11E-03	5.87E-03	1.19E-02
1.40E-03	1.40E+02	2.04E-05	1.56E+00	1.01E-02	1.11E-02	1.01E-02	6.84E-03	1.30E-02
1.60E-03	1.31E+02	2.04E-05	1.56E+00	8.90E-03	1.19E-02	8.90E-03	7.82E-03	1.41E-02

Depth [cm]	KERMA [J/kg ϒ]	σ_{KERMA} [%]	Dose [J/kg•ϒ]	σ_{dose} [%]	f_{CPE}	σ_{fCPE} [%]	VARSKIN 3 f_{CPE}	New Model f_{CPE}
1.80E-03	1.23E+02	2.04E-05	1.57E+00	9.39E-03	1.28E-02	9.39E-03	8.79E-03	1.51E-02
2.00E-03	1.16E+02	2.04E-05	1.53E+00	1.03E-02	1.32E-02	1.03E-02	9.76E-03	1.61E-02
2.20E-03	1.09E+02	2.04E-05	1.53E+00	8.59E-03	1.40E-02	8.59E-03	1.07E-02	1.70E-02
2.40E-03	1.03E+02	2.04E-05	1.54E+00	9.10E-03	1.49E-02	9.10E-03	1.17E-02	1.79E-02
2.60E-03	9.80E+01	2.04E-05	1.52E+00	9.15E-03	1.55E-02	9.15E-03	1.27E-02	1.88E-02
2.80E-03	9.31E+01	2.04E-05	1.49E+00	9.23E-03	1.60E-02	9.23E-03	1.36E-02	1.96E-02
3.00E-03	8.86E+01	2.04E-05	1.47E+00	9.47E-03	1.66E-02	9.47E-03	1.46E-02	2.05E-02
3.20E-03	8.44E+01	2.04E-05	1.46E+00	9.61E-03	1.73E-02	9.61E-03	1.56E-02	2.13E-02
3.40E-03	8.05E+01	2.04E-05	1.44E+00	9.07E-03	1.79E-02	9.07E-03	1.65E-02	2.21E-02
3.60E-03	7.69E+01	2.04E-05	1.39E+00	1.01E-02	1.80E-02	1.01E-02	1.75E-02	2.29E-02
3.80E-03	7.35E+01	2.04E-05	1.38E+00	1.07E-02	1.87E-02	1.07E-02	1.85E-02	2.37E-02
4.00E-03	7.04E+01	2.04E-05	1.38E+00	9.81E-03	1.95E-02	9.81E-03	1.94E-02	2.45E-02
4.20E-03	6.74E+01	2.04E-05	1.36E+00	9.86E-03	2.01E-02	9.86E-03	2.04E-02	2.52E-02
4.40E-03	6.46E+01	2.04E-05	1.35E+00	9.24E-03	2.09E-02	9.24E-03	2.14E-02	2.60E-02
4.60E-03	6.20E+01	2.04E-05	1.32E+00	8.86E-03	2.13E-02	8.86E-03	2.23E-02	2.67E-02
4.80E-03	5.95E+01	2.04E-05	1.31E+00	9.65E-03	2.20E-02	9.65E-03	2.33E-02	2.74E-02
5.00E-03	5.72E+01	2.04E-05	1.29E+00	8.53E-03	2.25E-02	8.53E-03	2.42E-02	2.82E-02
5.20E-03	5.50E+01	2.04E-05	1.23E+00	1.24E-02	2.25E-02	1.24E-02	2.52E-02	2.89E-02
5.40E-03	5.29E+01	2.04E-05	1.26E+00	8.12E-03	2.38E-02	8.12E-03	2.61E-02	2.96E-02
5.60E-03	5.09E+01	2.04E-05	1.21E+00	1.09E-02	2.37E-02	1.09E-02	2.71E-02	3.03E-02
5.80E-03	4.90E+01	2.04E-05	1.19E+00	9.75E-03	2.43E-02	9.75E-03	2.81E-02	3.10E-02
6.00E-03	4.72E+01	2.04E-05	1.17E+00	9.56E-03	2.49E-02	9.56E-03	2.90E-02	3.16E-02
6.20E-03	4.55E+01	4.08E-05	1.16E+00	1.04E-02	2.55E-02	1.04E-02	3.00E-02	3.23E-02
6.40E-03	4.39E+01	4.08E-05	1.13E+00	1.09E-02	2.58E-02	1.09E-02	3.09E-02	3.30E-02
6.60E-03	4.24E+01	4.08E-05	1.14E+00	1.06E-02	2.69E-02	1.06E-02	3.19E-02	3.37E-02
6.80E-03	4.09E+01	4.08E-05	1.12E+00	1.05E-02	2.73E-02	1.05E-02	3.28E-02	3.43E-02
7.00E-03	3.95E+01	4.08E-05	1.08E+00	1.12E-02	2.74E-02	1.12E-02	3.38E-02	3.50E-02
1.00E-02	2.46E+01	4.08E-05	8.91E-01	1.19E-02	3.62E-02	1.19E-02	4.79E-02	4.44E-02
2.00E-02	7.93E+00	8.16E-05	4.93E-01	2.08E-02	6.22E-02	2.08E-02	9.35E-02	7.26E-02
3.00E-02	3.75E+00	1.22E-04	3.48E-01	1.91E-02	9.30E-02	1.91E-02	1.37E-01	9.90E-02
4.00E-02	2.16E+00	1.63E-04	2.63E-01	2.02E-02	1.22E-01	2.02E-02	1.78E-01	1.25E-01
5.00E-02	1.39E+00	2.04E-04	2.12E-01	2.30E-02	1.52E-01	2.30E-02	2.18E-01	1.50E-01
6.00E-02	9.74E-01	2.45E-04	1.74E-01	3.02E-02	1.78E-01	3.02E-02	2.55E-01	1.76E-01

Depth [cm]	KERMA [J/kg Y]	σ_{KERMA} [%]	Dose [J/kg•Y]	σ_{dose} [%]	f_{CPE}	σ_{fCPE} [%]	VARSKIN 3 f_{CPE}	New Model f_{CPE}
7.00E-02	7.18E-01	2.86E-04	1.43E-01	6.22E-02	1.99E-01	6.22E-02	2.91E-01	2.02E-01
8.00E-02	5.51E-01	3.27E-04	1.25E-01	3.09E-02	2.27E-01	3.09E-02	3.25E-01	2.28E-01
9.00E-02	4.36E-01	3.67E-04	1.14E-01	3.43E-02	2.63E-01	3.43E-02	3.57E-01	2.54E-01
1.00E-01	3.53E-01	4.08E-04	1.02E-01	4.13E-02	2.88E-01	4.13E-02	3.88E-01	2.81E-01
1.10E-01	2.92E-01	4.49E-04	9.04E-02	5.39E-02	3.10E-01	5.39E-02	4.17E-01	3.08E-01
1.20E-01	2.46E-01	4.90E-04	8.21E-02	4.59E-02	3.34E-01	4.59E-02	4.45E-01	3.35E-01
1.30E-01	2.09E-01	5.31E-04	7.65E-02	5.32E-02	3.66E-01	5.32E-02	4.72E-01	3.62E-01
1.40E-01	1.81E-01	5.72E-04	6.98E-02	6.39E-02	3.86E-01	6.39E-02	4.97E-01	3.89E-01
1.50E-01	1.57E-01	6.12E-04	6.59E-02	7.78E-02	4.19E-01	7.78E-02	5.21E-01	4.16E-01
1.60E-01	1.38E-01	6.53E-04	6.51E-02	3.06E-02	4.70E-01	3.06E-02	5.44E-01	4.44E-01
1.70E-01	1.23E-01	6.94E-04	5.43E-02	7.17E-02	4.43E-01	7.17E-02	5.66E-01	4.71E-01
1.80E-01	1.09E-01	7.35E-04	5.28E-02	6.86E-02	4.83E-01	6.86E-02	5.86E-01	4.98E-01
1.90E-01	9.81E-02	7.76E-04	4.84E-02	6.64E-02	4.93E-01	6.64E-02	6.06E-01	5.25E-01
2.00E-01	8.85E-02	8.16E-04	4.51E-02	8.28E-02	5.09E-01	8.28E-02	6.25E-01	5.52E-01
2.10E-01	8.03E-02	8.57E-04	4.42E-02	6.08E-02	5.50E-01	6.08E-02	6.43E-01	5.79E-01
2.20E-01	7.31E-02	8.98E-04	4.55E-02	2.94E-02	6.22E-01	2.94E-02	6.60E-01	6.05E-01
2.30E-01	6.69E-02	9.39E-04	4.27E-02	5.40E-02	6.38E-01	5.40E-02	6.76E-01	6.31E-01
2.40E-01	6.15E-02	9.80E-04	3.94E-02	7.69E-02	6.42E-01	7.69E-02	6.92E-01	6.57E-01
2.50E-01	5.67E-02	1.02E-03	3.90E-02	5.78E-02	6.87E-01	5.78E-02	7.07E-01	6.82E-01
2.60E-01	5.24E-02	1.06E-03	3.61E-02	6.46E-02	6.90E-01	6.46E-02	7.21E-01	7.07E-01
2.70E-01	4.85E-02	1.10E-03	3.19E-02	8.00E-02	6.57E-01	8.00E-02	7.34E-01	7.31E-01
2.80E-01	4.51E-02	1.14E-03	3.30E-02	7.41E-02	7.32E-01	7.41E-02	7.47E-01	7.55E-01
2.90E-01	4.21E-02	1.18E-03	3.25E-02	5.62E-02	7.72E-01	5.62E-02	7.59E-01	7.78E-01
3.00E-01	3.93E-02	1.22E-03	3.27E-02	5.18E-02	8.31E-01	5.18E-02	7.70E-01	8.01E-01
3.10E-01	3.68E-02	1.27E-03	2.91E-02	5.75E-02	7.90E-01	5.75E-02	7.81E-01	8.23E-01
3.20E-01	3.45E-02	1.31E-03	2.79E-02	7.32E-02	8.07E-01	7.33E-02	7.92E-01	8.44E-01
3.30E-01	3.24E-02	1.35E-03	2.80E-02	6.50E-02	8.62E-01	6.50E-02	8.02E-01	8.65E-01
3.40E-01	3.05E-02	1.39E-03	2.93E-02	3.69E-02	9.60E-01	3.70E-02	8.11E-01	8.84E-01
3.50E-01	2.88E-02	1.43E-03	2.68E-02	4.50E-02	9.29E-01	4.50E-02	8.20E-01	9.03E-01
3.60E-01	2.72E-02	1.47E-03	2.35E-02	6.71E-02	8.65E-01	6.71E-02	8.29E-01	9.22E-01
3.70E-01	2.58E-02	1.52E-03	2.39E-02	7.19E-02	9.26E-01	7.20E-02	8.37E-01	9.40E-01
3.80E-01	2.44E-02	1.56E-03	2.53E-02	4.57E-02	1.04E+00	4.57E-02	8.45E-01	9.56E-01
3.90E-01	2.32E-02	1.60E-03	2.39E-02	7.11E-02	1.03E+00	7.11E-02	8.52E-01	9.72E-01

Depth [cm]	KERMA [J/kg ϒ]	σ_{KERMA} [%]	Dose [J/kg•ϒ]	σ_{dose} [%]	f_{CPE}	σ_{fCPE} [%]	VARSKIN 3 f_{CPE}	New Model f_{CPE}
4.00E-01	2.20E-02	1.64E-03	2.40E-02	4.63E-02	1.09E+00	4.64E-02	8.59E-01	9.88E-01
4.10E-01	2.09E-02	1.68E-03	2.18E-02	5.22E-02	1.04E+00	5.22E-02	8.66E-01	1.00E+00
4.20E-01	2.00E-02	1.72E-03	2.17E-02	5.48E-02	1.09E+00	5.49E-02	8.73E-01	1.02E+00

Table 6-10: The MCNP5 data that was used to construct the 1.8 MeV f_{CPE} curve and the corresponding values as calculated by VARSKIN 3 and the new model.

Depth [cm]	KERMA [J/kg•ϒ]	σ_{KERMA} [%]	Dose [J/kg•ϒ]	σ_{dose} [%]	f_{CPE}	σ_{fCPE} [%]	VARSKIN 3 f_{CPE}	New Model f_{CPE}
2.00E-04	3.02E+02	4.08E-05	1.19E+00	1.28E-02	3.94E-03	1.28E-02	6.46E-04	4.04E-03
4.00E-04	2.48E+02	4.08E-05	1.31E+00	1.21E-02	5.30E-03	1.21E-02	1.29E-03	5.88E-03
6.00E-04	2.17E+02	2.04E-05	1.34E+00	1.31E-02	6.16E-03	1.31E-02	1.94E-03	7.34E-03
8.00E-04	1.95E+02	2.04E-05	1.40E+00	1.08E-02	7.16E-03	1.08E-02	2.58E-03	8.61E-03
1.00E-03	1.78E+02	2.04E-05	1.40E+00	1.17E-02	7.84E-03	1.17E-02	3.22E-03	9.76E-03
1.20E-03	1.64E+02	2.04E-05	1.41E+00	9.98E-03	8.62E-03	9.98E-03	3.87E-03	1.08E-02
1.40E-03	1.52E+02	2.04E-05	1.42E+00	1.10E-02	9.29E-03	1.10E-02	4.51E-03	1.18E-02
1.60E-03	1.42E+02	2.04E-05	1.42E+00	9.68E-03	1.00E-02	9.68E-03	5.15E-03	1.28E-02
1.80E-03	1.34E+02	2.04E-05	1.43E+00	9.83E-03	1.07E-02	9.83E-03	5.80E-03	1.37E-02
2.00E-03	1.26E+02	2.04E-05	1.38E+00	1.17E-02	1.09E-02	1.17E-02	6.44E-03	1.45E-02
2.20E-03	1.19E+02	2.04E-05	1.38E+00	1.04E-02	1.16E-02	1.04E-02	7.08E-03	1.54E-02
2.40E-03	1.12E+02	2.04E-05	1.38E+00	1.01E-02	1.23E-02	1.01E-02	7.72E-03	1.62E-02
2.60E-03	1.07E+02	2.04E-05	1.35E+00	1.19E-02	1.26E-02	1.19E-02	8.36E-03	1.70E-02
2.80E-03	1.01E+02	2.04E-05	1.34E+00	1.16E-02	1.32E-02	1.16E-02	9.00E-03	1.77E-02
3.00E-03	9.63E+01	2.04E-05	1.35E+00	1.01E-02	1.40E-02	1.01E-02	9.64E-03	1.85E-02
3.20E-03	9.17E+01	2.04E-05	1.32E+00	1.15E-02	1.44E-02	1.15E-02	1.03E-02	1.92E-02
3.40E-03	8.75E+01	2.04E-05	1.31E+00	1.13E-02	1.49E-02	1.13E-02	1.09E-02	1.99E-02
3.60E-03	8.36E+01	2.04E-05	1.28E+00	1.03E-02	1.53E-02	1.03E-02	1.16E-02	2.06E-02
3.80E-03	7.99E+01	2.04E-05	1.24E+00	1.22E-02	1.55E-02	1.22E-02	1.22E-02	2.13E-02
4.00E-03	7.65E+01	2.04E-05	1.23E+00	1.17E-02	1.61E-02	1.17E-02	1.28E-02	2.20E-02
4.20E-03	7.33E+01	2.04E-05	1.23E+00	1.01E-02	1.68E-02	1.01E-02	1.35E-02	2.27E-02
4.40E-03	7.02E+01	2.04E-05	1.19E+00	1.19E-02	1.70E-02	1.19E-02	1.41E-02	2.34E-02
4.60E-03	6.74E+01	2.04E-05	1.20E+00	9.70E-03	1.78E-02	9.70E-03	1.47E-02	2.40E-02
4.80E-03	6.47E+01	2.04E-05	1.16E+00	1.15E-02	1.80E-02	1.15E-02	1.54E-02	2.46E-02

Depth [cm]	KERMA [J/kg•Y]	σ_{KERMA} [%]	Dose [J/kg•Y]	σ_{dose} [%]	f_{CPE}	σ_{fCPE} [%]	VARSKIN 3 f_{CPE}	New Model f_{CPE}
5.00E-03	6.22E+01	2.04E-05	1.16E+00	9.39E-03	1.87E-02	9.39E-03	1.60E-02	2.53E-02
5.20E-03	5.98E+01	2.04E-05	1.11E+00	1.37E-02	1.85E-02	1.37E-02	1.67E-02	2.59E-02
5.40E-03	5.75E+01	2.04E-05	1.14E+00	9.33E-03	1.99E-02	9.33E-03	1.73E-02	2.65E-02
5.60E-03	5.53E+01	2.04E-05	1.09E+00	1.15E-02	1.97E-02	1.15E-02	1.79E-02	2.72E-02
5.80E-03	5.33E+01	2.04E-05	1.07E+00	1.29E-02	2.00E-02	1.29E-02	1.86E-02	2.78E-02
6.00E-03	5.13E+01	2.04E-05	1.07E+00	1.16E-02	2.09E-02	1.16E-02	1.92E-02	2.84E-02
6.20E-03	4.95E+01	4.08E-05	1.03E+00	1.40E-02	2.09E-02	1.40E-02	1.98E-02	2.90E-02
6.40E-03	4.77E+01	4.08E-05	1.02E+00	1.22E-02	2.13E-02	1.22E-02	2.05E-02	2.96E-02
6.60E-03	4.61E+01	4.08E-05	1.02E+00	1.23E-02	2.21E-02	1.23E-02	2.11E-02	3.01E-02
6.80E-03	4.45E+01	4.08E-05	1.01E+00	1.02E-02	2.27E-02	1.02E-02	2.17E-02	3.07E-02
7.00E-03	4.30E+01	4.08E-05	9.79E-01	1.30E-02	2.28E-02	1.30E-02	2.24E-02	3.13E-02
1.00E-02	2.68E+01	4.08E-05	8.04E-01	1.26E-02	3.00E-02	1.26E-02	3.18E-02	3.95E-02
2.00E-02	8.62E+00	8.16E-05	4.64E-01	1.93E-02	5.38E-02	1.93E-02	6.26E-02	6.39E-02
3.00E-02	4.07E+00	1.22E-04	3.17E-01	1.71E-02	7.79E-02	1.71E-02	9.24E-02	8.64E-02
4.00E-02	2.34E+00	1.63E-04	2.48E-01	3.06E-02	1.06E-01	3.06E-02	1.21E-01	1.08E-01
5.00E-02	1.52E+00	2.04E-04	1.92E-01	2.28E-02	1.27E-01	2.28E-02	1.49E-01	1.30E-01
6.00E-02	1.06E+00	2.45E-04	1.61E-01	3.03E-02	1.52E-01	3.03E-02	1.76E-01	1.51E-01
7.00E-02	7.81E-01	2.86E-04	1.24E-01	7.68E-02	1.59E-01	7.68E-02	2.02E-01	1.73E-01
8.00E-02	5.99E-01	3.27E-04	1.16E-01	5.31E-02	1.93E-01	5.31E-02	2.28E-01	1.94E-01
9.00E-02	4.74E-01	3.67E-04	1.01E-01	5.35E-02	2.14E-01	5.35E-02	2.52E-01	2.16E-01
1.00E-01	3.84E-01	4.08E-04	9.32E-02	2.99E-02	2.43E-01	2.99E-02	2.76E-01	2.38E-01
1.10E-01	3.18E-01	4.49E-04	8.26E-02	5.09E-02	2.60E-01	5.09E-02	2.99E-01	2.60E-01
1.20E-01	2.67E-01	4.90E-04	7.78E-02	4.41E-02	2.91E-01	4.41E-02	3.21E-01	2.83E-01
1.30E-01	2.28E-01	5.31E-04	7.21E-02	4.74E-02	3.17E-01	4.74E-02	3.43E-01	3.05E-01
1.40E-01	1.96E-01	5.72E-04	6.47E-02	7.66E-02	3.30E-01	7.66E-02	3.64E-01	3.28E-01
1.50E-01	1.71E-01	6.12E-04	6.17E-02	4.84E-02	3.60E-01	4.84E-02	3.84E-01	3.51E-01
1.60E-01	1.50E-01	6.53E-04	5.49E-02	7.77E-02	3.65E-01	7.77E-02	4.04E-01	3.74E-01
1.70E-01	1.33E-01	6.94E-04	5.02E-02	6.91E-02	3.76E-01	6.91E-02	4.23E-01	3.97E-01
1.80E-01	1.19E-01	7.35E-04	4.86E-02	6.15E-02	4.09E-01	6.15E-02	4.41E-01	4.20E-01
1.90E-01	1.07E-01	7.76E-04	4.35E-02	6.71E-02	4.08E-01	6.71E-02	4.59E-01	4.44E-01
2.00E-01	9.62E-02	8.16E-04	4.44E-02	5.80E-02	4.61E-01	5.80E-02	4.76E-01	4.67E-01
2.10E-01	8.73E-02	8.57E-04	4.16E-02	5.49E-02	4.76E-01	5.49E-02	4.93E-01	4.90E-01
2.20E-01	7.95E-02	8.98E-04	4.21E-02	6.25E-02	5.29E-01	6.25E-02	5.09E-01	5.14E-01

Depth [cm]	KERMA [J/kg•Y]	σ_{KERMA} [%]	Dose [J/kg•Y]	σ_{dose} [%]	f_{CPE}	σ_{fCPE} [%]	VARSKIN 3 f_{CPE}	New Model f_{CPE}
2.30E-01	7.28E-02	9.39E-04	4.00E-02	5.69E-02	5.50E-01	5.69E-02	5.24E-01	5.37E-01
2.40E-01	6.68E-02	9.80E-04	3.76E-02	5.61E-02	5.62E-01	5.61E-02	5.39E-01	5.60E-01
2.50E-01	6.16E-02	1.02E-03	3.57E-02	4.90E-02	5.80E-01	4.90E-02	5.54E-01	5.84E-01
2.60E-01	5.70E-02	1.06E-03	3.38E-02	6.65E-02	5.93E-01	6.65E-02	5.68E-01	6.07E-01
2.70E-01	5.28E-02	1.10E-03	3.34E-02	6.51E-02	6.33E-01	6.51E-02	5.82E-01	6.29E-01
2.80E-01	4.91E-02	1.14E-03	3.38E-02	4.94E-02	6.88E-01	4.94E-02	5.95E-01	6.52E-01
2.90E-01	4.58E-02	1.18E-03	3.07E-02	3.87E-02	6.71E-01	3.87E-02	6.08E-01	6.74E-01
3.00E-01	4.28E-02	1.22E-03	3.09E-02	5.58E-02	7.24E-01	5.58E-02	6.21E-01	6.97E-01
3.10E-01	4.00E-02	1.27E-03	2.88E-02	6.63E-02	7.19E-01	6.63E-02	6.33E-01	7.19E-01
3.20E-01	3.75E-02	1.31E-03	2.67E-02	8.00E-02	7.11E-01	8.00E-02	6.44E-01	7.40E-01
3.30E-01	3.53E-02	1.35E-03	2.79E-02	6.74E-02	7.90E-01	6.74E-02	6.56E-01	7.62E-01
3.40E-01	3.32E-02	1.39E-03	2.33E-02	6.67E-02	7.02E-01	6.67E-02	6.67E-01	7.83E-01
3.50E-01	3.13E-02	1.43E-03	2.09E-02	1.05E-01	6.68E-01	1.05E-01	6.77E-01	8.03E-01
3.60E-01	2.96E-02	1.47E-03	2.45E-02	5.30E-02	8.26E-01	5.30E-02	6.87E-01	8.23E-01
3.70E-01	2.80E-02	1.52E-03	2.47E-02	6.16E-02	8.82E-01	6.16E-02	6.97E-01	8.43E-01
3.80E-01	2.65E-02	1.55E-03	2.50E-02	4.04E-02	9.43E-01	4.04E-02	7.07E-01	8.63E-01
3.90E-01	2.52E-02	1.60E-03	2.13E-02	6.43E-02	8.43E-01	6.43E-02	7.16E-01	8.81E-01
4.00E-01	2.39E-02	1.64E-03	1.85E-02	8.52E-02	7.72E-01	8.52E-02	7.25E-01	9.00E-01
4.10E-01	2.28E-02	1.68E-03	2.18E-02	5.97E-02	9.58E-01	5.98E-02	7.34E-01	9.18E-01
4.20E-01	2.17E-02	1.72E-03	1.98E-02	8.21E-02	9.14E-01	8.21E-02	7.42E-01	9.35E-01
4.30E-01	2.07E-02	1.76E-03	1.94E-02	7.25E-02	9.37E-01	7.25E-02	7.51E-01	9.52E-01
4.40E-01	1.98E-02	1.80E-03	1.93E-02	7.10E-02	9.75E-01	7.10E-02	7.59E-01	9.69E-01
4.50E-01	1.89E-02	1.84E-03	1.84E-02	5.73E-02	9.71E-01	5.73E-02	7.66E-01	9.85E-01
4.60E-01	1.81E-02	1.88E-03	1.79E-02	6.93E-02	9.89E-01	6.93E-02	7.74E-01	1.00E+00
4.70E-01	1.73E-02	1.93E-03	1.81E-02	5.79E-02	1.04E+00	5.79E-02	7.81E-01	1.02E+00
4.80E-01	1.66E-02	1.97E-03	1.21E-02	8.14E-02	7.27E-01	8.14E-02	7.88E-01	1.03E+00
4.90E-01	1.59E-02	2.01E-03	1.56E-02	6.48E-02	9.78E-01	6.48E-02	7.95E-01	1.04E+00
5.00E-01	1.53E-02	2.05E-03	1.59E-02	6.00E-02	1.04E+00	6.00E-02	8.01E-01	1.06E+00
5.10E-01	1.47E-02	2.09E-03	1.72E-02	5.79E-02	1.17E+00	5.79E-02	8.07E-01	1.07E+00
5.20E-01	1.41E-02	2.13E-03	1.44E-02	6.84E-02	1.02E+00	6.85E-02	8.14E-01	1.08E+00
5.30E-01	1.36E-02	2.17E-03	1.43E-02	6.21E-02	1.06E+00	6.22E-02	8.19E-01	1.09E+00
5.40E-01	1.31E-02	2.21E-03	1.39E-02	6.62E-02	1.06E+00	6.62E-02	8.25E-01	1.10E+00

Table 6-11: The MCNP5 data that was used to construct the 2.0 MeV f_{CPE} curve and the corresponding values as calculated by VARSKIN 3 and the new model.

Depth [cm]	KERMA [J/kg Y]	σ_{KERMA} [%]	Dose [J/kg•Y]	σ_{dose} [%]	f_{CPE}	σ_{fCPE} [%]	VARSKIN 3 f_{CPE}	New Model f_{CPE}
2.00E-04	3.26E+02	4.08E-05	1.10E+00	1.28E-02	3.37E-03	1.28E-02	4.25E-04	3.71E-03
4.00E-04	2.67E+02	4.08E-05	1.20E+00	1.37E-02	4.51E-03	1.37E-02	8.50E-04	5.38E-03
6.00E-04	2.34E+02	2.04E-05	1.25E+00	1.33E-02	5.33E-03	1.33E-02	1.28E-03	6.71E-03
8.00E-04	2.10E+02	2.04E-05	1.29E+00	1.13E-02	6.16E-03	1.13E-02	1.70E-03	7.86E-03
1.00E-03	1.92E+02	2.04E-05	1.29E+00	1.42E-02	6.73E-03	1.42E-02	2.12E-03	8.91E-03
1.20E-03	1.77E+02	2.04E-05	1.30E+00	1.22E-02	7.35E-03	1.22E-02	2.55E-03	9.87E-03
1.40E-03	1.64E+02	2.04E-05	1.33E+00	9.69E-03	8.07E-03	9.69E-03	2.97E-03	1.08E-02
1.60E-03	1.53E+02	2.04E-05	1.29E+00	1.25E-02	8.44E-03	1.25E-02	3.40E-03	1.16E-02
1.80E-03	1.44E+02	2.04E-05	1.29E+00	1.25E-02	8.96E-03	1.25E-02	3.82E-03	1.24E-02
2.00E-03	1.35E+02	2.04E-05	1.29E+00	1.15E-02	9.53E-03	1.15E-02	4.24E-03	1.32E-02
2.20E-03	1.28E+02	2.04E-05	1.26E+00	1.23E-02	9.87E-03	1.23E-02	4.67E-03	1.40E-02
2.40E-03	1.21E+02	2.04E-05	1.26E+00	1.31E-02	1.04E-02	1.31E-02	5.09E-03	1.47E-02
2.60E-03	1.15E+02	2.04E-05	1.26E+00	1.13E-02	1.09E-02	1.13E-02	5.51E-03	1.54E-02
2.80E-03	1.09E+02	2.04E-05	1.22E+00	1.43E-02	1.12E-02	1.43E-02	5.94E-03	1.61E-02
3.00E-03	1.04E+02	2.04E-05	1.22E+00	1.24E-02	1.17E-02	1.24E-02	6.36E-03	1.68E-02
3.20E-03	9.88E+01	2.04E-05	1.22E+00	1.35E-02	1.23E-02	1.35E-02	6.78E-03	1.74E-02
3.40E-03	9.43E+01	2.04E-05	1.18E+00	1.13E-02	1.25E-02	1.13E-02	7.20E-03	1.81E-02
3.60E-03	9.01E+01	2.04E-05	1.17E+00	1.21E-02	1.30E-02	1.21E-02	7.63E-03	1.87E-02
3.80E-03	8.61E+01	2.04E-05	1.15E+00	1.26E-02	1.34E-02	1.26E-02	8.05E-03	1.93E-02
4.00E-03	8.24E+01	2.04E-05	1.12E+00	1.32E-02	1.36E-02	1.32E-02	8.47E-03	2.00E-02
4.20E-03	7.89E+01	2.04E-05	1.13E+00	1.18E-02	1.44E-02	1.18E-02	8.89E-03	2.06E-02
4.40E-03	7.57E+01	2.04E-05	1.10E+00	1.32E-02	1.45E-02	1.32E-02	9.31E-03	2.11E-02
4.60E-03	7.26E+01	2.04E-05	1.10E+00	1.02E-02	1.52E-02	1.02E-02	9.73E-03	2.17E-02
4.80E-03	6.97E+01	2.04E-05	1.07E+00	1.40E-02	1.54E-02	1.40E-02	1.02E-02	2.23E-02
5.00E-03	6.70E+01	2.04E-05	1.06E+00	1.28E-02	1.58E-02	1.28E-02	1.06E-02	2.29E-02
5.20E-03	6.44E+01	2.04E-05	1.04E+00	1.45E-02	1.61E-02	1.45E-02	1.10E-02	2.34E-02
5.40E-03	6.19E+01	2.04E-05	1.02E+00	1.37E-02	1.64E-02	1.37E-02	1.14E-02	2.40E-02
5.60E-03	5.96E+01	2.04E-05	9.84E-01	1.58E-02	1.65E-02	1.58E-02	1.18E-02	2.45E-02
5.80E-03	5.74E+01	2.04E-05	1.00E+00	1.22E-02	1.74E-02	1.22E-02	1.23E-02	2.51E-02
6.00E-03	5.53E+01	2.04E-05	9.79E-01	1.21E-02	1.77E-02	1.21E-02	1.27E-02	2.56E-02
6.20E-03	5.33E+01	4.08E-05	9.47E-01	1.60E-02	1.78E-02	1.60E-02	1.31E-02	2.62E-02

Depth [cm]	KERMA [J/kg Y]	σ_{KERMA} [%]	Dose [J/kg•Y]	σ_{dose} [%]	f_{CPE}	σ_{fCPE} [%]	VARSKIN 3 f_{CPE}	New Model f_{CPE}
6.40E-03	5.14E+01	4.08E-05	9.40E-01	1.48E-02	1.83E-02	1.48E-02	1.35E-02	2.67E-02
6.60E-03	4.96E+01	4.08E-05	9.27E-01	1.37E-02	1.87E-02	1.37E-02	1.39E-02	2.72E-02
6.80E-03	4.79E+01	4.08E-05	9.14E-01	1.55E-02	1.91E-02	1.55E-02	1.44E-02	2.77E-02
7.00E-03	4.63E+01	4.08E-05	8.95E-01	1.52E-02	1.93E-02	1.52E-02	1.48E-02	2.82E-02
1.00E-02	2.89E+01	4.08E-05	7.34E-01	1.47E-02	2.55E-02	1.47E-02	2.10E-02	3.55E-02
2.00E-02	9.29E+00	8.16E-05	4.18E-01	2.16E-02	4.50E-02	2.16E-02	4.16E-02	5.70E-02
3.00E-02	4.39E+00	1.22E-04	2.93E-01	2.63E-02	6.68E-02	2.63E-02	6.18E-02	7.66E-02
4.00E-02	2.52E+00	1.63E-04	2.26E-01	2.41E-02	8.96E-02	2.41E-02	8.15E-02	9.54E-02
5.00E-02	1.63E+00	2.04E-04	1.79E-01	4.04E-02	1.10E-01	4.04E-02	1.01E-01	1.14E-01
6.00E-02	1.14E+00	2.45E-04	1.52E-01	4.22E-02	1.33E-01	4.22E-02	1.20E-01	1.32E-01
7.00E-02	8.41E-01	2.86E-04	1.14E-01	7.86E-02	1.35E-01	7.86E-02	1.38E-01	1.50E-01
8.00E-02	6.45E-01	3.27E-04	1.09E-01	5.47E-02	1.69E-01	5.47E-02	1.56E-01	1.69E-01
9.00E-02	5.11E-01	3.67E-04	9.92E-02	3.30E-02	1.94E-01	3.30E-02	1.74E-01	1.87E-01
1.00E-01	4.14E-01	4.08E-04	8.23E-02	5.68E-02	1.99E-01	5.68E-02	1.92E-01	2.06E-01
1.10E-01	3.42E-01	4.49E-04	8.44E-02	3.34E-02	2.46E-01	3.34E-02	2.09E-01	2.24E-01
1.20E-01	2.88E-01	4.90E-04	6.36E-02	7.58E-02	2.21E-01	7.58E-02	2.25E-01	2.43E-01
1.30E-01	2.45E-01	5.31E-04	6.56E-02	5.14E-02	2.68E-01	5.14E-02	2.42E-01	2.62E-01
1.40E-01	2.12E-01	5.72E-04	5.47E-02	7.66E-02	2.58E-01	7.66E-02	2.57E-01	2.81E-01
1.50E-01	1.84E-01	6.12E-04	5.68E-02	5.02E-02	3.08E-01	5.02E-02	2.73E-01	3.00E-01
1.60E-01	1.62E-01	6.53E-04	5.36E-02	4.96E-02	3.31E-01	4.97E-02	2.88E-01	3.19E-01
1.70E-01	1.44E-01	6.94E-04	4.93E-02	4.80E-02	3.43E-01	4.80E-02	3.03E-01	3.38E-01
1.80E-01	1.28E-01	7.35E-04	4.50E-02	7.20E-02	3.51E-01	7.20E-02	3.18E-01	3.58E-01
1.90E-01	1.15E-01	7.76E-04	4.09E-02	7.11E-02	3.56E-01	7.11E-02	3.32E-01	3.77E-01
2.00E-01	1.04E-01	8.16E-04	4.51E-02	4.31E-02	4.35E-01	4.31E-02	3.46E-01	3.96E-01
2.10E-01	9.40E-02	8.57E-04	4.08E-02	5.06E-02	4.34E-01	5.06E-02	3.60E-01	4.16E-01
2.20E-01	8.57E-02	8.98E-04	3.97E-02	5.15E-02	4.63E-01	5.15E-02	3.74E-01	4.35E-01
2.30E-01	7.84E-02	9.39E-04	3.37E-02	7.18E-02	4.30E-01	7.18E-02	3.87E-01	4.55E-01
2.40E-01	7.20E-02	9.80E-04	3.32E-02	6.46E-02	4.61E-01	6.46E-02	4.00E-01	4.75E-01
2.50E-01	6.64E-02	1.02E-03	3.16E-02	8.09E-02	4.76E-01	8.09E-02	4.12E-01	4.94E-01
2.60E-01	6.14E-02	1.06E-03	3.18E-02	7.33E-02	5.18E-01	7.34E-02	4.25E-01	5.13E-01
2.70E-01	5.69E-02	1.10E-03	2.90E-02	6.66E-02	5.10E-01	6.66E-02	4.37E-01	5.33E-01
2.80E-01	5.29E-02	1.14E-03	2.80E-02	7.82E-02	5.30E-01	7.82E-02	4.49E-01	5.52E-01
2.90E-01	4.93E-02	1.18E-03	2.97E-02	4.90E-02	6.03E-01	4.90E-02	4.60E-01	5.71E-01

Depth [cm]	KERMA [J/kg Y]	σ_{KERMA} [%]	Dose [J/kg•Y]	σ_{dose} [%]	f_{CPE}	σ_{fCPE} [%]	VARSKIN 3 f_{CPE}	New Model f_{CPE}
3.00E-01	4.61E-02	1.22E-03	2.73E-02	6.12E-02	5.92E-01	6.12E-02	4.72E-01	5.90E-01
3.10E-01	4.31E-02	1.27E-03	2.39E-02	7.78E-02	5.54E-01	7.78E-02	4.83E-01	6.09E-01
3.20E-01	4.05E-02	1.31E-03	2.57E-02	6.79E-02	6.35E-01	6.79E-02	4.94E-01	6.28E-01
3.30E-01	3.80E-02	1.35E-03	1.93E-02	9.32E-02	5.09E-01	9.32E-02	5.04E-01	6.47E-01
3.40E-01	3.58E-02	1.39E-03	2.53E-02	6.13E-02	7.07E-01	6.13E-02	5.15E-01	6.65E-01
3.50E-01	3.38E-02	1.43E-03	2.37E-02	5.74E-02	7.02E-01	5.74E-02	5.25E-01	6.83E-01
3.60E-01	3.19E-02	1.47E-03	2.13E-02	8.02E-02	6.68E-01	8.02E-02	5.35E-01	7.01E-01
3.70E-01	3.02E-02	1.52E-03	1.78E-02	8.07E-02	5.89E-01	8.07E-02	5.45E-01	7.19E-01
3.80E-01	2.86E-02	1.55E-03	2.01E-02	5.76E-02	7.04E-01	5.76E-02	5.54E-01	7.37E-01
3.90E-01	2.72E-02	1.60E-03	2.39E-02	5.36E-02	8.81E-01	5.37E-02	5.64E-01	7.54E-01
4.00E-01	2.58E-02	1.64E-03	1.86E-02	7.58E-02	7.20E-01	7.58E-02	5.73E-01	7.71E-01
4.10E-01	2.45E-02	1.68E-03	1.82E-02	6.66E-02	7.40E-01	6.66E-02	5.82E-01	7.88E-01
4.20E-01	2.34E-02	1.72E-03	1.93E-02	4.97E-02	8.27E-01	4.97E-02	5.91E-01	8.04E-01
4.30E-01	2.23E-02	1.76E-03	2.00E-02	4.49E-02	8.95E-01	4.49E-02	5.99E-01	8.20E-01
4.40E-01	2.13E-02	1.80E-03	1.90E-02	5.84E-02	8.90E-01	5.85E-02	6.08E-01	8.36E-01
4.50E-01	2.04E-02	1.85E-03	1.82E-02	5.76E-02	8.92E-01	5.76E-02	6.16E-01	8.51E-01
4.60E-01	1.95E-02	1.88E-03	1.78E-02	6.80E-02	9.14E-01	6.81E-02	6.24E-01	8.66E-01
4.70E-01	1.87E-02	1.92E-03	1.77E-02	7.50E-02	9.46E-01	7.51E-02	6.32E-01	8.81E-01
4.80E-01	1.79E-02	1.97E-03	1.59E-02	7.21E-02	8.92E-01	7.21E-02	6.40E-01	8.95E-01
4.90E-01	1.72E-02	2.01E-03	1.65E-02	5.41E-02	9.61E-01	5.41E-02	6.47E-01	9.09E-01
5.00E-01	1.65E-02	2.05E-03	1.46E-02	6.01E-02	8.85E-01	6.01E-02	6.55E-01	9.23E-01
5.10E-01	1.58E-02	2.09E-03	1.47E-02	8.09E-02	9.29E-01	8.09E-02	6.62E-01	9.36E-01
5.20E-01	1.52E-02	2.13E-03	1.50E-02	7.29E-02	9.84E-01	7.29E-02	6.69E-01	9.49E-01
5.30E-01	1.46E-02	2.18E-03	1.46E-02	7.61E-02	9.94E-01	7.62E-02	6.76E-01	9.62E-01
5.40E-01	1.41E-02	2.22E-03	1.44E-02	5.81E-02	1.02E+00	5.82E-02	6.83E-01	9.74E-01
5.50E-01	1.36E-02	2.26E-03	1.35E-02	5.87E-02	9.91E-01	5.88E-02	6.89E-01	9.86E-01
5.60E-01	1.31E-02	2.30E-03	1.29E-02	7.83E-02	9.82E-01	7.83E-02	6.96E-01	9.97E-01
5.70E-01	1.27E-02	2.34E-03	1.34E-02	7.83E-02	1.06E+00	7.83E-02	7.02E-01	1.01E+00
5.80E-01	1.22E-02	2.38E-03	1.31E-02	7.52E-02	1.07E+00	7.52E-02	7.09E-01	1.02E+00
5.90E-01	1.18E-02	2.42E-03	1.25E-02	5.00E-02	1.05E+00	5.01E-02	7.15E-01	1.03E+00
6.00E-01	1.14E-02	2.46E-03	1.07E-02	6.06E-02	9.38E-01	6.06E-02	7.21E-01	1.04E+00
6.10E-01	1.11E-02	2.50E-03	1.24E-02	8.62E-02	1.12E+00	8.62E-02	7.27E-01	1.05E+00
6.20E-01	1.07E-02	2.54E-03	1.14E-02	6.92E-02	1.07E+00	6.93E-02	7.32E-01	1.06E+00